

①

AD A 951 904



FINAL TECHNICAL REPORT  
High Frequency Aircraft Antennas

The Ohio State University  
**ElectroScience Laboratory**

Department of Electrical Engineering  
Columbus, Ohio 43212

DTIC  
FEB 1 1968  
H

FINAL TECHNICAL REPORT 2235-5  
3 May 1968

APPROVED FOR PUBLIC RELEASE  
DISTRIBUTION UNLIMITED

DTIC FILE COPY

83 01 31 083

REPORT  
by  
The Ohio State University ElectroScience Laboratory  
(formerly Antenna Laboratory)  
Columbus, Ohio 43212

Investigation of High Frequency Aircraft Antennas

Subject of Report Final Technical Report

Submitted by ElectroScience Laboratory  
Department of Electrical Engineering

Date 3 May 1968

N00019-67-C-0063

APPROVED FOR PUBLIC RELEASE  
DISTRIBUTION UNLIMITED



Accession For	<input checked="" type="checkbox"/>
ADIS (M&I)	<input type="checkbox"/>
ADIS (S)	<input type="checkbox"/>
Approved	<input type="checkbox"/>
Justification	
By	
Distribution/	
Availability Codes	
Avail and/or	
Special	
<b>A</b>	
<b>UNANNOUNCED</b>	

REPORTS PUBLISHED  
Under Project 2235

- 2235-1 Annual Summary Report, "High Frequency Aircraft Antennas,"  
27 July 1967
- 2235-2 Richards, G.A., "A Boundary-Value Technique for Computing  
the Patterns of an Antenna Near a Conducting Body of Arbitrary  
Shape," September 1967
- 2235-3 Flaig, T.L., "Impedance and Efficiency of Multiturn Loop  
Antennas," 3 April 1968
- 2235-4 Munk, B.A. and Flaig, T.L., "Radiation Resistance and  
Efficiency of Multiturn Loop Antennas, April 1968
- 2235-5 Final Technical Report, "High Frequency Aircraft Antennas,"  
April 1968

STIC  
FEB 1 1983  
S D  
H

## ABSTRACT

A new HF aircraft antenna system with improved performance characteristics is described and studied. Two prominent features of the system are the use of small multiturn loop elements of greater efficiency than conventional loops of the same size, and the use of several of these elements to inductively excite radiating currents on the aircraft structure. An analysis of this system is followed by a systematic design procedure which applies to any specific aircraft. Conclusions on the feasibility and relative merits of this system are presented.

## TABLE OF CONTENTS

	Page
I. INTRODUCTION	1
II. STUDY OF THE BASIC LOOP ELEMENT	4
A. <u>Introduction</u>	4
B. <u>Description of the Small Multiturn Loop Antenna</u>	4
C. <u>Analysis of the Small Multiturn Loop Element in Free Space</u>	6
D. <u>Experimental Investigation of the Loop Element</u>	15
1. <u>Pattern</u>	15
2. <u>Impedance</u>	20
3. <u>Efficiency</u>	20
4. <u>Dielectric loading</u>	23
E. <u>Element Tuning and Matching</u>	23
III. STRUCTURE EFFECTS ON PATTERN AND IMPEDANCE	29
A. <u>Pattern Effects</u>	29
1. <u>Computer program analysis</u>	29
2. <u>Computer-aided optimization</u>	34
3. <u>Application over a wide bandwidth</u>	39
B. <u>Impedance Effects</u>	39
1. <u>Experimental measurements</u>	39
2. <u>Computer analysis for total impedance effects</u>	46
3. <u>Simplified computer analysis for resistive impedance effects</u>	49
C. <u>Treatment of the Loop Cavity</u>	51

TABLE OF CONTENTS (cont.)

	Page
IV. DESIGN PROCEDURE	52
A. <u>Element Location Design for Best Pattern</u>	53
B. <u>Loop Design for Optimum Efficiency</u>	54
C. <u>System Design for Pattern and Efficiency</u>	56
D. <u>Tuning and Matching Network Design</u>	56
V. CONCLUSIONS AND RECOMMENDATIONS	56
APPENDIX I      EXCITATION OF RADIATING CURRENTS ON THE STRUCTURES	60
APPENDIX II     COMPUTER PROGRAM FOR OPTIMIZING LOCATIONS OF FOUR ANTENNA ELEMENTS ON A WIRE- GRID AIRCRAFT MODEL	67
APPENDIX III    STRUCTURE IMPEDANCE EFFECTS COMPUTER CALCULATION PROGRAM	78
APPENDIX IV     RADIATION RESISTANCE FROM FAR- FIELD PATTERN INTEGRATION	85
APPENDIX V      MAGNETIC DIPOLE REPRESENTATION OF A SMALL ELECTRIC CURRENT LOOP	89
REFERENCES	95

## FINAL TECHNICAL REPORT

### I. INTRODUCTION

The conventional approach to a high-frequency aircraft antenna system is to use an electric element such as a tail cap, trailing wire, or notch antenna. Generally satisfactory results have been obtained but there are definite shortcomings in the conventional system.

First of all, such systems have not fully taken into account structural distortion of the antenna pattern. Some adjustment of antenna position might be made to reduce pattern scalloping effects by the aircraft structure, but very limited control is available with but one element as in a tail cap antenna system.

Secondly, even if good azimuth coverage could be obtained from a tail cap antenna, it behaves essentially like a vertical stub and thus has very poor response directly overhead or below. Poor overhead response means missing some sky wave propagation.

Thirdly, although the electric element by itself might be efficient, it is generally used well below its first natural resonance ( $\lambda/4$  in length for a stub) where it is highly capacitive, hence requires a relatively large tuning coil. Losses in the tuning coil and matching circuitry can result in a system with low efficiency.

And finally, the single antenna limits the total power that can be radiated and reduces the reliability and security of the communications system. If something happens to the single antenna, communication is completely lost.

The object of the present program has been to study the feasibility and develop a design procedure for a new high-frequency aircraft antenna system which does not have the shortcomings mentioned above. The performance goals for this system are omnidirectional radiation with good efficiency at frequencies from 3 to 30 MHz and a number of radiating elements to give improved power handling capability, reliability, and security. To minimize structural and aerodynamic problems, each element must be small and flush-mounted.

The system under consideration uses several relatively small, multiturn loops as antenna elements. These elements are mounted, along with individual power amplifiers and transmit/receive networks,

in cavities at appropriate locations on the aircraft structure. A sketch showing the general layout of this system is shown in Fig. 1. If conventional design approaches were used for this system, the results would be quite unsatisfactory. The small loop elements would have very low efficiency and the pattern of the array of elements on an actual structure would be quite different from that predicted by conventional array theory, probably exhibiting deep scalloping in some directions. However, based on the results of this research effort, two significant departures from conventional practice for applying this system are presented, which change its character drastically.

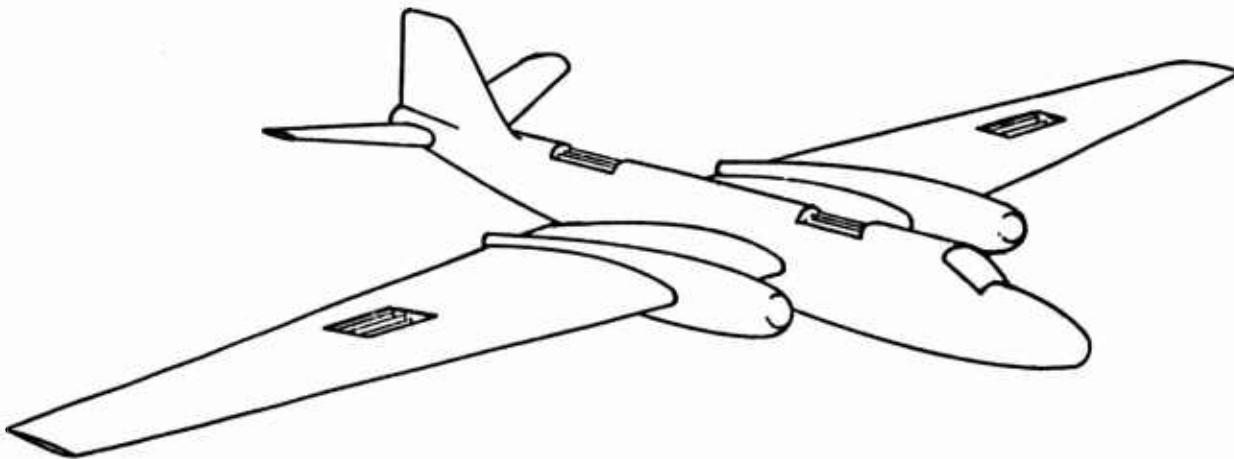


Fig. 1. Illustration of HF antenna system concept.

First, rather than ignoring the structure effects and trying to minimize them, it is proposed that they be used to advantage. A well-known characteristic of antennas in general is that the larger their effective aperture is, the more satisfactory their impedance and efficiency characteristics are when correctly designed. Thus by properly exciting sizable radiating currents over the aircraft structure, the effective aperture of this system, and hence its efficiency, may be greatly increased. Furthermore, the use of multiple elements at selected locations and with



selected drive signals allows a high degree of control of the structure excitation. This excitation control can be used to obtain significantly improved radiation patterns for communication or also to obtain D.F. and homing modes of operation. This new H-F antenna system is very flexible due to the use of a number of radiating elements.

A loop antenna element was chosen for this system primarily because of its suitability for coupling energy onto the structure through its magnetic field. However, even accounting for the structure effects discussed above, the efficiency of a conventional loop is prohibitively low for transmitting applications. A second major departure from conventional practice has been made in order to solve this problem.

It has been found that loops of small area but of many turns, where the total wire length,  $l$ , is on the order of  $\lambda/2$  or more, exhibit a resonant behavior near  $l = \lambda/2, \lambda, 3\lambda/2$ , etc. which is not predicted by the conventional loop antenna analysis. A more accurate analysis has shown that near the resonant frequencies corresponding to  $l \approx \lambda/2, 3\lambda/2, 5\lambda/2 \dots$ , the radiation resistance increases at a much greater rate than the loss resistance, and a peak in the loop antenna efficiency is observed. Thus, by operating the multiturn loop antenna elements just below these resonant frequencies, and optimizing the element geometry for a given cavity size, a practical element for transmitting applications has been achieved. Also, at these operating points, the antenna impedance is inductive and the resulting capacitive matching network is much more efficient than the tuning coils used with conventional, capacitive, high-frequency aircraft antennas.

When these two innovations are properly applied, the resulting system is slightly more complicated but has distinct advantages over a conventional high-frequency aircraft antenna system. However, because of the more complicated nature of this new system, more accurate analyses and a more sophisticated design procedure must be developed. These topics are the subject of this report.

Sections II and III are concerned with analysis of the system. Because of the characteristics of this system, it is convenient to divide the analysis into two parts. In Section II, the multiturn loop element is analyzed in free space. The parameters of primary interest are impedance and efficiency as a function of element geometry. The analysis is accompanied by experimental data and discussions of element loading and element tuning. In Section III, the effects of adding the structure are analyzed. An arbitrary structure is treated as a scatterer, illuminated by one or more of the loop antenna elements. The two parts of this section analyze pattern effects, and impedance and efficiency effects. It is found that these structure effects depend mainly on structure shape and on location and orientation of the elements.

Section IV outlines a design procedure for applying this new high-frequency antenna system to an arbitrary aircraft. Conclusions and recommendations of this study program are presented in Section V.

## II. STUDY OF THE BASIC LOOP ELEMENT

### A. Introduction

Because of space limitations, an aircraft antenna at HF must be relatively small electrically. This generally implies an undesirable impedance characteristic and low efficiency. In the new HF antenna system an attempt is made to overcome these problems by purposely exciting currents on the aircraft structure in order to make use of a larger radiating surface. Currents on a conducting surface are associated with an external tangential magnetic field that is maximum at the conducting surface. Such a magnetic field can generally be established more effectively by a loop element than by a stub or dipole element. Hence a loop antenna has been chosen as the basic element of the new HF antenna system.

The small single-turn loop antenna is too inefficient to be used as the basic radiating element in a feasible HF antenna system. However, the efficiency of the basic loop element can be greatly enhanced by increasing the number of turns. The characteristics of this type of loop antenna are discussed in the following paragraphs.

### B. Description of the Small Multiturn Loop Antenna

The small multiturn loop antenna has turns which are electrically small in area but sufficient in number such that the total wire length may be a significant portion of a wavelength. Since it is required that the antenna system be flush-mounted to eliminate aerodynamic problems, the individual loop elements must be mounted in cavities in the aircraft surface.

A prototype loop element has been designed and is shown mounted in a 18 by 18 by 5 inch cavity in Fig. 2. The antenna consists of 13 turns (approximately rectangular), each 3 in. by 12 in. The coil is constructed of 3/4 in. diameter copper tubing in order to maximize conductor area (minimize losses) while maintaining low weight. The analysis which leads to the design of the prototype loop element is reviewed in the following section.

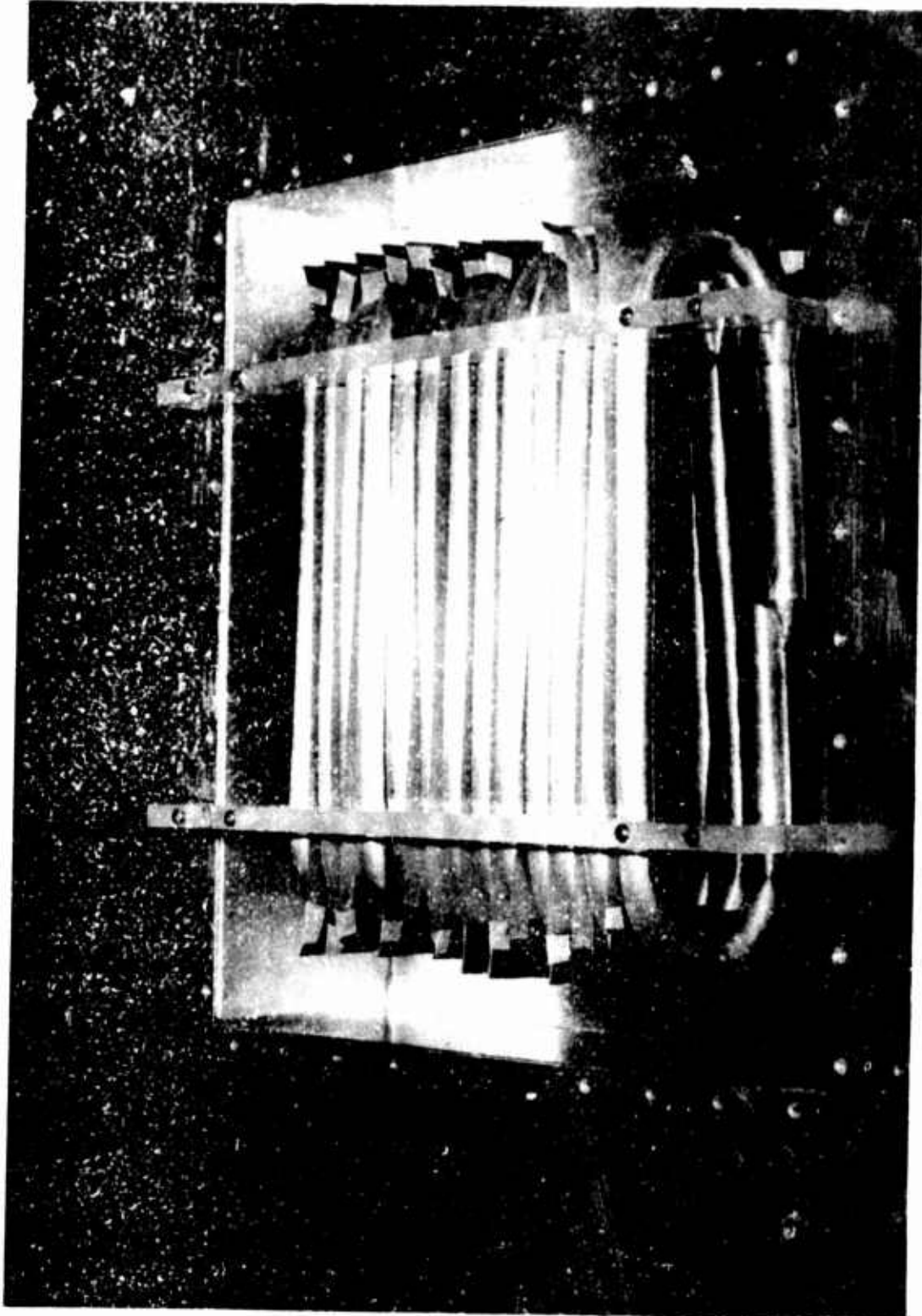


Fig. 2. 13-turn loop antenna.

### C. Analysis of the Small Multiturn Loop Element in Free Space

The basic assumption used by most authors<sup>1,2</sup> in the analysis of the small single-turn loop antenna is that the current on the loop is uniform and in-phase at all points on the loop. In the case of the small multiturn loop, the assumption of uniform in-phase current is not valid if the number of turns is such that the total length of wire in the loop is a significant portion of a wavelength. For this reason, the results of the usual analyses of small loop antennas are useless for predicting the behavior of the type of small multiturn loop antenna discussed here.

A more realistic description of the multiturn loop antenna is obtained if the current on the loop is assumed to be a superposition of two oppositely directed uniform traveling-wave currents of equal amplitude (i.e., sinusoidal current distribution). An analysis based on this assumed form of the current distribution has been performed by B.A. Munk<sup>3</sup> and the far-field pattern, radiation resistance, loss resistance, and efficiency have been calculated. A brief outline of Munk's analysis follows.

The current on the loop is assumed to be of the form

$$(1) \quad \bar{I}(\phi') = \hat{\phi}' I_0 \cos k_0 a \phi' *$$

where  $k_0 = \omega \sqrt{\mu_0 \epsilon_0}$ .

The geometry is illustrated in Fig. 3.

The magnetic far-field of a circular source is given by<sup>4</sup>

$$(2) \quad \bar{H} = \frac{jk_0 a}{4\pi r} e^{-jk_0 r} \int_{-N\pi}^{N\pi} \bar{I}(\phi') \times \hat{r}' e^{jk_0 a \sin \theta \cos(\phi - \phi')} d\phi'$$

and the components of the electric field are given by

$$(3) \quad \begin{cases} E_\theta = \frac{k_0}{\omega \epsilon_0} H_\phi \\ E_\phi = -\frac{k_0}{\omega \epsilon_0} H_\theta \end{cases} .$$

\* Henceforth, bars (—) denote vectors and hats (Λ) denote unit vectors.

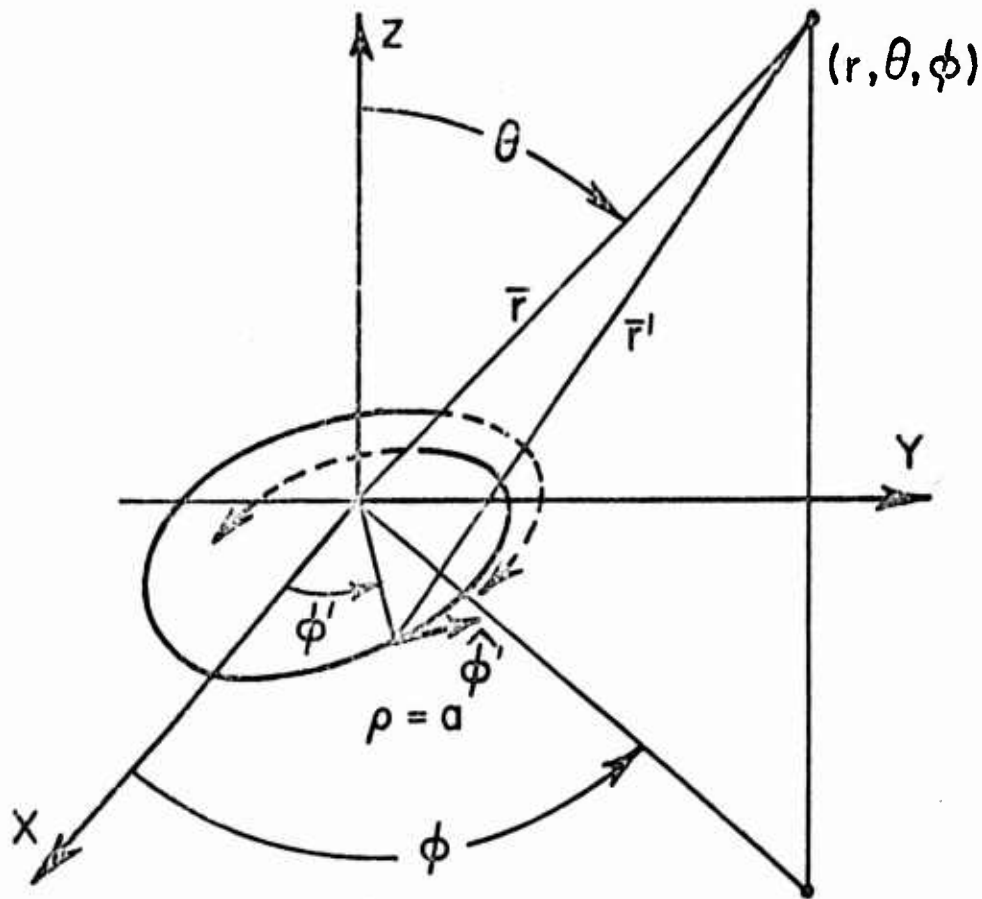


Fig. 3. Coordinate system for Munk's analysis of the multi-turn loop.

By using Eq. (1) in Eq. (2) and inserting the result into Eq.(3) Munk obtains the components of the electric field as:

$$\begin{aligned}
 (4) \quad E_{\theta} = & \frac{j\omega\mu_0 a e^{-jk_0 z} I_0}{8r} \cos \theta \frac{\sin(N\pi k_0 a)}{\sin(\pi k_0 a)} \\
 & \times \left[ e^{jk_0 a \left(\phi + \frac{\pi}{2}\right)} \begin{pmatrix} \mathbb{J}_{k_0 a + 1}(z) & \mathbb{J}_{k_0 a - 1}(z) \end{pmatrix} \right. \\
 & \left. + e^{-jk_0 a \left(\phi + \frac{\pi}{2}\right)} \begin{pmatrix} \mathbb{J}_{k_0 a + 1}(-z) & \mathbb{J}_{k_0 a - 1}(-z) \end{pmatrix} \right]
 \end{aligned}$$

and

$$(5) \quad E_{\phi} = -\frac{\omega \mu_0 a I_0 e^{-jk_0 r}}{4r} \frac{\sin(N\pi k_0 a)}{\sin(\pi k_0 a)} \\ \times \left[ \begin{array}{cc} e^{jk_0 a \left(\phi + \frac{\pi}{2}\right)} & e^{-jk_0 a \left(\phi + \frac{\pi}{2}\right)} \\ \mathbb{J}'(z) & \mathbb{J}'(z) \\ k_0 a & -k_0 a \end{array} \right]$$

where  $z = k_0 a \sin \theta$  and  $\mathbb{J}_{\alpha}(\beta)$  is the Anger Function of order  $\alpha$  with argument  $\beta$ .

The radiation resistance  $R_R$  of the N-turn loop is calculated from Eqs. (4) and (5) by the standard technique of Poynting Vector integration in the far-field. The radiated power  $P_R$  is

$$(6) \quad P_R = \frac{1}{2} R_R I^2_{\text{Terminal}} = \int_0^{2\pi} \int_0^{\pi} \frac{|\overline{E}|^2}{2Z_0} r^2 \sin \theta d\theta d\phi .$$

With simplifying approximations made, the integral in Eq. (6) is evaluated giving

$$(7) \quad R_R = \frac{8\pi^2 f_{\text{MHz}}^2 a^2}{9 \times 10^3} \tan^2(N\pi k_0 a) ,$$

at the terminals where  $f_{\text{MHz}}$  is the frequency in MHz.

The power lost in the antenna,  $P_L$ , and the loss resistance,  $R_L$ , are related to the current on the antenna as follows:

$$(8) \quad P_L = \frac{1}{2} R_L I^2_{\text{Terminal}} = \frac{1}{2} \int_{-N\pi}^{N\pi} \frac{R_s}{2\pi b} I^2(\phi') a d\phi' ,$$

where  $R_s$  is the surface resistivity of the copper wire given by<sup>5</sup>

$$(9) \quad R_s = 2.16 \times 10^{-4} \sqrt{f_{\text{MHz}}} \Omega .$$

In evaluating Eq. (8), Munk obtains

$$(10) \quad R_L = \frac{4.16 \times 10^{-5}}{b} \frac{N\pi a \sqrt{f_{\text{MHz}}}}{\cos^2(N\pi k_0 a)} \left[ 1 + \frac{\sin(2N\pi k_0 a)}{2N\pi k_0 a} \right]$$

at the terminals.

The radiation efficiency of an antenna is customarily defined as<sup>6</sup>

$$(11) \quad E = \frac{P_R}{P_R + P_L}$$

Using Eqs (6) and (8) in Eq. (11) gives

$$E = \frac{\frac{1}{2} R_A I^2_{\text{Terminal}}}{\frac{1}{2} R_A I^2_{\text{Terminal}} + \frac{1}{2} R_L I^2_{\text{Terminal}}}$$

or,

$$(12) \quad E = \frac{R_R}{R_R + R_L}$$

When the values of  $R_R$  and  $R_L$  from Eqs. (6) and (10) are substituted into Eq. (12), the efficiency is obtained.

From Eqs. (4) and (5) it is seen that  $|E_\theta| \ll |E_\phi|$ . Thus the far-field power pattern is proportional to  $|E_\phi|^2$ . Using only the first term in the series expansion for  $J_{\pm k_0 a}(z)$  yields

$$(13) \quad |E_\phi|^2 = (\text{Constant}) \sin^2 \theta$$

The results of Munk's analysis are reviewed below.

Far-field power pattern;

$$(14) \quad f(\theta, \phi) = \sin^2 \theta$$

Radiation resistance at the loop terminals;

$$(15) \quad R_R = \frac{8\pi \cdot 10^{-3}}{9} f_{\text{MHz}}^2 (\pi a^2) \tan^2 \left( \frac{N(2\pi a)\pi f_{\text{MHz}}}{300} \right) ,$$

Loss resistance at the loop terminals;

$$(16) \quad R_L = \frac{4.16 \cdot 10^{-5} \sqrt{\rho_r} N(2\pi a) \sqrt{f_{\text{MHz}}}}{d_m \cos^2 \left( \frac{(2\pi a) N \pi f_{\text{MHz}}}{300} \right)} \left[ 1 + \frac{\sin \left( \frac{(2\pi a) 2\pi N f_{\text{MHz}}}{300} \right)}{\frac{(2\pi a) 2\pi N f_{\text{MHz}}}{300}} \right]$$

Radiation efficiency;

$$(17) \quad E = \frac{R_R}{R_R + R_L} ,$$

where

$f_{\text{MHz}}$  = frequency in MHz,

$a$  = loop radius in meters,

$N$  = number of turns,

$d_m$  = wire diameter in meters,

$\rho_r$  = relative resistivity of the wire material

$$= \frac{\rho_{\text{wire material}}}{\rho_{\text{copper}}} ,$$

$\phi$  = azimuthal angle of the spherical coordinate system,

$\theta$  = polar angle of the spherical coordinate system.

Munk's analysis of the small circular multiturn loop antenna can be adapted to apply to loops of other than circular shape by replacing  $(\pi a^2)$  by the area of one turn of the noncircular loop, and replacing  $(2\pi a)$  by the perimeter of one turn of the noncircular loop, in Eqs. (15) and (16).



Munk's analysis yields the resistive component of the input impedance of the small multiturn loop antenna. The input reactance, although of less importance than the input resistance, is also of interest. Since calculation of the input reactance of even the simplest antenna is a difficult problem, a simplified approach was adopted. The multiturn loop was represented as a network of coupled single-turn loops, each with uniform in-phase current. An R-L-C equivalent circuit was then formulated and the values of mutual inductance and capacitance between loops and of the self-impedance of each loop were obtained from the literature.<sup>7</sup> Figure 4 shows the R-L-C equivalent circuit for a 5-turn loop antenna. A computer program was written to solve the network equations and calculate the complex input impedance of the equivalent circuit for a particular 5-turn loop. The results were compared with actual measurements made on a 5-turn loop identical to the one analyzed by the equivalent circuit method. It was found that the predictions of the equivalent circuit were not sufficiently accurate to establish this technique as a reliable method of calculating input impedance. The equivalent circuit does, however, provide a physical picture (from the circuit viewpoint) of the operation of the multiturn loop antenna.

Another qualitative method of explaining the behavior of the multiturn loop antenna is to regard it as a shorted section of transmission line of length equal to one half the total length of wire in the loop. The first resonance occurs when the transmission line is about a quarter wavelength long. This would normally be considered an anti-resonance or parallel resonance, since there is a peak in the terminal impedance. Below the first resonance the reactance is inductive. This would generally be the preferred region of operation, since tuning and matching could then be accomplished by a simple low-loss capacitive network. Similar resonances occur for wire lengths of  $3\lambda/2$ ,  $5\lambda/2$ , etc.

Equations (15), (16), and (17) were used to calculate the input resistance and efficiency for the 13-turn loop previously described and also for a 5-turn, 0.4 m diameter circular loop constructed of 1/16 in. diameter copper wire as shown in Fig. 5. The predicted input resistance and efficiency for the 5-turn and 13-turn loops are shown in Figs. 6, 8, 9 and 11. As seen from Fig. 11 the predicted maximum efficiency for the 13-turn loop is about 16.5% and occurs at about 19 MHz.

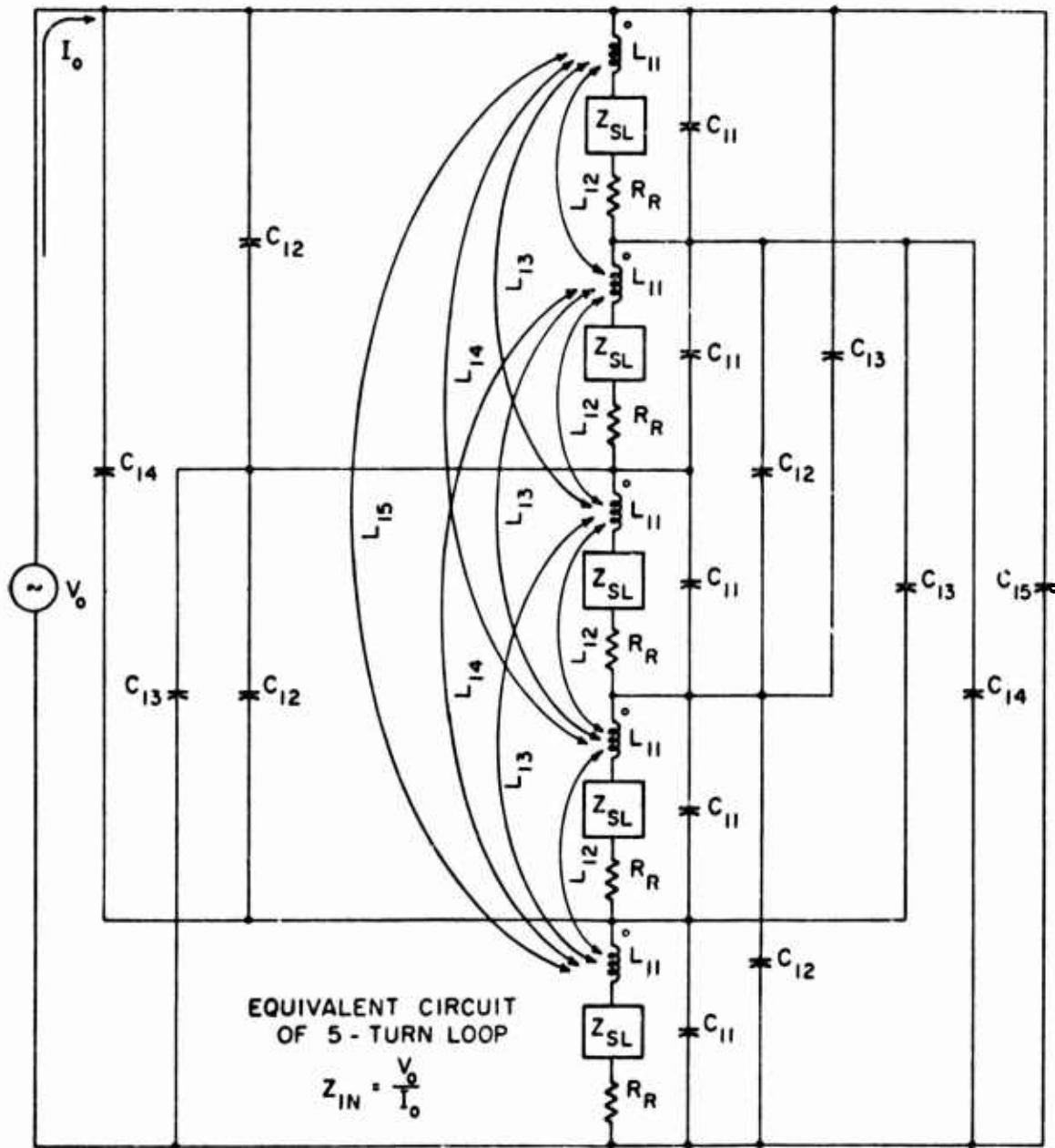


Fig. 4. Equivalent circuit of a five-turn loop antenna.

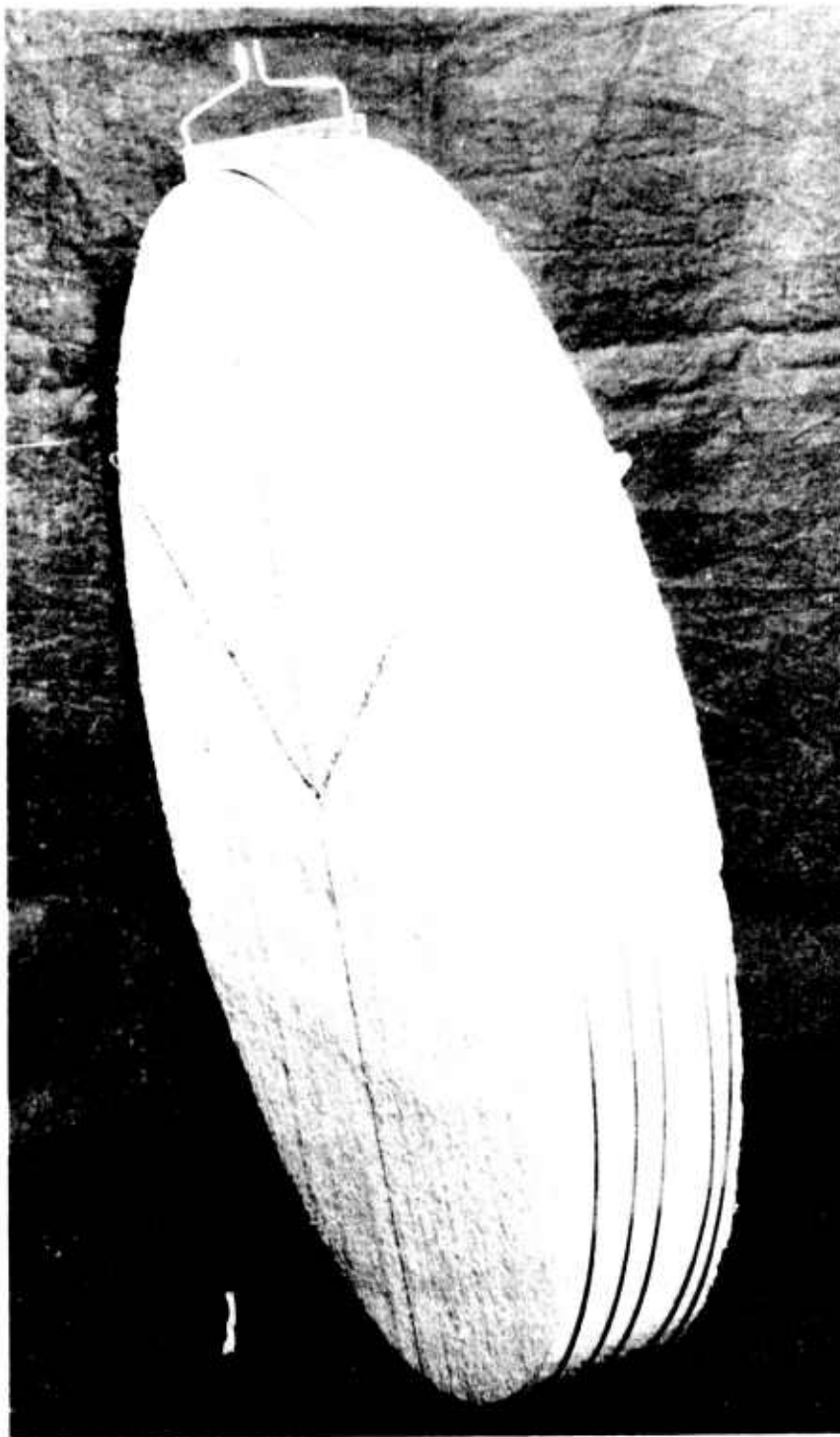


Fig. 5. Five-turn loop antenna.

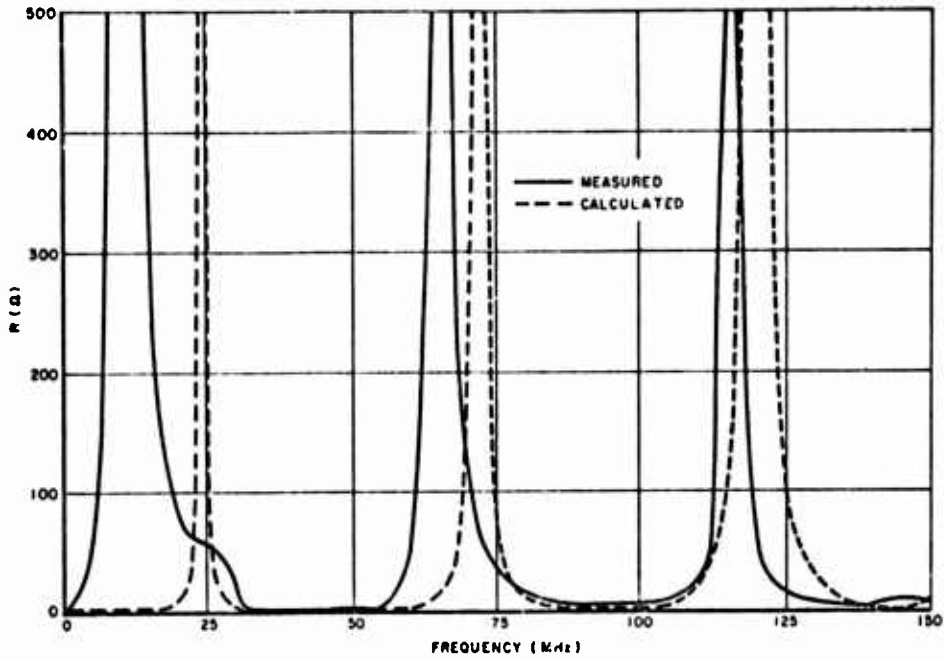


Fig. 6. Input resistance of the 5-turn loop antenna.

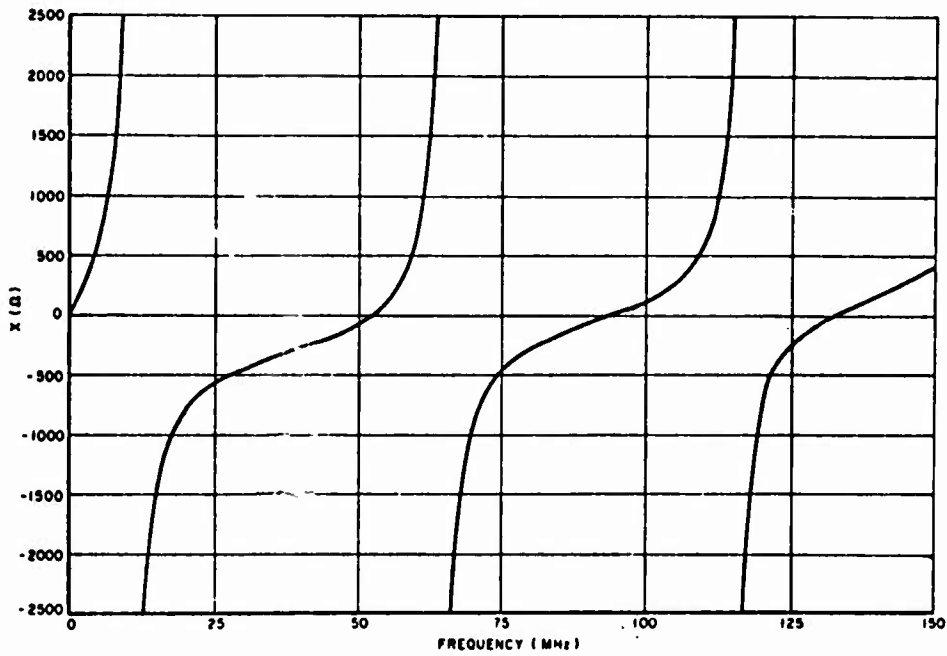


Fig. 7. Input reactance of the 5-turn loop antenna.

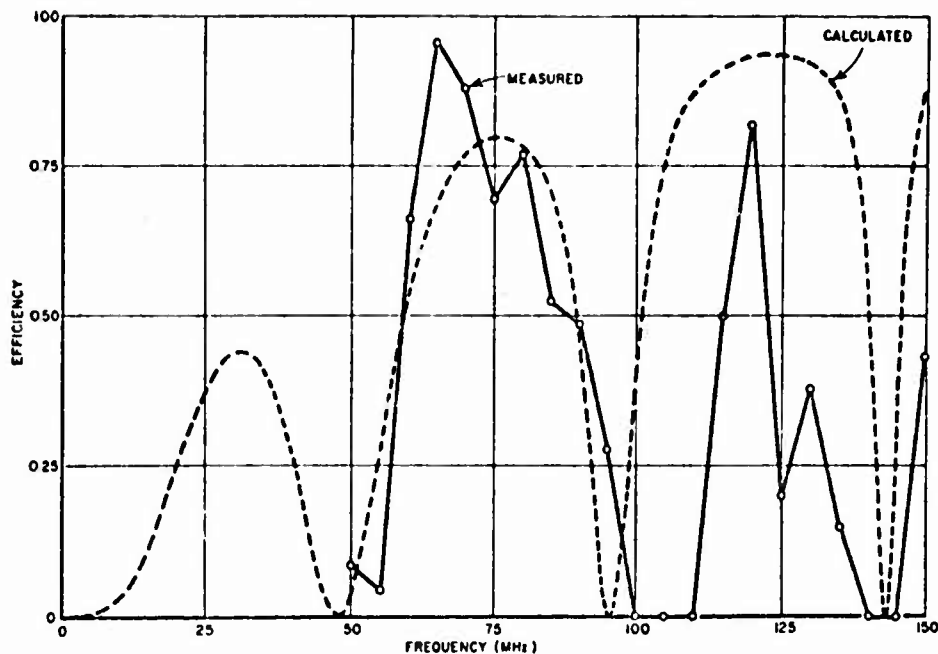


Fig. 8. Efficiency of the 5-turn loop antenna.

#### D. Experimental Investigation of the Loop Element

In order to verify the theoretical results stated in the previous section, impedance and efficiency measurements were made on the 5-turn and 13-turn loop models previously described. Additionally, a far-field power pattern of the 5-turn loop was measured in order to verify the prediction that the pattern function is independent of the angle  $\phi$ . The results of these measurements and the methods by which the measurements were made are described in this section.

##### 1. Pattern

The far-field power pattern of the 5-turn loop model, described in Section II-A, was measured at 125 MHz. The pattern, shown in Fig. 12 is a record of  $\phi$ -polarized radiation in the  $\theta = \pi/2$  plane. As seen from Fig. 12, the pattern is approximately circular (i.e., independent of  $\phi$ ) as predicted by Munk.

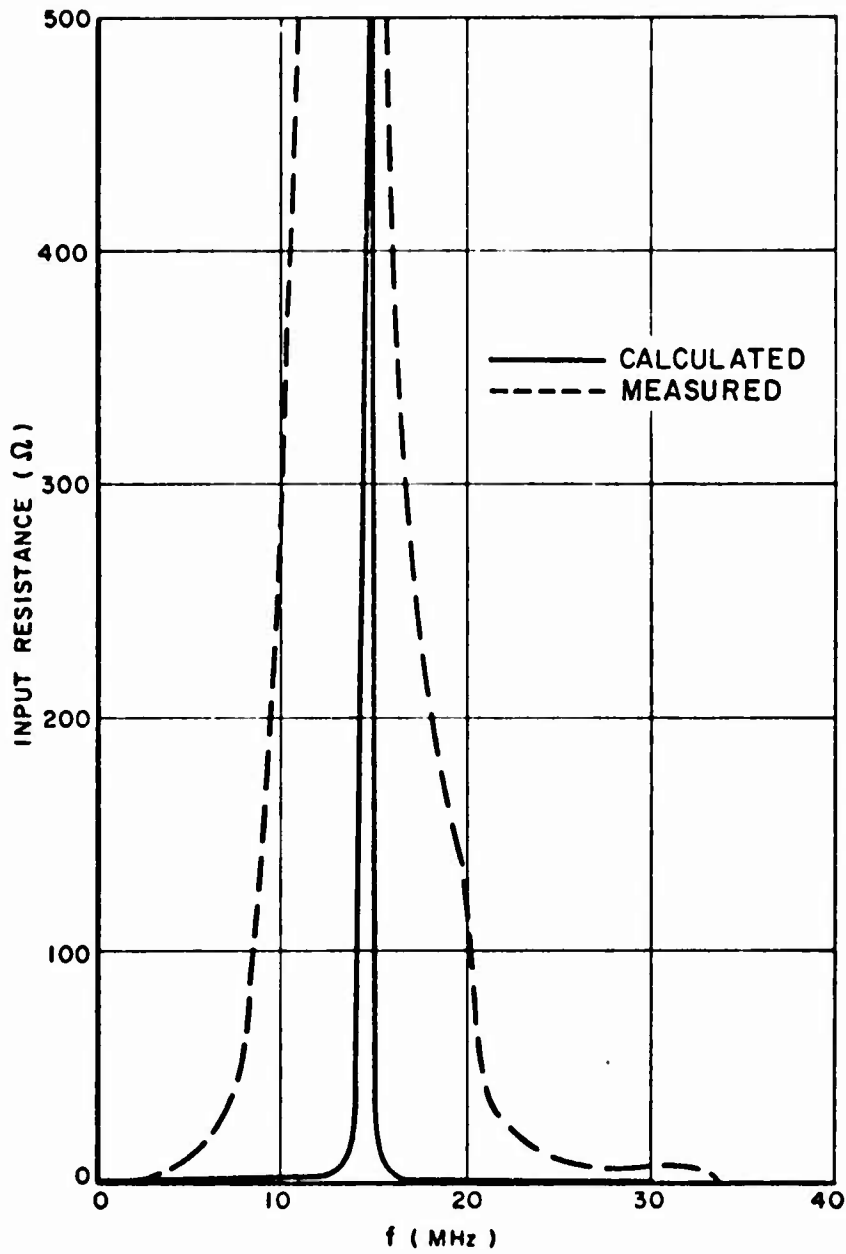


Fig. 9. Input resistance of the 13-turn loop antenna.

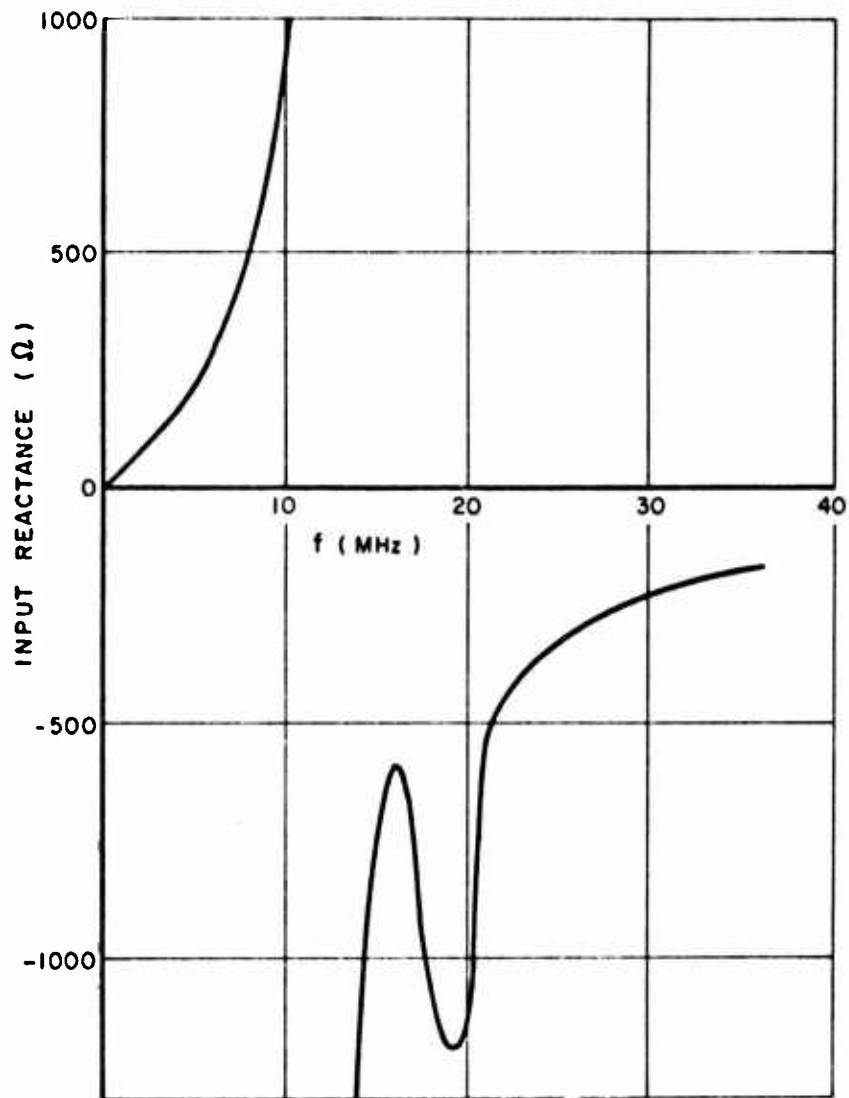


Fig. 10. Input reactance of the 13-turn loop antenna.

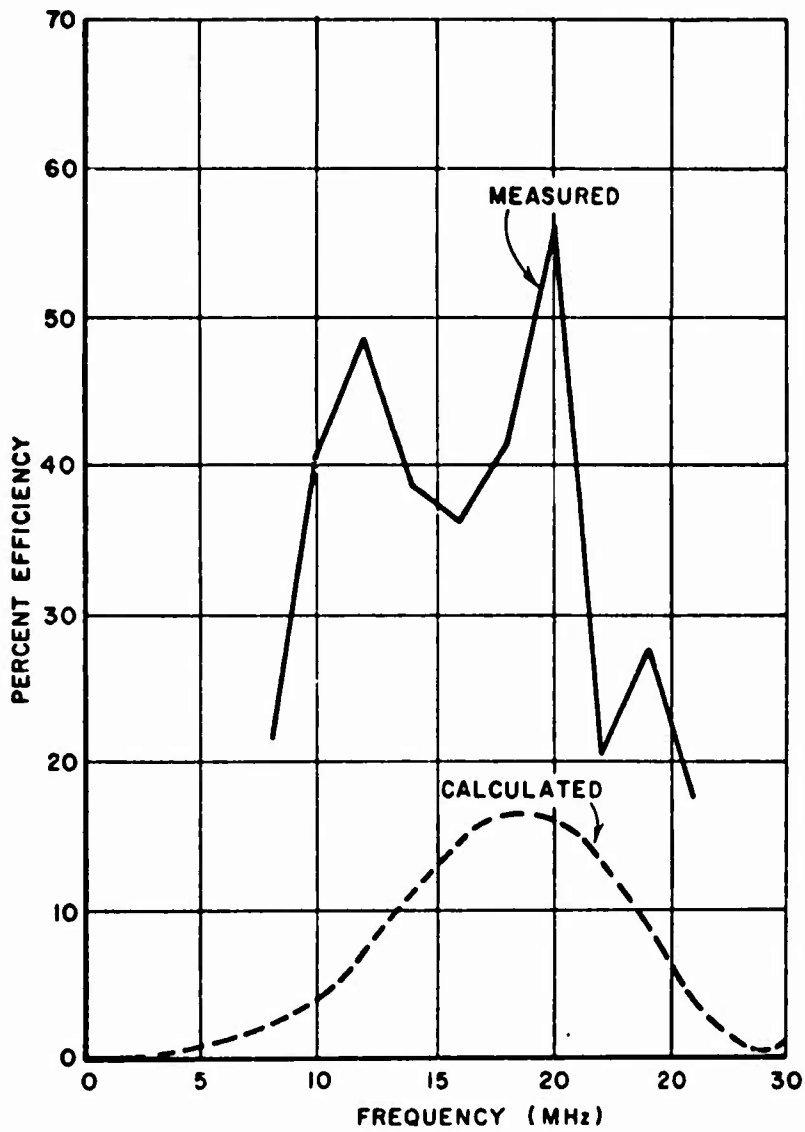


Fig. 11. Efficiency of the 13-turn loop antenna.



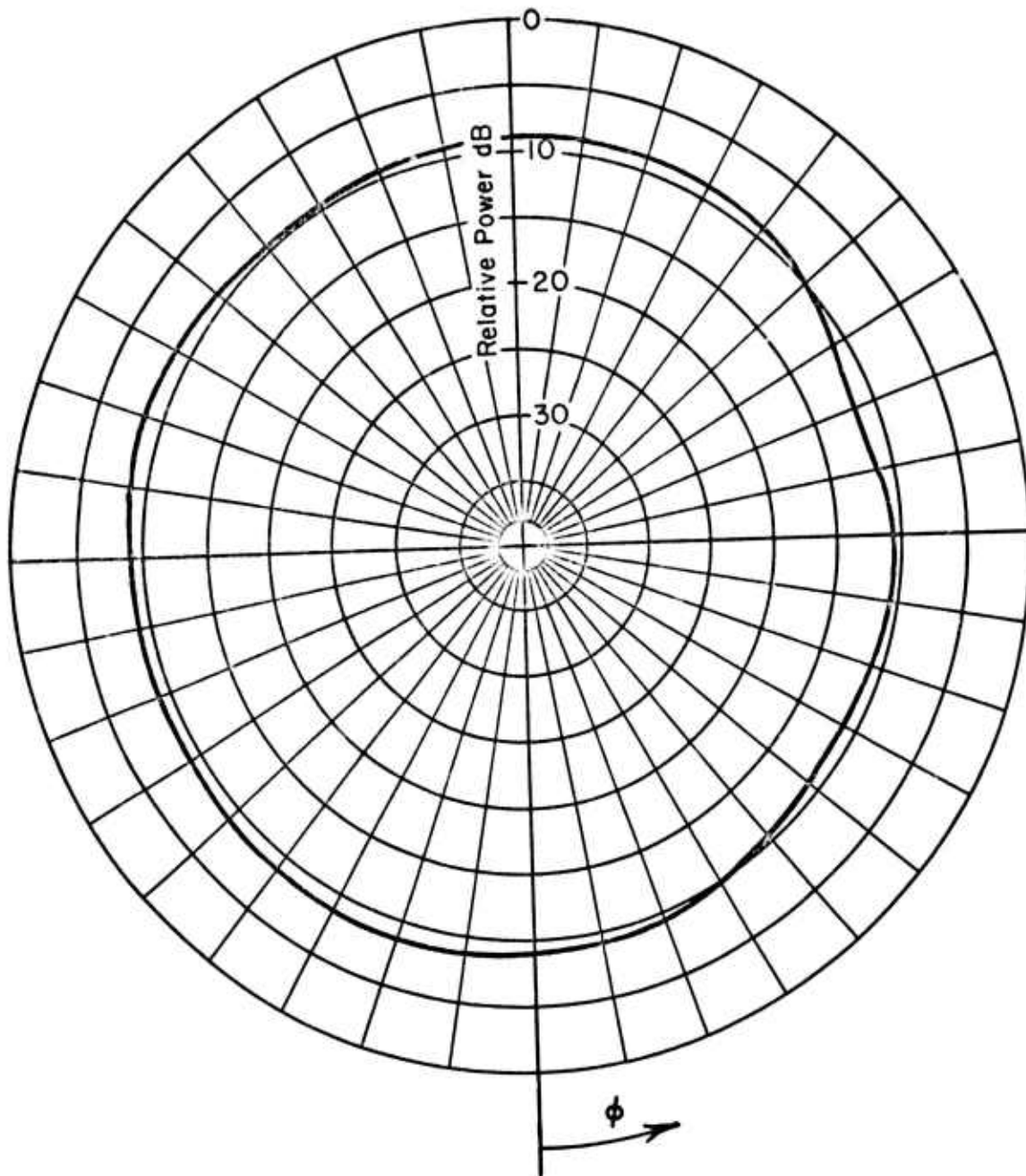


Fig. 12. Far-field power pattern of the 5-turn loop antenna.

## 2. Impedance

The terminal impedances of the 5-turn and 13-turn loop models were measured by the VHF bridge and Vector-Voltmeter techniques described in Report Number 2235-3. During the making of these measurements, it was found that at lower frequencies, the surroundings in which the antenna is located have a significant effect on the impedance measured. In order to reduce these effects, the measurements at frequencies below 50 MHz were made out-of-doors.

Impedance measurements were made on the 5-turn loop in the frequency range from 0 to 150 MHz. The results are shown plotted in Figs. 6 and 7, where Fig. 6 depicts the input resistance, both measured and calculated and Fig. 7 shows the measured input reactance. As seen in Fig. 6, the calculated results agree quite well in form; however, the frequencies at which the resistance peaks actually occur are somewhat lower than the frequencies at which the theory predicts that the peaks should occur. Also, Fig. 7 shows that the antenna has the type of resonance behavior which is characteristic of an R-L-C circuit such as the one shown in Fig. 4.

Figure 13 shows the impedance of the 5-turn loop plotted on a 500 ohm Smith chart. It is seen that the 5-turn loop does behave approximately as a shorted section of transmission line, in that the plot is almost circular and is near the edge of the chart.

The measured input impedance of the 13-turn loop antenna is shown in Fig. 9 and 10. Figure 9 shows measured and calculated input resistance and the measured input reactance is shown in Fig. 10. As in the case of the 5-turn loop, the measured values of input resistance are somewhat different from those predicted by theory, although the general shape of the theoretical curve is verified. From Fig. 10 it is seen that the reactance behaves essentially as that of an R-L-C circuit or a shorted section of transmission line.

## 3. Efficiency

The radiation efficiency of the multiturn loop antennas has been measured by comparing the terminal resistance of one antenna to that of a geometrically identical antenna constructed of different material.<sup>8</sup> This method of efficiency measurement was developed specifically for use in the HF-VHF range of frequencies, since no established method was considered satisfactory at these frequencies. With the terminal

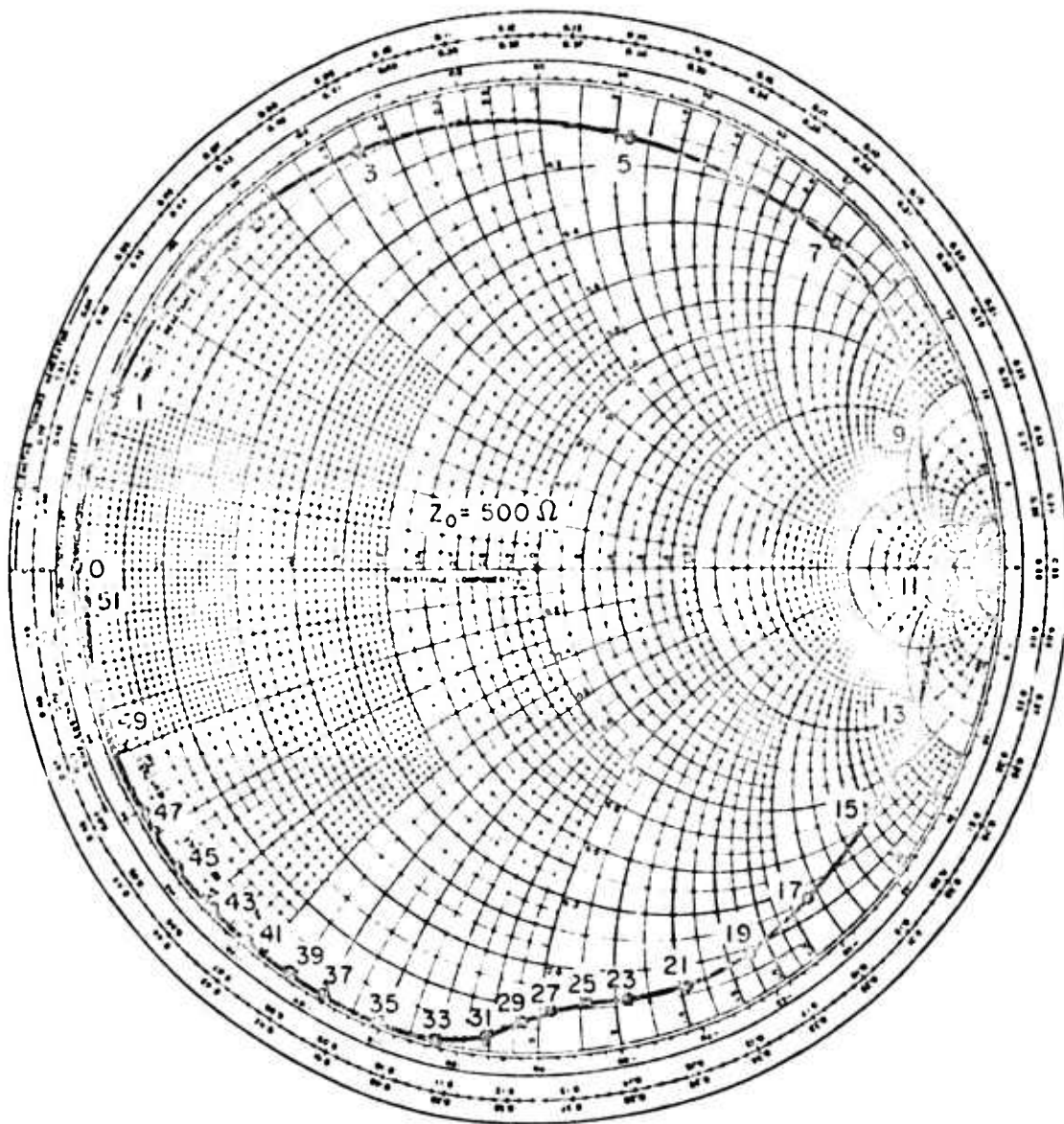


Fig. 13. Smith chart plot of the complex input impedance of the 5-turn loop antenna.

resistances of the two antennas denoted by  $R^{(1)}$  and  $R^{(2)}$  respectively, the efficiency  $E^{(1)}$  of antenna number 1 is given by

$$(18) \quad E^{(1)} = \frac{r R^{(1)} - R^{(2)}}{R^{(1)} (r - 1)}$$

where  $r$  denotes the ratio of the surface resistivity of antenna number 2 to that of antenna number 1.

Measurements on 5-turn loop antennas of copper and brass were made for the purpose of testing this newly developed method of efficiency measurement. The values of efficiency for the copper loop were measured at frequencies between 50 and 150 MHz and are shown plotted in Fig. 8 with the calculated values from Munk's analysis. As indicated in Fig. 8, the measurements are somewhat scattered but tend to substantiate the predictions of the theory.

The radiation efficiency of the 13-turn loop antenna has been measured by three different methods. These are

- (a) comparison of the terminal resistance of geometrically identical but materially different loop models<sup>8</sup>
- (b) comparison of input and radiated power to that of a short dipole<sup>9</sup>
- (c) measuring the effect on terminal resistance when the antenna is enclosed by a radiation shield.<sup>10</sup>

Since the loop element must be mounted in a cavity on the surface of the aircraft, it is the efficiency of the loop in the cavity that is of greatest interest. The three measurement methods described in the previous paragraph were applied to the 13-turn loop element in a cavity as shown in Fig. 2. The results of the three methods of measurement have been averaged and are shown plotted in Fig. 11 with the calculated values of efficiency for the 13-turn loop in free space. The measured efficiency for the loop in the cavity is seen in Fig. 11 to be substantially higher than that predicted by theory for the loop in free space. Part of this disparity may be attributed to the effects of the cavity, as discussed in Section III and Appendix I. However, some measurement error is indicated also.

#### 4. Dielectric loading

If the permittivity of the medium in which the loop is placed is increased, the effect will be to slow down the traveling wave currents on the loop and thus make the loop appear larger in size. Equations (6), (7), and (10) indicate that the effects will be to decrease the frequency at which the resistance peaks occur and to increase the radiation resistance.

In order to verify these predictions, measurements were taken on a 1/12 scale model of the 13-turn loop antenna described previously. The impedance of the 1/12 scale model was measured in the band from 70 MHz to 90 MHz with the model tuned for 88 MHz resonance. The model was then loaded with paraffin and the impedance was again measured. The results are shown plotted in Fig. 14. As shown in Fig. 14, the input resistance is increased while the frequency of maximum input resistance is decreased. Thus dielectric loading provides a means of effectively reducing loop size for a given level of performance.

#### E. Element Tuning and Matching

If the HF antenna system is to operate over a wide band of frequencies, some provision must be made for tuning the basic loop element over the band. In order to operate in the region of maximum efficiency, the geometry of the loop must be adjusted to the frequency to be transmitted. This can be accomplished by disconnecting turns so that as the frequency is increased the length of the loop remains slightly less than one-half wavelength. Fine tuning can then be accomplished by placing a capacitor either in series with or in parallel with the loop element.

Parallel capacitive tuning is illustrated in Fig. 15. Figure 15 is a Smith chart plot of the terminal impedance of the 1/12 scale model 13-turn loop with and without a 0.75 pf. capacitor connected across its terminals. As seen in Fig. 15, the loop alone resonates at about 190 MHz while the loop and capacitor combination resonates at about 129 MHz. Thus the resonance frequency of the loop can be greatly altered by a parallel tuning capacitor.

The relative bandwidth of an antenna is the interval of frequencies over which the antenna reactance is less than the antenna resistance, divided by the resonance frequency. From Fig. 15, the bandwidth of the tuned and untuned 1/12 scale model 13-turn loop is seen to be about 26.3 per cent for the untuned loop and about 11.5 per cent when the loop is tuned to resonate at 129 MHz. It should be noted that the bandwidth of the actual model would be slightly greater than that measured on the

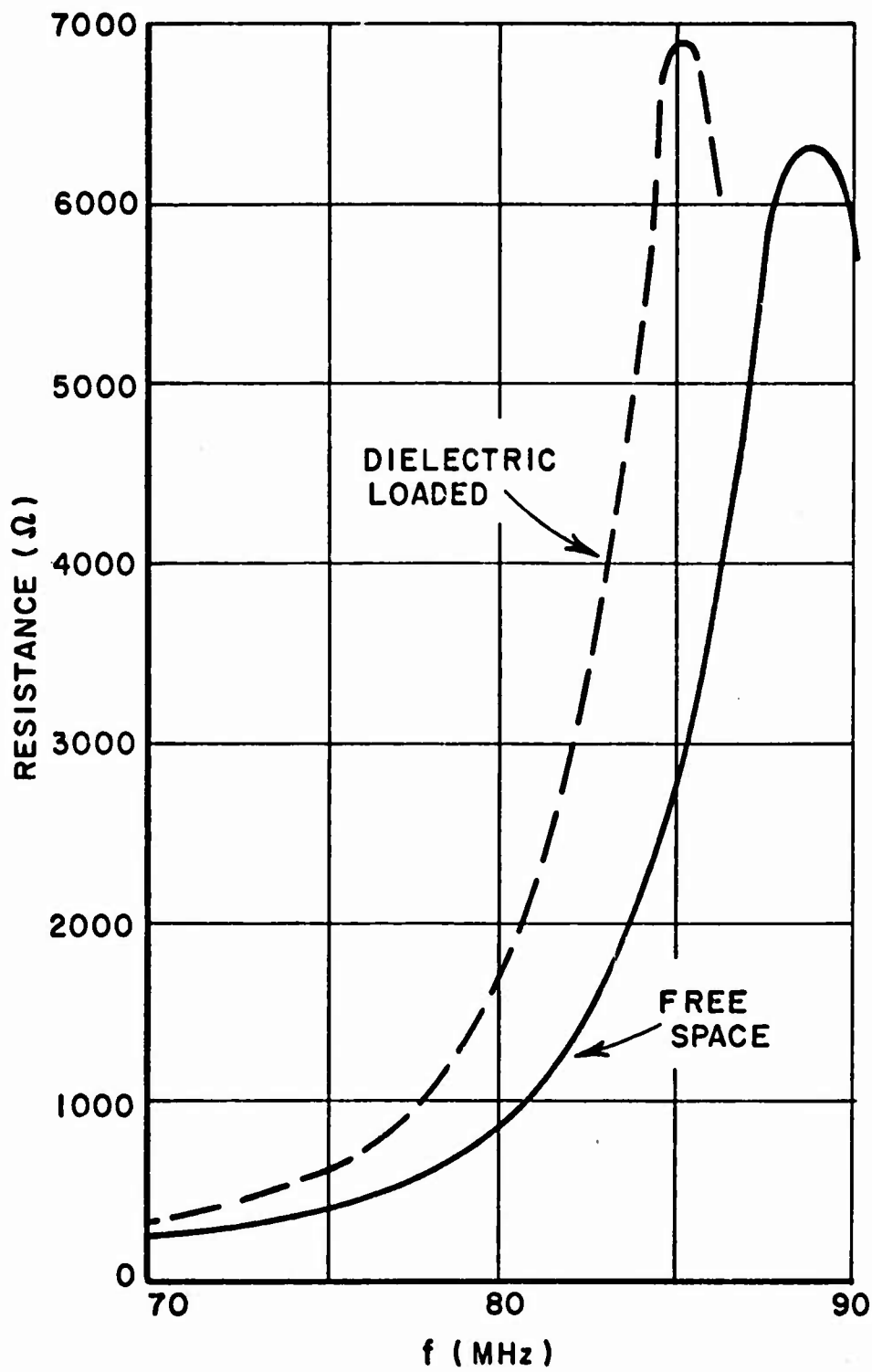


Fig. 14. Input resistance of the 13-turn 1/12 scale model loop antenna with dielectric loading.

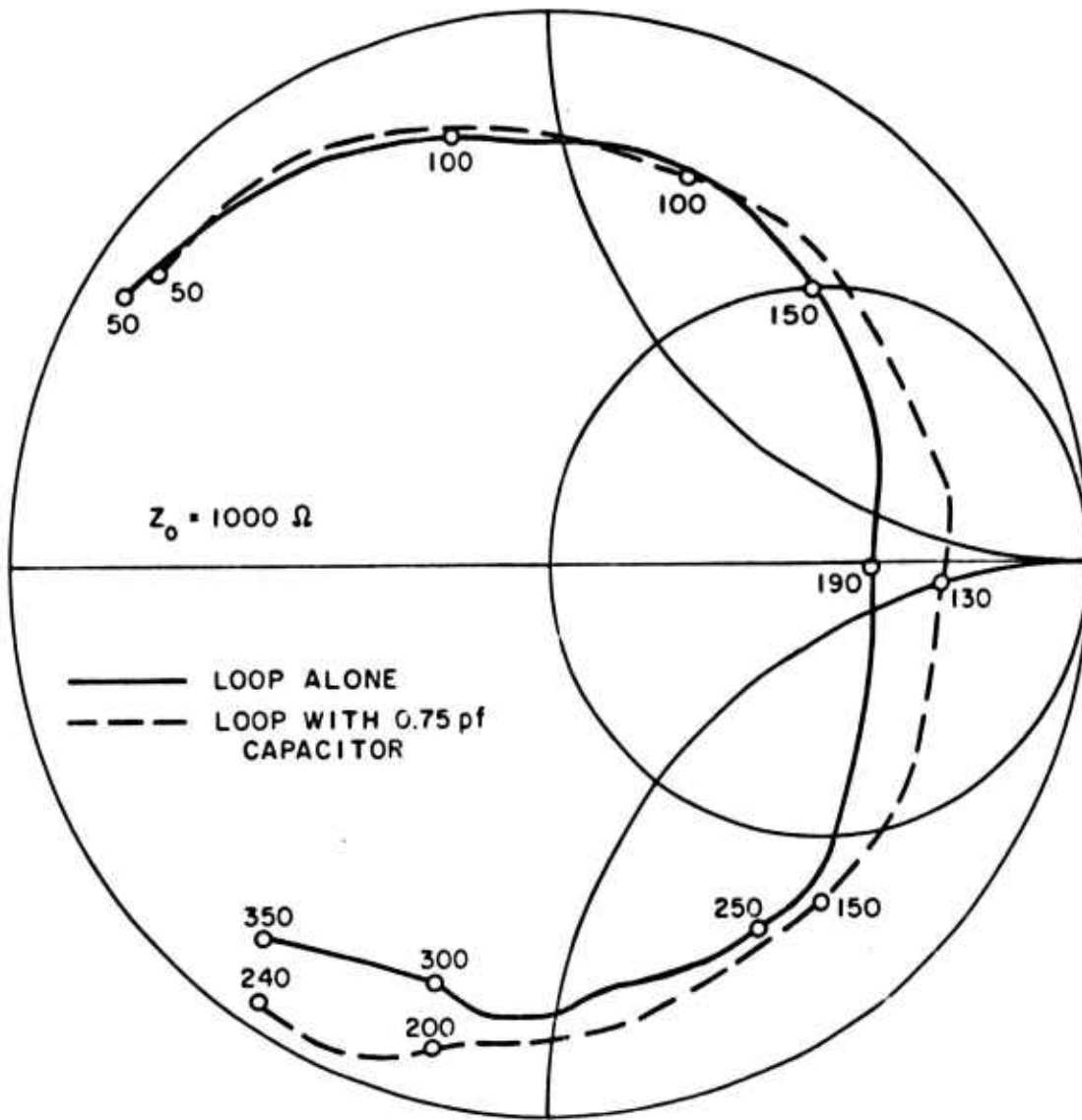


Fig. 15. Input impedance of the 13-turn 1/12 scale model loop antenna with parallel capacitive tuning.

scale model, since the loss resistance would be scaled down, relative to the radiation resistance and reactance.

The relative bandwidth was measured on the actual model with series capacitive tuning and is shown plotted in Fig. 16. In Fig. 16 it is seen that the relative bandwidth is 20 per cent or greater at frequencies between 6 and 12 MHz.

By choosing the number of turns and tuning so that the loop element operates below the first resistance peak, the reactive part of the input impedance of the multiturn loop element may be made positive. In this case, the balanced loop element can be matched to a balanced power amplifier by a purely capacitive matching network. This system eliminates matching coils, a major source of loss in conventional antenna systems.

One particular capacitive matching circuit which has been studied is shown in Fig. 17. Analysis of this circuit shows that the load impedance  $Z$  presented to the amplifier can be made real and equal to a

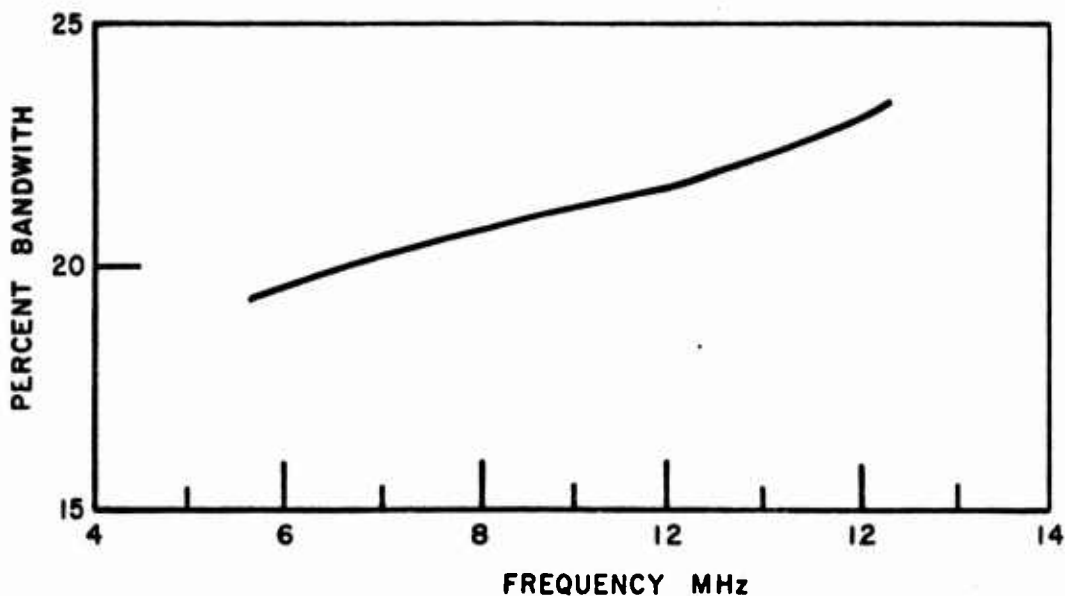


Fig. 16. Tuning bandwidth of the 13-turn loop-in-cavity.



prescribed value  $R_z$  if the capacitors  $X_{c1}$  and  $X_{c2}$  are chosen according to the equations

$$(19) \quad X_{c1} = R_z \sqrt{\frac{R}{R_z - R}}$$

and

$$(20) \quad X_{c2} = \frac{X}{2} - \frac{X_{c1}}{4} + \frac{1}{2} \sqrt{\frac{X_{c1}^2}{4} - R^2}$$

From Eqs. (19) and (20) it is seen that two conditions which must hold are

$$R_z > R,$$

and

$$X_{c1} \geq 2R.$$

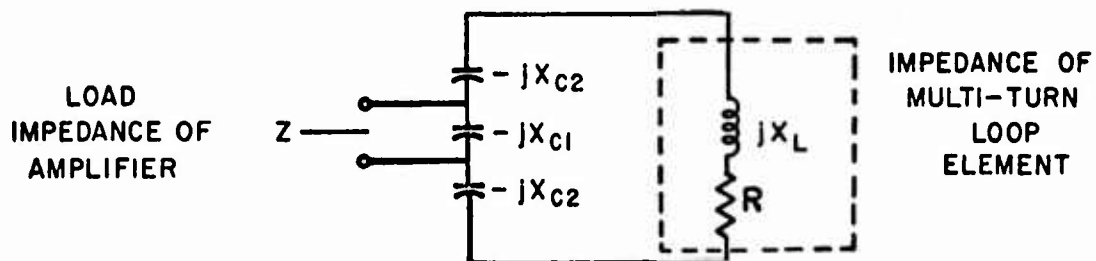


Fig. 17. Capacitive matching network.

The correct value of  $R_z$  for a given push-pull power amplifier can be found from the following equations<sup>11</sup>

$$(21) \quad \text{Total power output} \quad P_o = \frac{I_{\max} E_b}{2} \left( 1 - \frac{E_{\min}}{E_b} \right) ,$$

$$(22) \quad \text{Output stage efficiency} \quad \eta = \frac{\pi}{4} \left( 1 - \frac{E_{\min}}{E_b} \right) , \quad \left( \leq \frac{\pi}{4} \right)$$

$$(23) \quad \text{Proper load resistance} \quad R_L = \frac{4E_b}{I_{\max}} \left( 1 - \frac{E_{\min}}{E_b} \right) ,$$

where

$I_{\max}$  = peak output current of each cycle

$E_{\min}$  = minimum plate or collector potential reached on each cycle,

$E_b$  = supply voltage.

Equations (21), (22), and (23) may be solved simultaneously for  $R_L$  in terms of  $\eta$ ,  $E_b$ , and  $P_o$ . The result is

$$(24) \quad R_z = \frac{32 \eta^2 E_b^2}{\pi^2 P_o}$$

Equation (24) applies to Class B tube type push-pull power amplifiers. Analogous equations can be derived for transistor amplifiers. There are many other types of capacitive networks which might be used to match the loop element to a power amplifier.

### III. STRUCTURE EFFECTS ON PATTERN AND IMPEDANCE

When loop antenna elements are strongly coupled to a conducting structure, currents on the structure significantly affect the pattern, the efficiency, and the impedance of the antenna system. The general character of these effects has been ascertained in a preliminary experimental study, which is presented in Appendix I.

Based on the results of Appendix I, it is evident that the radiation pattern is primarily dependent on the structure currents. And to a first approximation, a method of obtaining nearly isotropic radiation is to excite a crossed-dipole current configuration on the aircraft structure. Also, it is evident that increases in efficiency of up to an order of magnitude can be obtained when the loop elements are placed on the conducting structure.

More accurate methods for the analysis and prediction of structure effects for an arbitrary structure with arbitrary element locations will now be discussed. The methods utilize high-speed digital computers and form the basis for a systematic design procedure for the new HF antenna system. The presentation of the complete design procedure for this system is the subject of Section IV.

#### A. Pattern Effects

##### 1. Computer program analysis

A digital computer program can be used to calculate the far-field patterns of a radiating element mounted on a conducting body of arbitrary shape. The theory behind the development of this computer program and a detailed description of the method by which the computer calculates the far-field of the composite radiating system can be found in Technical Report 2235-2. However, for completeness a brief recapitulation is given here.

The computer program embodies a boundary-value technique wherein the electromagnetic field boundary conditions are enforced at discrete points on the surface of a perfect electric conductor. In order to program this operation, a continuous conducting surface is represented as a grid of perfectly conducting straight wire segments, each short compared to a wavelength. A system of linear equations involving the unknown currents on the wire segments is solved for those currents. The  $i$ -th equation is of the form

$$(25) \quad \sum_{j=1}^N S_{ij} I_j = -E_i$$

where  $N$  is the number of wire-grid segments.  $S_{ij}$  is called a "scattering coefficient" and represents the tangential component of the electric field incident at the center of segment  $i$  that is generated by unit current on segment  $j$ .  $I_j$  is the unknown complex current on segment  $j$ , and  $E_i$  is the tangential electric field at the center of segment  $i$  generated by the radiating element, or antenna.

After the induced current on each segment of the wire grid has been computed, the far-field pattern of the antenna in the presence of the conducting structure is calculated by adding the far-field contribution from each wire-grid segment in free space to that generated by the antenna itself in free space. If the antenna has been represented in the computer as a set of segments like those of the wire-grid structure, differing only in that the current on each of these segments is specified, then the same far-field expressions apply to the segments of the antenna itself as apply to the segments of the wire grid structure. Both dipoles and small square loops have been successfully modeled as a series of short segments on each of which is specified a constant current.

Two examples are presented to illustrate the accuracy of the computer program outlined above. Figure 18 compares calculated and experimental patterns for a  $0.2\lambda$  horizontal dipole mounted over a two-dimensional wire-grid model of an aircraft. The experimental model and the structure modeled in the computer were identical. The patterns are horizontally polarized in the horizontal plane, i.e., the plane containing the wire-grid model. Very good agreement is observed both in the relative magnitudes of the two maxima and in the locations of the maxima and minima.

Another example of the accuracy of the computer program is shown in Fig. 19. Again, calculated and measured patterns are compared, but this time the radiating system is a small rectangular loop mounted on a conducting cylinder  $0.5\lambda$  long and  $0.06\lambda$  in diameter. The patterns are taken with the horizontal component of the field in the horizontal plane, i.e., the plane containing both the loop itself and the axis of the cylinder. Very good agreement between calculated and measured patterns is observed.

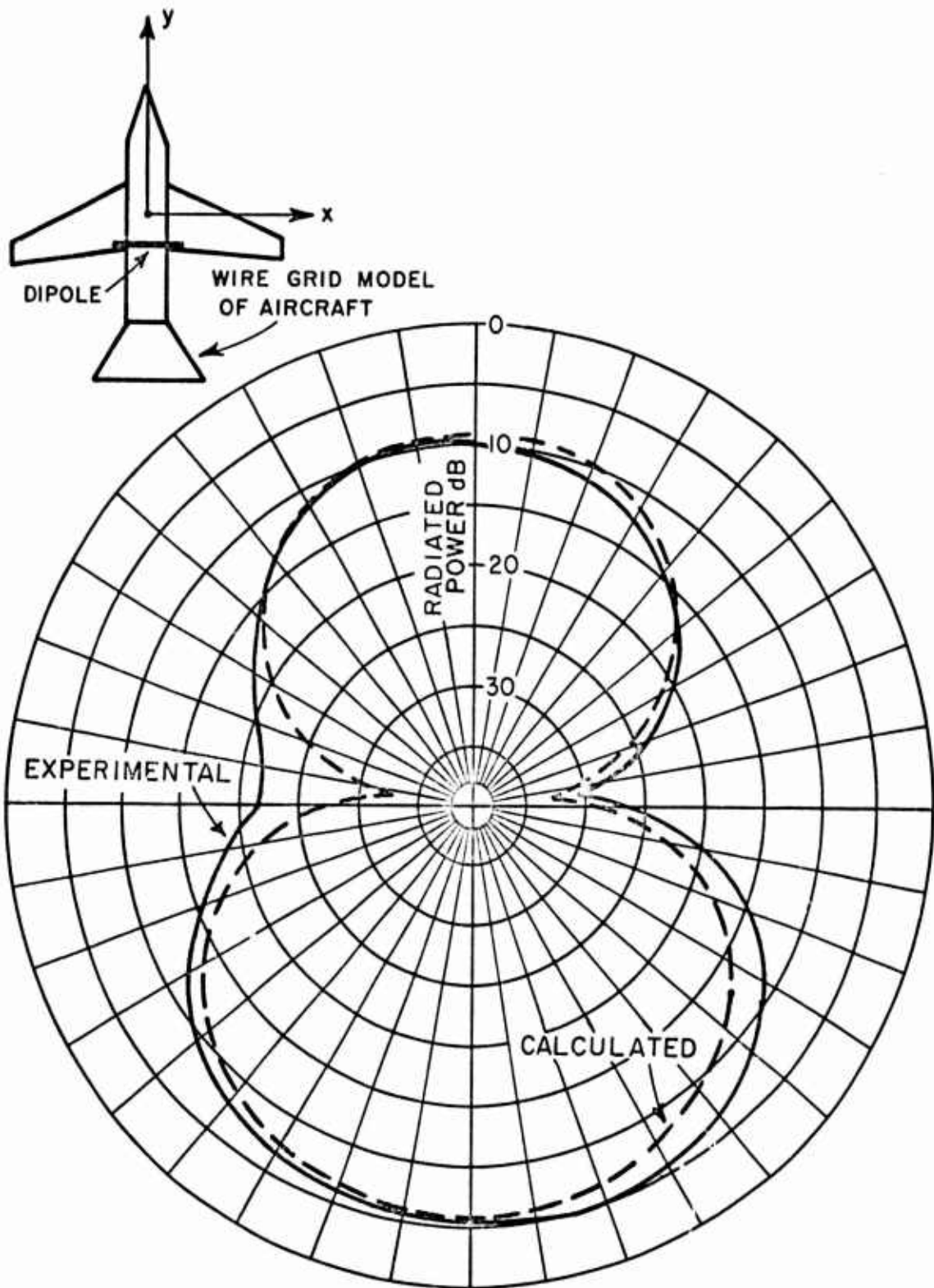


Fig. 18. xy-plane dB plot of the field of a  $0.2\lambda$  dipole mounted on wire-grid aircraft model.

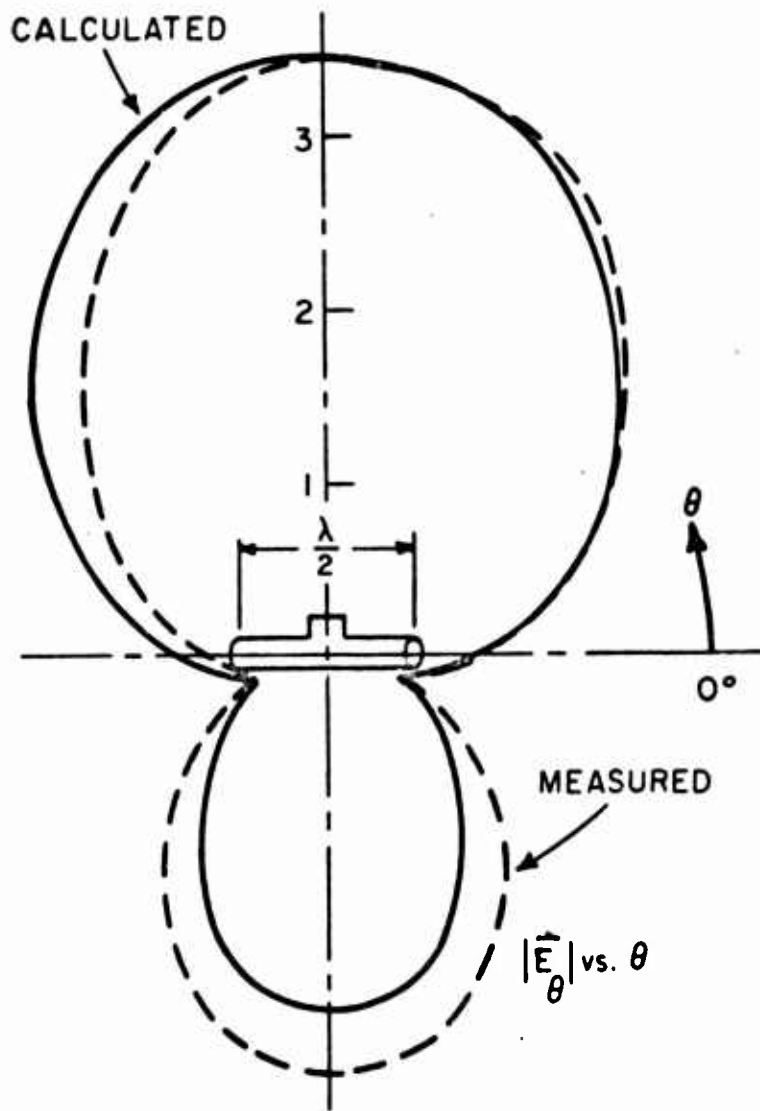


Fig. 19. Calculated vs. experimental loop-excited cylinder pattern.

Due to restrictions on computer storage capabilities, the present development of the point-matching approach to computing antenna patterns has been restricted mainly to antennas mounted on essentially planar aircraft structures. In the 5 - 15 MHz frequency range, though, an aircraft can be grossly represented by a horizontal two-dimensional conducting surface plus a vertical tail section. This has been done for an existing aircraft. Figure 20 shows a wire-grid model of the B-57B aircraft at 4.92 MHz. The straight-line grid is composed of 100 short segments. The antenna elements used to excite the structure were four single-turn square loops, each  $0.01\lambda$  on a side. These were mounted on the structure at the segments noted A, B, C, and D in Fig. 20. All

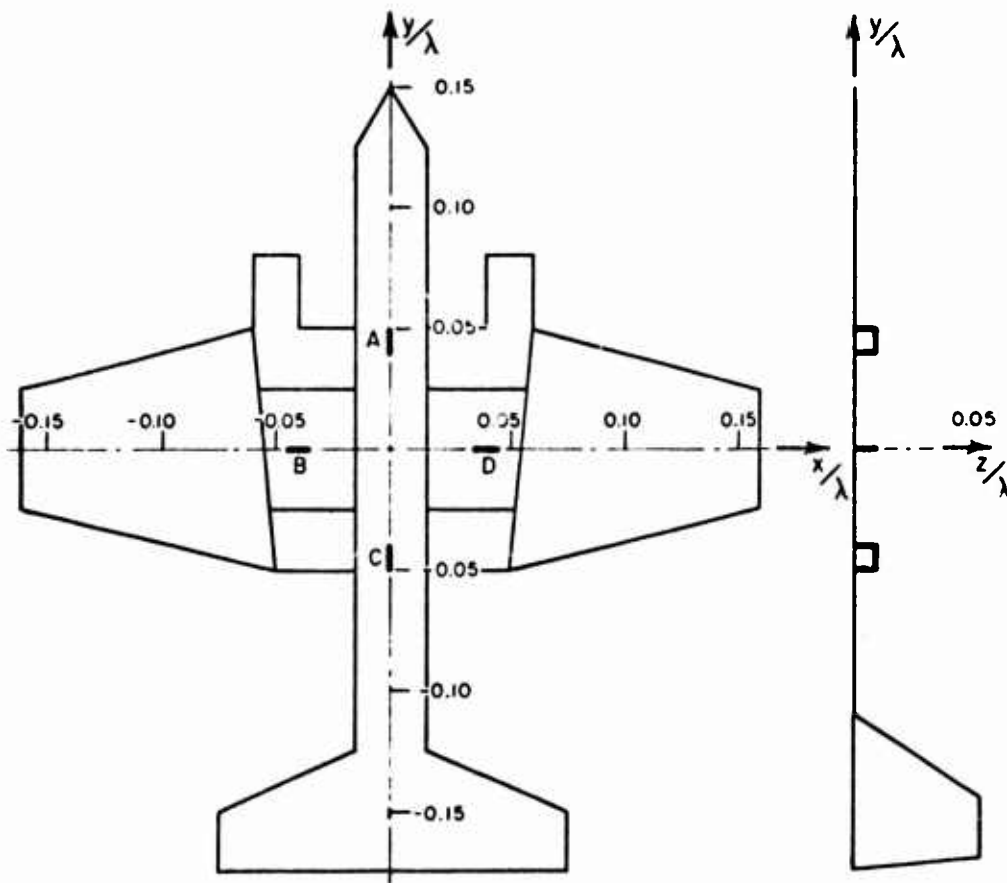


Fig. 20. Wire-grid model of B-57B aircraft at 4.92 MHz showing locations of four small single turn loops.

four loops were excited with currents of one ampere magnitude, and the loops located at segments A and C were excited  $90^\circ$  out of phase with the loops located at segments B and D. Figure 21 shows both the horizontally polarized and vertically polarized far-field power patterns calculated in the plane of the aircraft. Notice that the vertically polarized pattern is not affected greatly by the presence of the structure, mainly because this component is perpendicular to the plane of most of the conducting structure. The horizontal component of the power pattern, if considered from a simplified viewpoint, should be closely related to the almost uniform pattern in that plane of two crossed dipoles excited  $90^\circ$  out of phase with each other. This is clearly not the case, for several reasons. First, the small loops are probably not located where they would most strongly excite dipole-mode currents on the wings and fuselage of the aircraft. Secondly, the wing section does not give the same representation of a dipole as does the fuselage. Finally, even if one assumes adequate dipole representation of the wings and fuselage, these dipole-like structures do not intersect one another in their respective centers. The cumulative effect of all three of these reasons helps explain why the horizontal component of the power pattern in Fig. 21 is not isotropic for the loop array considered above.

## 2. Computer-aided optimization

The basic computer program described previously can be altered to optimize the design of an antenna system mounted on an airframe. Although each system would have its definition of an optimum system, this discussion will consider a fairly simple approach and will illustrate two of several parameters with respect to which a designer may want to optimize his system.

The computer program used here facilitates the use of an iterative type of procedure that a program must eventually utilize in order to pick out the best of several alternatives. This feature of the computer program is seen as follows: if the frequency for which optimization is to be carried out is fixed, then the matrix of scattering coefficients needs to be calculated only once. Furthermore, this square matrix has to be inverted only once. Thus, if the quantity to be varied is the location of the active elements and/or the excitation of any of these elements, or even the number of active elements to be used, then the only quantities that need to be recalculated for each iteration are the values of the tangential electric field that is generated by the antenna elements, themselves, evaluated at the centers of all the wire-grid segments. The inversion of the matrix is then completed, and the new values for the induced currents on the wire-grid segments are obtained much more quickly than if the entire matrix of coefficients had to be generated and then inverted.



WIRE GRID MODEL OF RB-57

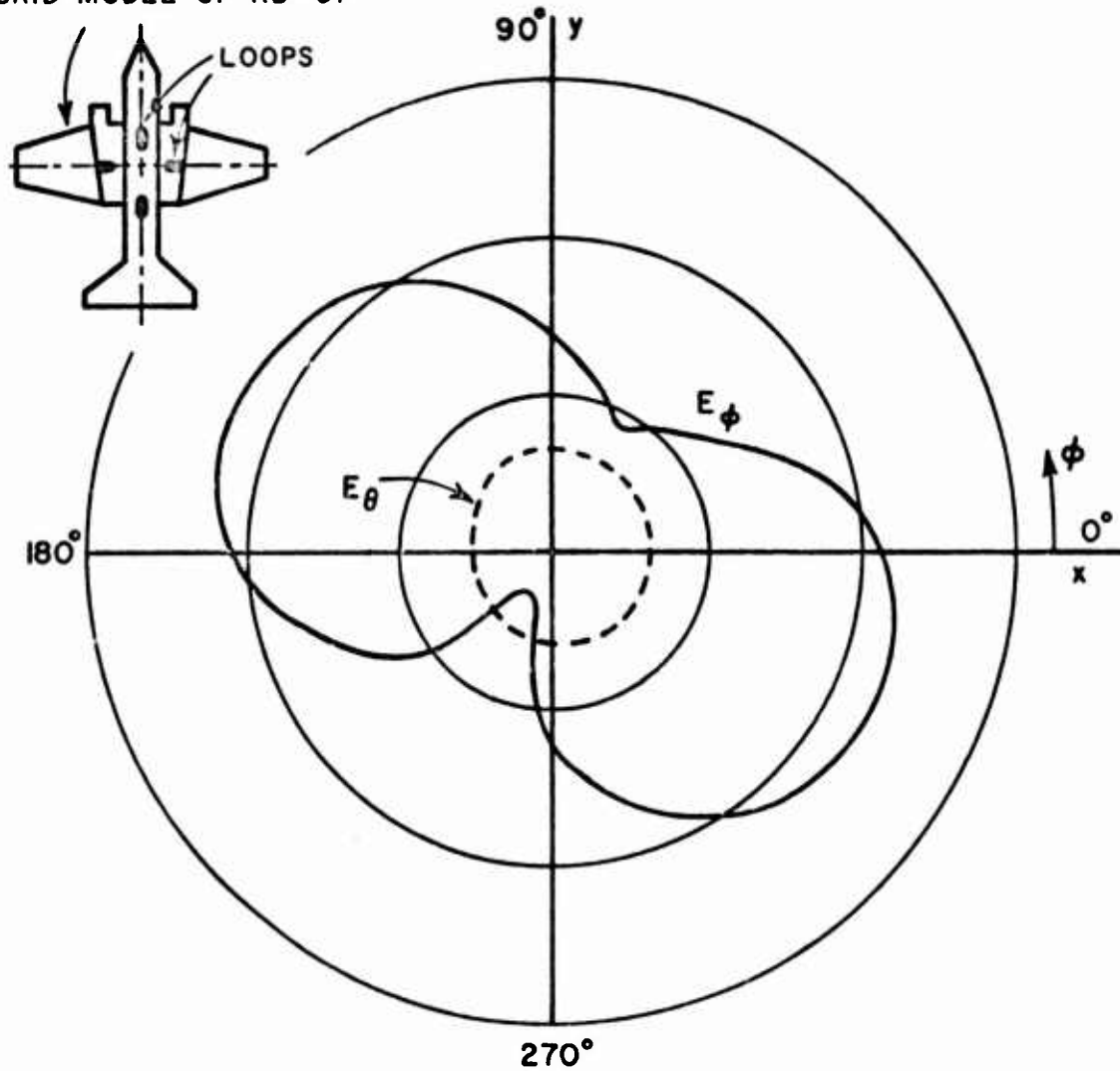


Fig. 21. Calculated horizontal patterns for four small single-turn loops mounted on wire-grid structure of Fig. 20.

As an illustration of this optimization capability, the basic computer program has been adjusted to optimize the locations of two out of four single-turn loops mounted on the wire-grid model of Fig. 20. Because the far-field patterns do not change significantly for incremental changes in element positions, the criterion used to decide the most acceptable locations was the lowest maximum-to-minimum power ratio in some far-field pattern cut (i.e., the smallest difference in dB in the horizontal plane, for example). The computer program was given the excitations and the initial locations of all four loops. Also given was an acceptable figure for the power ratio (3 dB, for instance). The program, by calculating the far-field of the radiating system in some plane, determined whether the power ratio was acceptable. If so, the run was terminated. If not, the program automatically chose new locations for the pair of elements to be moved and recalculated the power ratio for the same pattern cut. If this was a more acceptable power ratio than the original one had been, the program continued to move the elements in the same direction as before. If the power ratio was less acceptable than before, the program shifted the locations of the pair of elements in the opposite direction. In either case, another power ratio was calculated for the new locations. If this ratio was more favorable, the positions were again shifted in the direction they had previously been moved, within bounds on the locations that had been set at the beginning of the program. If the newest power ratio was better than the previous one, then the program continued to shift the elements in the same direction, within set bounds on the locations. If at any point thereafter either a bound was reached or a less acceptable power ratio was calculated, then the best set of locations, as determined by the computer, was printed and the program terminated.

Figure 22 shows patterns which were calculated during an optimization run for locations of a pair of single-turn loops mounted on a wire-grid model of the B-57B aircraft. Notice that the pattern does not change greatly as the positions are changed, since the increment of distance is only  $0.01\lambda$ . For this particular pattern, the magnitudes of the currents on all four loops were equal, and the phasing was  $90^\circ$  between the fuselage pair and the wing pair of elements.

The details of this program are given in Appendix II. This particular program is useful for either the pair of elements on the wings of the aircraft or on the fuselage, depending on the order in which the elements are read into the computer originally.

This program can be changed to optimize the excitations of the elements rather than the positions of the elements. By replacing the iterations of the element positions by iterations of the magnitude and/or

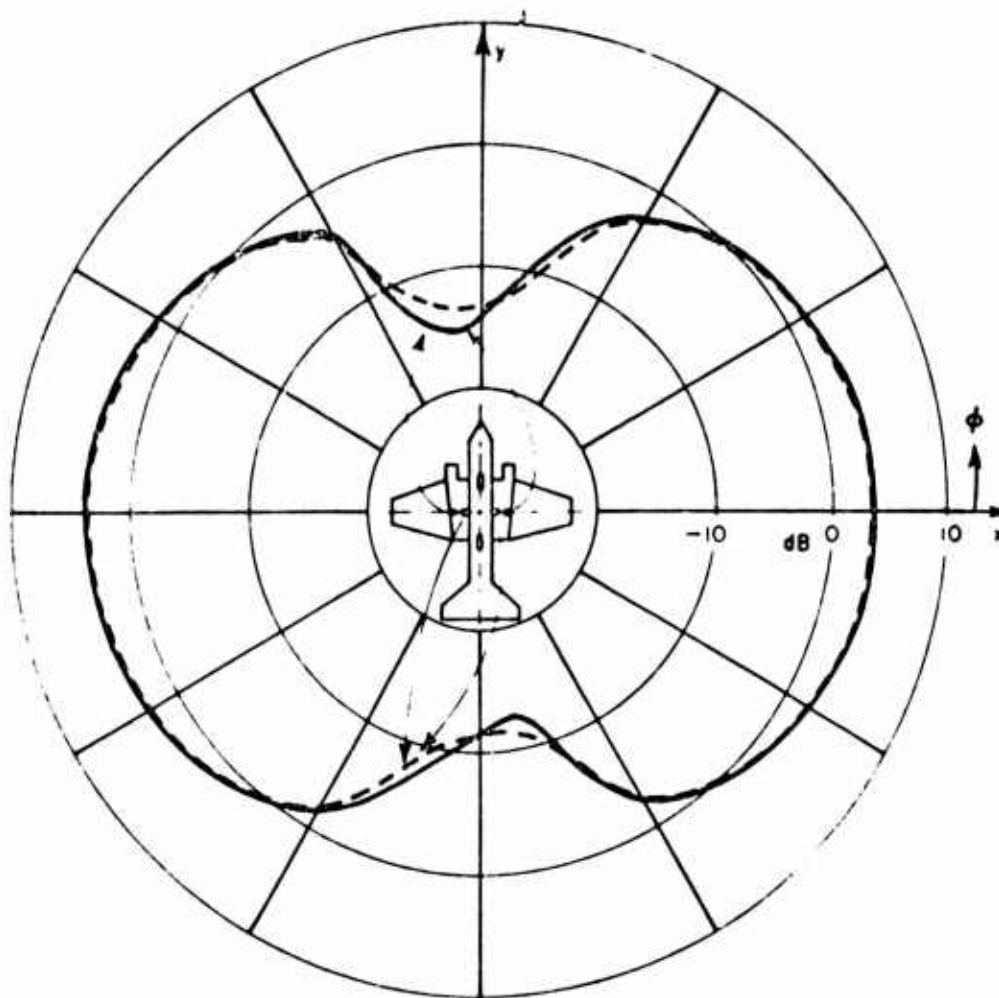


Fig. 22. dB patterns calculated during optimization run for locations of a pair of loops on B-57B.

phase of the elemental current values, the program can be used to find a best set of excitations for one pair of elements, given the excitations of the other pair. Extensions of this approach would allow optimization to be carried out first on one pair of elements, then on the other pair, etc. In addition, a successively finer increment of current could be employed to more accurately determine the optimum values.

Figure 23 shows how the pattern may be changed by varying the relative phase between the elements. The example involves a pair of crossed, but not centered, half-wavelength dipoles which are excited at two different relative phases. The magnitudes of the excitations are the same for both dipoles. Although not isotropic, the pattern for  $90^\circ$

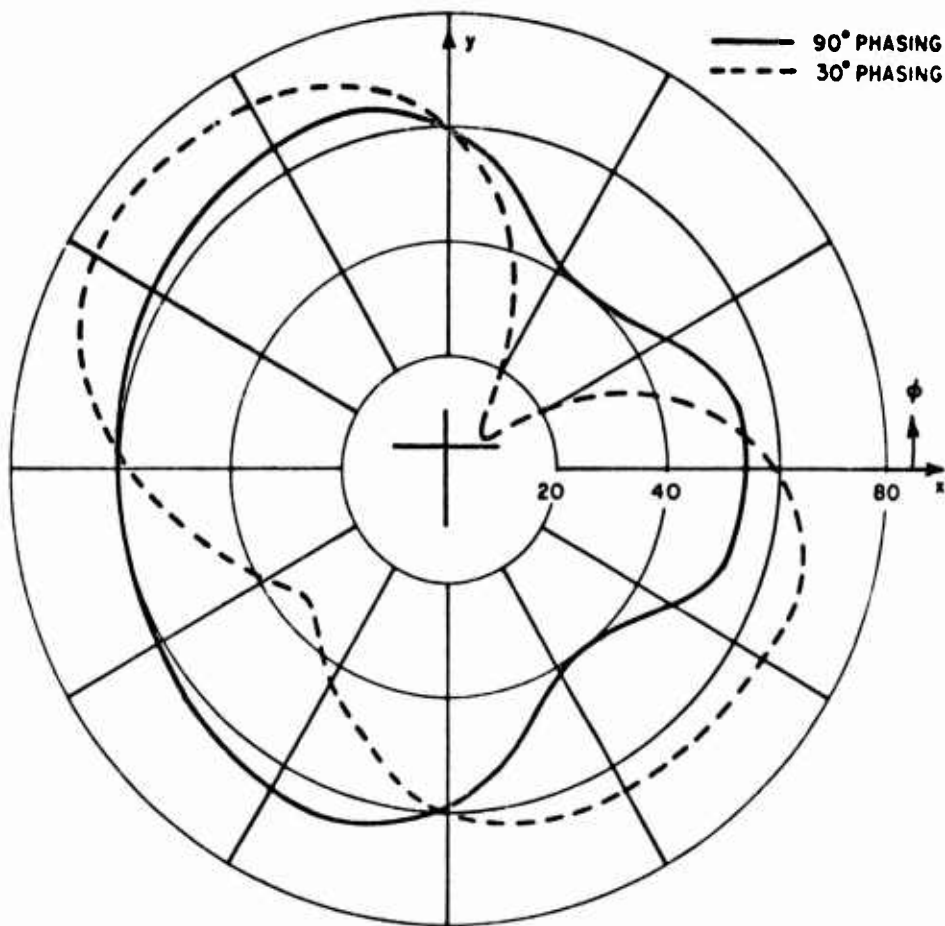


Fig. 23. Patterns from two crossed but non-centered  $\lambda/2$  dipoles for different current phasings.

phasing is more nearly uniform than the pattern for  $30^\circ$  relative phasing. Whether the  $90^\circ$  case would always be more acceptable if the relative magnitudes of the excitations were varied is not known, but by altering the optimization program as noted previously, this information could be obtained. The very process of obtaining this information would be to optimize the phase of a given pair of elements with respect to the other pair, having first altered the relative magnitudes of the pairs of elements. A more elaborate alteration of the program would allow the user to vary both the amplitude and phase of the excitation of each element separately, rather than in a pair-wise fashion.

### 3. Application over a wide bandwidth

The wire-grid model approach to antenna system design through analysis permits more than one quantity to be varied over almost any desired range. However, the frequency for which computations are made is a fixed quantity determining the dimensions, in wavelengths, of the antenna elements and the wire-grid aircraft structure. This means that a configuration that is optimized at one frequency may not be the optimum configuration at a different frequency. Another factor to consider, though, is that the program, by the necessity of limited storage in the computer, \* can be successfully applied only to relatively low-frequency cases (5 - 15 MHz) for typical aircraft sizes. A variation of one to two MHz from the design frequency will probably have little effect on the far-field patterns because the electrical dimensions of the bodies involved do not change greatly in wavelengths. However, in order to design an antenna system to cover a wide range of frequencies, such as the entire HF band, it is necessary to model the system at a number of different frequencies over the band and either strike an acceptable compromise over the entire frequency range from the individual optimizations, or utilize each optimized design within its band of applicability (this implies tuning or step-switching of element excitations).

#### B. Impedance Effects

It is expected that the structure will affect the impedance characteristics of the flush-mounted loop as well as the radiation pattern. Some measurements have been made to determine the extent and character of these impedance effects. Also, techniques for predicting these effects have been investigated.

##### 1. Experimental measurements

The experimental model consisted of a 1/12 scale model of the 13-turn copper loop shown in Fig. 24. The impedance was measured for

---

\* The core storage of IBM 7094 limits analysis to structures about one wavelength in extent. This is not a fundamental limitation on the point-matching method, however. The next generation of computers, already available, extend this to structures about  $3\lambda$  in extent. Use of tape input can extend the range but at the cost of computer time.



Fig. 24. Photo of 1/12 scale model 13-turn loop.

this loop in free space, and also mounted in a 1" deep  $\times$  2" square cavity centered on the surface of a 68" long by 8" diameter copper cylinder. The measurements, made from 50 MHz to around 250 MHz, do not scale exactly since the loss resistance of the scale model loop is increased approximately proportional to  $\sqrt{12}$  because of the smaller skin depth at higher frequencies. Radiation resistance and reactance for the two models should scale exactly, however, assuming that the current distributions are not altered by skin effect.

Figure 25 shows a Smith chart plot of the impedance of the scale model loop, on and off the cylinder. A characteristic impedance of  $700 \Omega$  was chosen arbitrarily to spread the data points over a larger portion of the chart. For the impedance measurements shown on the  $1000 \Omega$  Smith chart of Fig. 26, the loop was tuned to resonate at 81 MHz using a parallel capacitor of  $\approx 3$  pf. The real part of these impedances of Fig. 26 are shown in Fig. 27. The Smith chart of Fig. 28 shows measured impedances for the loop tuned to resonate at 138 MHz using a parallel capacitor of  $\approx 0.75$  pf. A plot of the real part of these impedances is shown in Fig. 29.

All of these measurements exhibit two major structure effects on the loop impedance. First, the resonant frequency is changed somewhat. This effect can be attributed to the structure disturbing the near field distribution of the loop. Since the reactive fields of the full size model are very similar to those of the scale model, this resonant frequency change should occur similarly on the full size model. Also, as can be seen from the peaks of the terminal resistance curves, the radiation resistance is changed somewhat by the structure. Since the radiation resistance is a larger portion of the total resistance for the full size model, this effect should be enhanced (by approximately  $\sqrt{12}$ ) for the full size model.

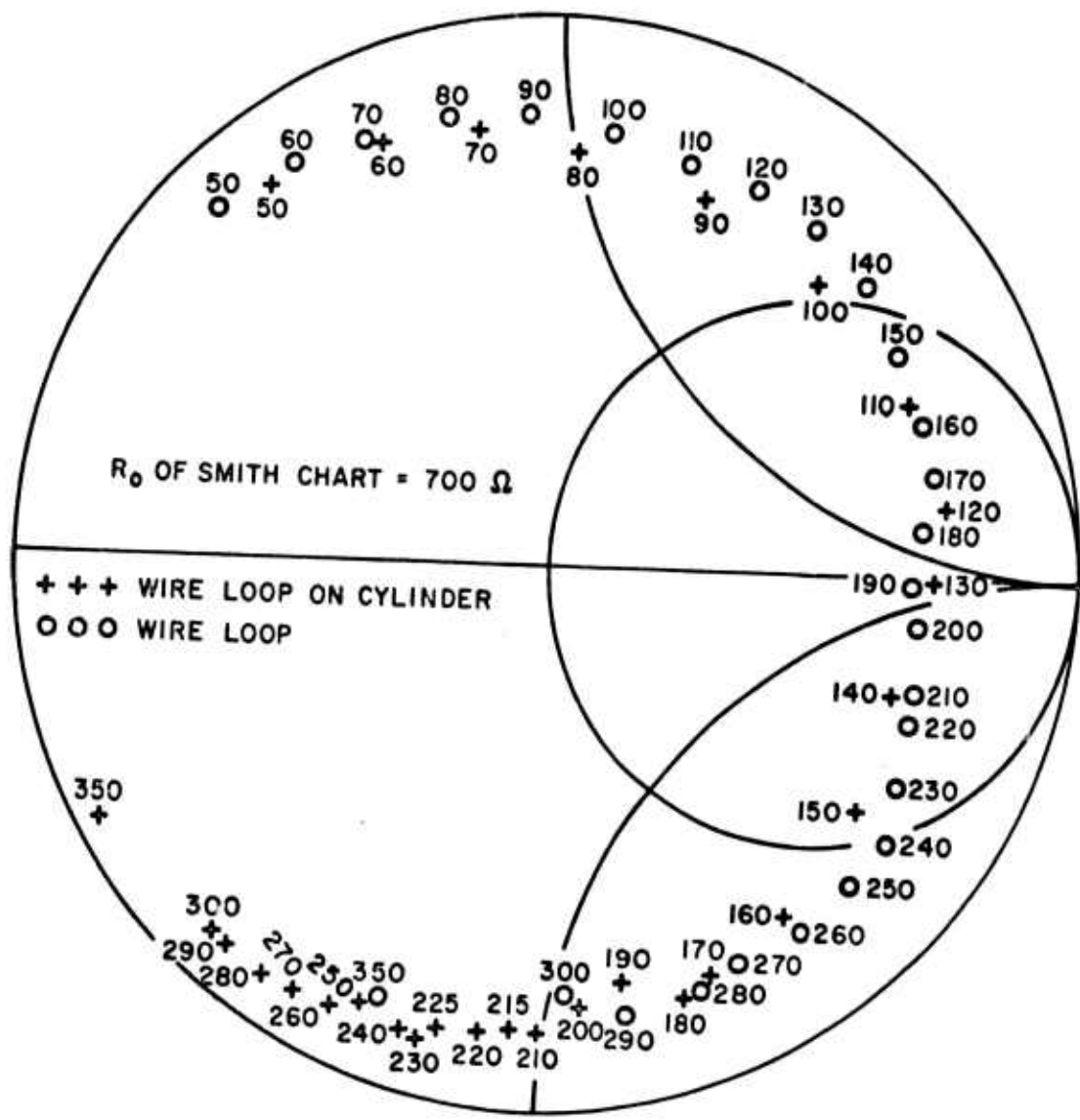


Fig. 25. Impedance of untuned loop on and off structure.

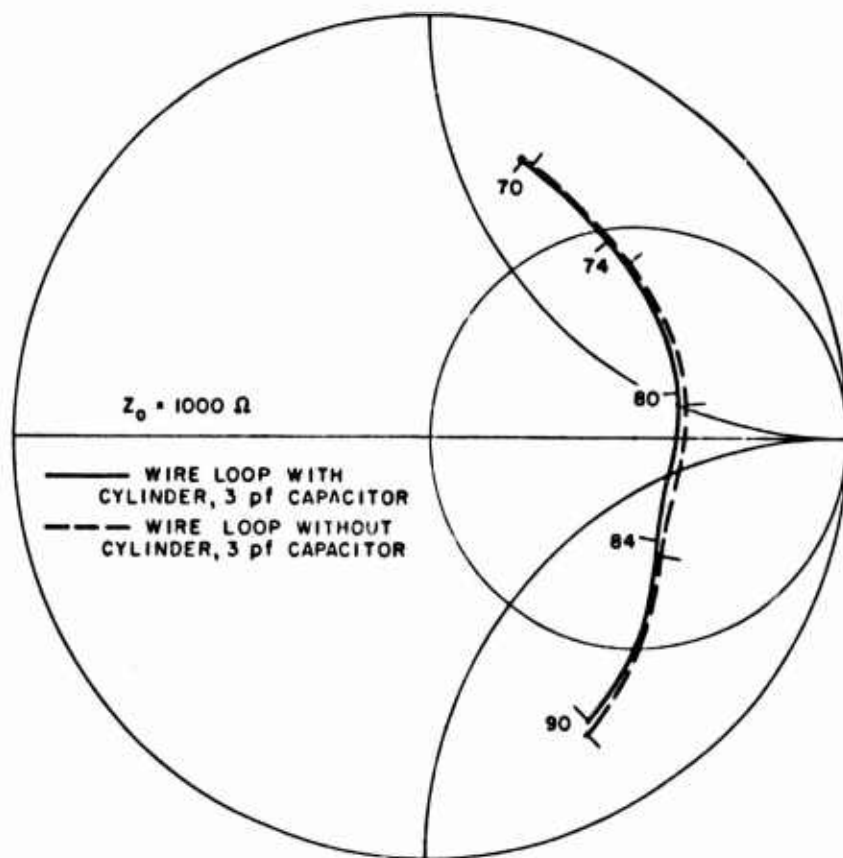


Fig. 26. Impedance of loop, tuned to 81 MHz resonance, on and off structure.



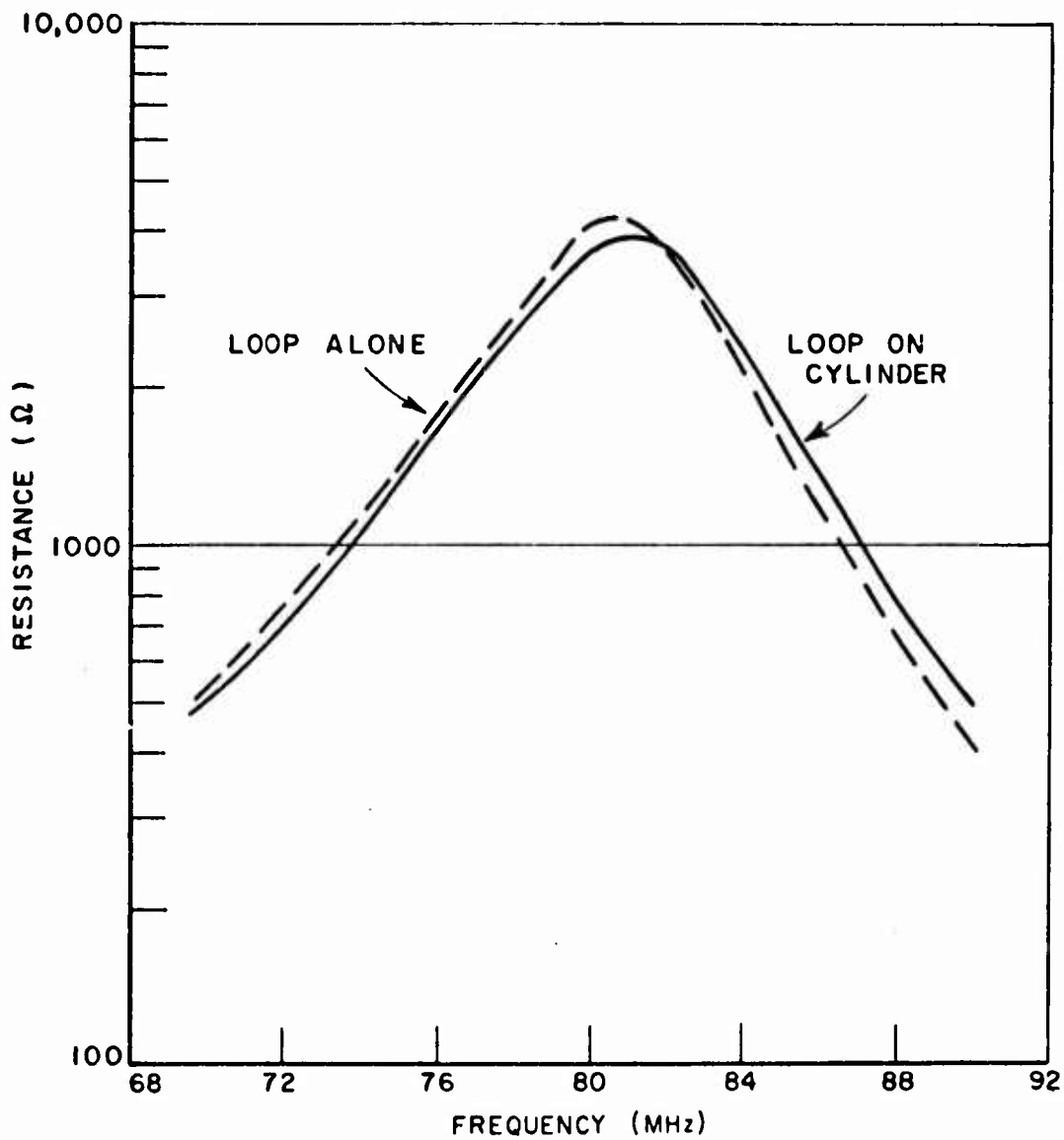


Fig. 27. Real part of the impedances of Fig. 26.

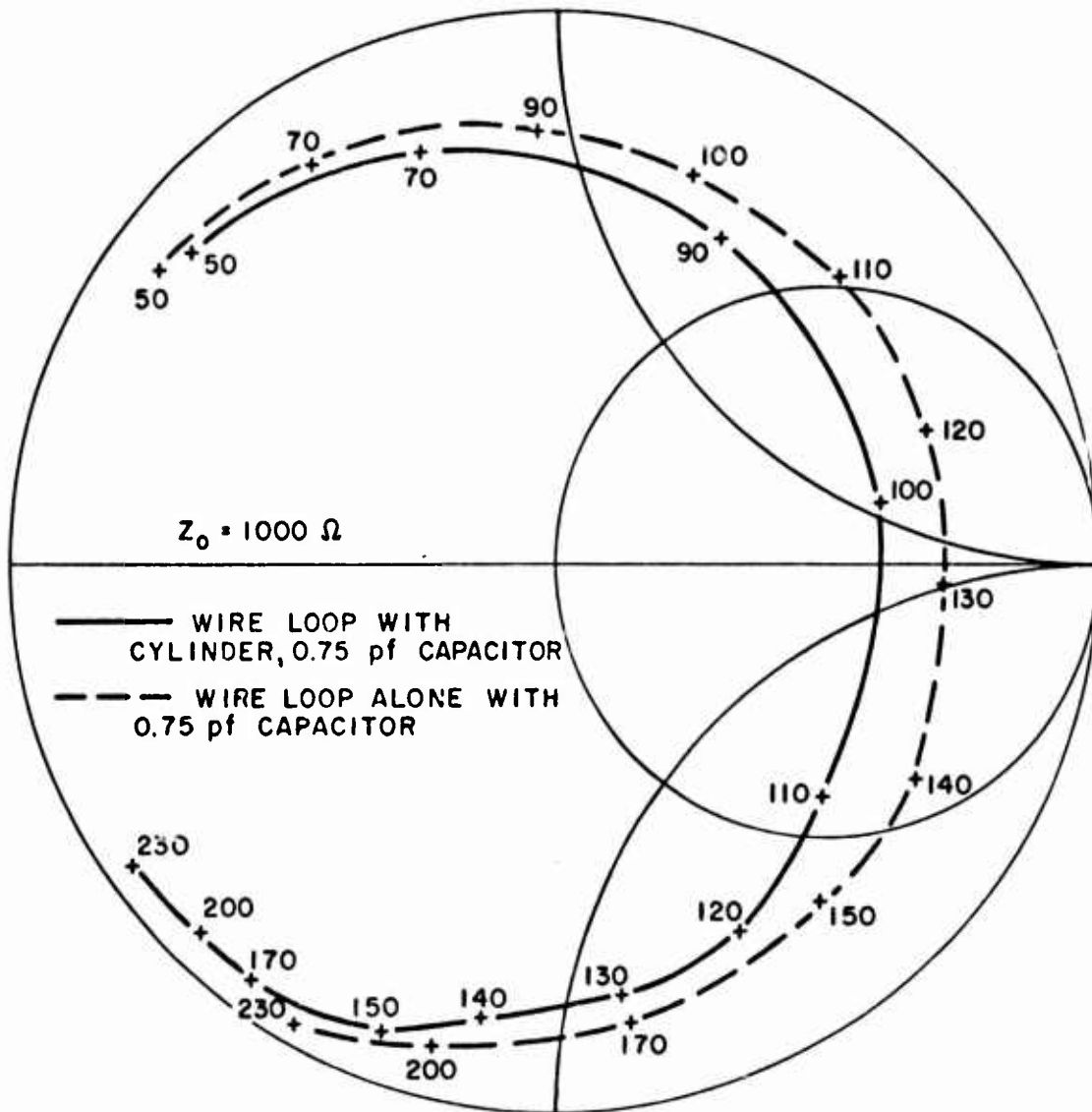


Fig. 28. Impedance of loop, tuned to 123 MHz resonance, on and off structure.

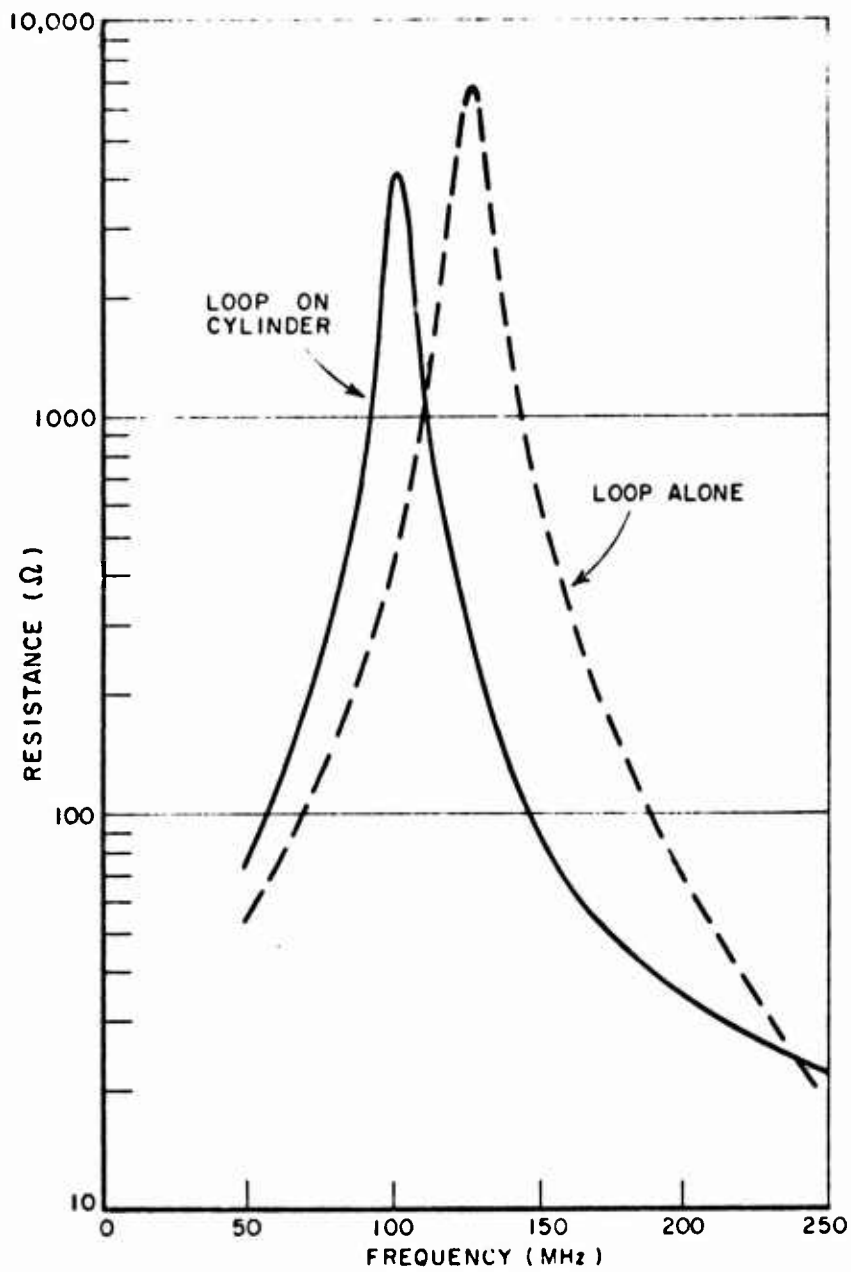


Fig. 29. Real part of the impedances of Fig. 28.

Based on tests with a single-turn cavity-mounted loop and the pattern results of this section already discussed, it can be deduced that these structure effects are dependent on frequency, loop geometry, structure size and shape, and location of the antenna on the structure. Therefore, because of the many parameters involved, the complexity of the dependence of the impedance on these parameters, and the variety of specific aircraft structures that might be considered, a computer technique for the analysis of the structure effects seems to be the most appropriate approach. Such a program has been written.

## 2. Computer analysis for total impedance effects

The basis of the analysis method is a novel form of the reaction theorem, derived by Richmond.<sup>13</sup> This theorem is applied to the generalized geometry shown in Fig. 30, consisting of a source region and a scattering region. For this application, assume that the source region is filled by the loop antenna element, and the scattering region is filled by the perfectly conducting aircraft structure. Then the total terminal impedance, including structure effects, is

$$(26) \quad Z' = Z - \frac{1}{I^2} \int_{S_2} \bar{J}' \cdot \bar{E} \, ds,$$

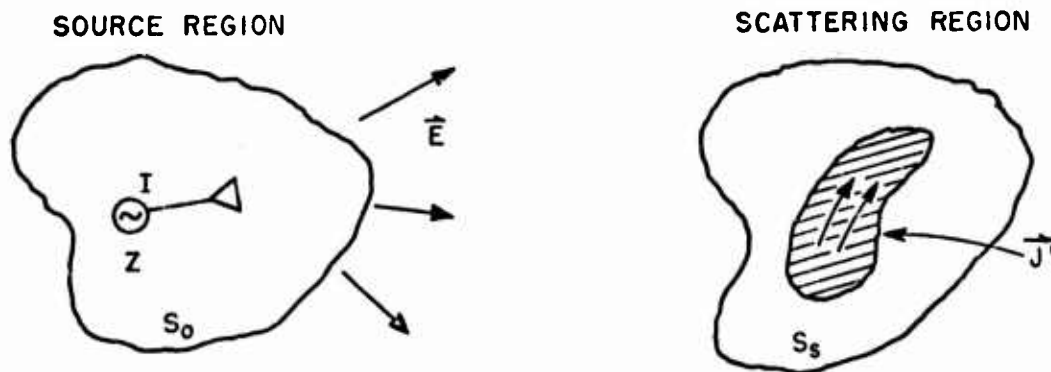


Fig. 30. General geometry for reaction theorem.

where  $Z$  is the known impedance of the source antenna in free space,  $\bar{E}$  is the free-space electric field of the source antenna evaluated on the surface of the structure,  $\bar{J}'$  is the current density induced on the surface of the structure,  $I$  is the terminal current of the source antenna, and the integration is performed over the surface of the "scattering" structure.

A statement listing for a computer program utilizing this technique for calculating structure impedance effects is shown in Appendix II. The point-boundary matching computer program for pattern calculation forms the basis for this impedance program. The values of  $\bar{E}$  of the structure are known from the "scattering coefficients" calculated in the pattern program. Also, the pattern program solves for the structure current  $\bar{J}'$  at discrete points on the structure before it computes the pattern. These features have been preserved in the impedance program.

However, it is well known that accurate computation for complex antenna impedance requires a more detailed and exact representation of the near field and/or surface currents than pattern calculations do. The much more involved techniques used to compute accurately the complex impedance of a simple dipole antenna<sup>14</sup> are a good example of this fact. In an attempt to obtain the increased detail from the limited number of constants dictated by computer capacity, several modifications in the computer program approach have been made. First, the currents on the structure are described by a set of orthonormal modes with unknown mode coefficients rather than by constant current segments as before. Using this approach, for example, the sinusoidal current distribution on a dipole could be described by a single mode coefficient, rather than several discrete constant current segments which only approximate a sinusoid, as shown in Fig. 31. With careful selection of the form of the orthonormal modes, this technique should improve accuracy substantially. Also, the structure is represented as a series of adjacent perfectly conducting rectangular surface elements, which may be flat or curved, each element having a "longitudinal" and "lateral" component of current. A more detailed outline of the program operation, and required inputs and outputs, is presented in Appendix III.

This program has been applied to the test case of coupling between two  $\lambda/2$  dipoles, placed side by side at a spacing of  $\lambda/2$ . An infinitely thin dipole is treated as the antenna element, and the second dipole, with an 8 to 1 aspect ratio, was defined as the "scattering surface" in the computer program. For unit current excitation, the current distribution on the scattering dipole is shown in Fig. 32, corresponding to a mutual impedance between the dipoles of  $Z_{12} = 26.9/-118^\circ$ . This compares to the accepted value of  $Z_{12} = 32.4/-112.75^\circ$  for two infinitely thin dipoles.

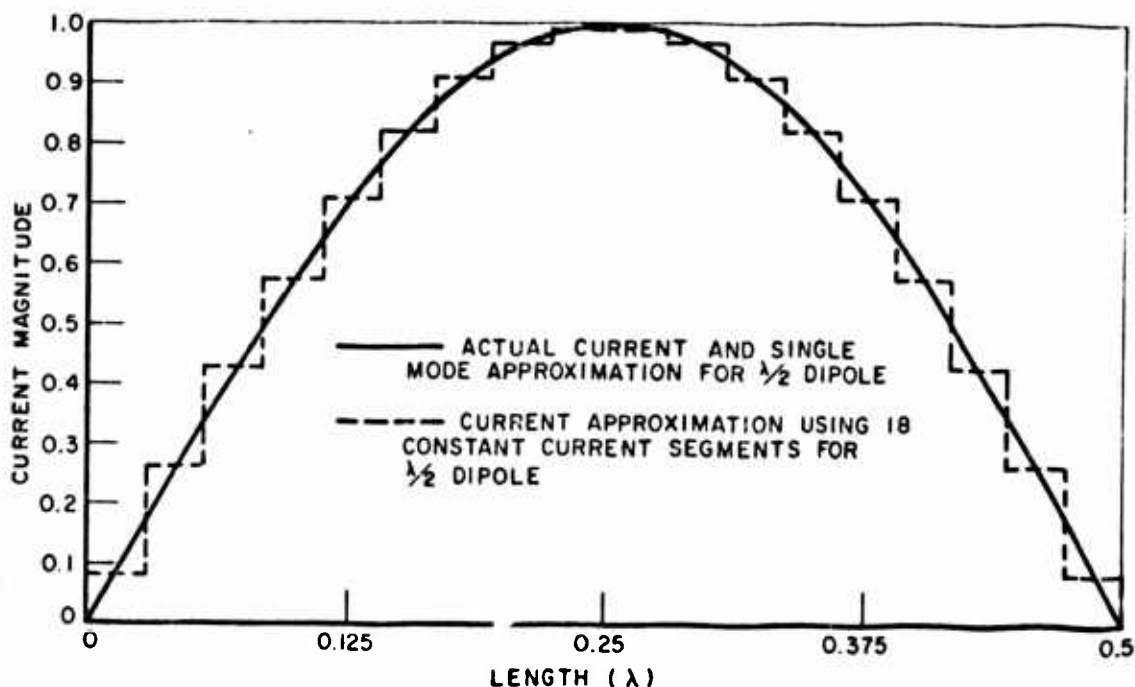


Fig. 31. Mode current vs. discrete current segment approximation of  $\lambda/2$  dipole current.

This test case solution displayed several drawbacks. First, 15 mode currents were needed to obtain the demonstrated solution on this simple cylindrical shape. This implies that, despite the improved detail of the mode current approach, the 100 unknown-coefficients capacity of the computer presently used would still not permit sufficiently accurate current representation on the much more complicated aircraft structure. Also, satisfactory data was obtained only when the boundary conditions were enforced on the axis of the cylinder, rather than its surface. This implies that the computer program would only solve for current modes which are constant around the circumference of the cylinder, an obviously unrealistic case when loop elements are placed on only one side of the cylinder.

Because of time considerations and its present drawbacks, development of this computer technique was suspended after its test case application. However, this method is still regarded as promising, in that it is a systematic, rigorous, analytical method applicable to real, irregularly

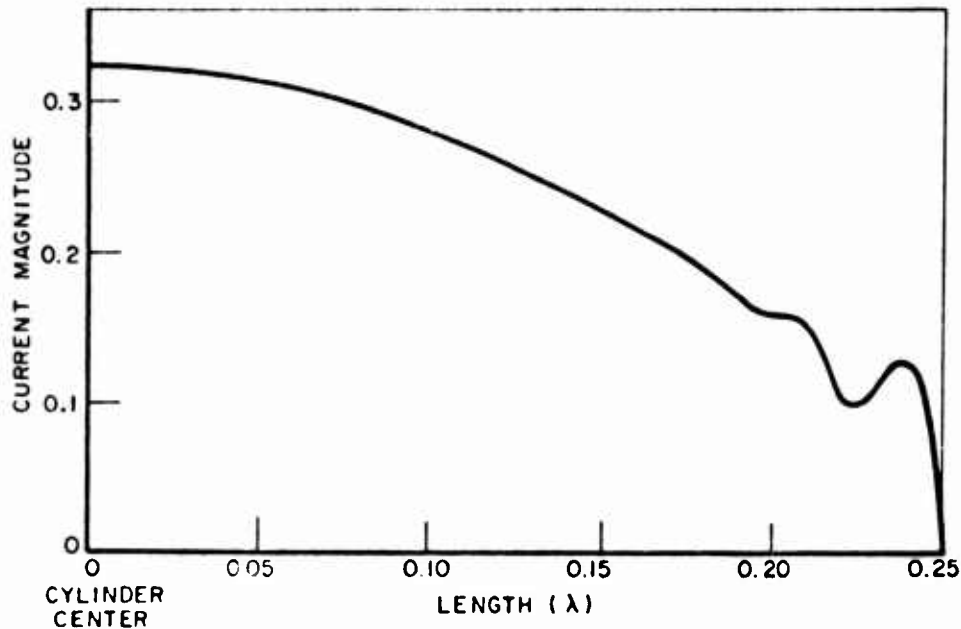


Fig. 32. Computed current distribution on scattering cylinder.

shaped aircraft structures. Among improvements contemplated which should make it more practical are better expressions for the fields produced by a specified current on the rectangular surface elements and possibly a variational technique for determining the mode current coefficients in order to circumvent the capacity limitation of the computer (at the cost of increased computation time).

A simple adaptation of this program technique, when it becomes practical, would allow computation of the mutual impedance between two antennas in the presence of the structure. This calculation would involve computation of the structure currents induced by a unit current in antenna #1, and the "scattering coefficients" between the structure and antenna #2.

### 3. Simplified computer analysis for resistive impedance effects

A less ambitious modification of the pattern calculation computer program has been developed which calculates the effects on radiation

resistance of the aircraft structure. Generally, dipole-mode radiation, such as that for the structure, is very efficient, and thus, to a good approximation, there is no significant loss resistance contribution from the structure. Thus in effect, this computer program modification computes the total resistive effects of the structure on the loop antenna impedance.

The added program subsection is located just after the pattern calculation section of the pattern program, and is shown in Appendix IV. An integration of the Poynting vector associated with the computed radiation pattern is performed over a closed surface in the far-field of the antenna-structure combination.

This calculation has been applied to the two-dipole case, as before. The calculated and accepted values<sup>15</sup> of input resistance of dipole #1 in the presence of shorted dipole #2 vs. spacing are shown in Table I.

TABLE I

Dipole Spacing	Calculated R	Accepted R
0.5 $\lambda$	76.02	75.8
0.4 $\lambda$	89.64	89.3
0.3 $\lambda$	88.48	88.9
0.2 $\lambda$	61.56	64.8

This computer program calculation can also be used to determine the effects of the structure on system efficiency, providing the structure is assumed to be lossless.\* The Poynting vector integration is performed first for the loop element alone with assumed unity current maximum,

---

\* This limitation applies to the present programs. However, there is no fundamental limitation here. A revised program can be written which would include losses in the structure. Time did not permit this to be done on the present investigation.



and then for the antenna structure combination with an equal assumed antenna current. Defining these two integrals as  $P_{LOOP}$  and  $P_{LOOP+STRUCTURE}$ , the total system efficiency can be expressed as

$$(27) \quad EFF_{TOTAL} = \frac{EFF_{LOOP}}{1 + \left( \frac{P_L}{P_{L+S}} - 1 \right) (1 - EFF_{LOOP})}$$

### C. Treatment of the Loop Cavity

For flush mounting of the antenna system, each loop must be embedded in a cavity which would be considered as part of the scattering structure in the computer analysis techniques presented above. In all of the computer programs thus far the antenna elements have been situated on the surface of the structure, as if a cavity was not being used. There is a reason for this omission. To adequately model the cavity requires several wire segments, and due to the present limitation of computer capacity, a sacrifice in the detail of the rest of the structure must be made. To resolve this dilemma, some experimental tests were made to determine where modeling detail is most important. It was found that the far-field radiation characteristics of the loop element on the surface were a very good approximation of those for the cavity-mounted loop. Therefore, for pattern and resistive effects calculation, it is believed that valid results can be achieved when the cavities are ignored in the computer calculation programs.

It is expected that the primary effects of the cavity are on the reactive impedance behavior of the loop antenna elements. The resonant frequency changes demonstrated in Figs. 26 and 28 are to a certain extent dependent on the cavity which was used. Since the reactive impedance changes cannot be treated yet by the computer techniques presented, a thorough study of reactive effects vs. cavity parameters has not been done, and any design effort in this area is still limited to a cut-and-try approach. (Fortunately, tuning network impedance values are the only antenna system parameters depending on this design area, as shown in the next section.)

Toward the end of this investigation, some work was done on determining a more accurate representation for the loop-in-cavity for use with the computer analysis techniques, which is still economical in terms of wire segments. There was not sufficient time to complete this effort, but results which were obtained are presented in Appendix V.

In the approach studied, the multiturn loop is represented by a series of very short constant current magnetic dipoles, one located at the center of each turn and with magnetic current proportional to the electric current in that turn. The total length of this collinear array of magnetic dipoles would be equal to the coiled length of the multiturn loop. In order to represent the loop-in-cavity configuration, this collinear array of magnetic dipoles is located flush with the surface of the structure and surrounded by a wire segment rectangle whose dimensions correspond to the surface opening of the cavity.

The computer program alterations for calculating the scattering coefficients of the magnetic current source are explained in Appendix V. Unfortunately, these have not yet been incorporated into the computer calculation programs to obtain pattern and impedance data. However, this approach can serve as a guide if it is deemed advisable during a design effort to obtain a more accurate element-in-cavity configuration.

#### IV. DESIGN PROCEDURE

Based on the techniques developed during this investigation, a procedure can be outlined for designing a multiturn loop HF antenna system for an arbitrary aircraft. The chief feature of this procedure is that it allows optimization of two of the most important transmitting antenna parameters, pattern shape and efficiency, without any cut-and-try measurements. Pattern shape and system efficiency are the performance goals of highest priority in this design procedure. Impedance and tuning ease, although important, are secondary considerations.

In its initial stages, the design is split into two parts. First, using the computer program, the locations on the structure and excitation currents for a satisfactory approximation of an isotropic pattern are found. Second, the geometry of the loop antenna for maximum practical efficiency in the operating region is determined. For both of these calculations, there are some basic limitations caused by the structure, power amplifier, etc., which are specified as initial assumptions. Next the loop design and structure design are combined, and total system parameters, including pattern and efficiency are calculated. Further optimization, considering these parameters, is done at this point if necessary. Finally, the tuning and excitation network for this system is designed.

### A. Element Location Design for Best Pattern

The computer program approach to locating the antenna elements, using a wire-grid model, has been discussed in Section III-A. For a computer which has a capacity equivalent to an IBM Model 7094, this approach is applicable over the frequency range where the extreme dimensions of the aircraft are less than a wavelength, or where the surface area of the conducting body does not exceed about a square wavelength. At a frequency at which an optimized design is desired, the structure dimensions in wavelengths are determined, and a wire-grid model of correct dimensions is specified. This wire-grid model should consist of 100 or fewer straight wire segments,\* each  $0.01\lambda$  to  $0.05\lambda$  long, which give an accurate outline of the structure and as much filling inside of the outline as possible. The wires must form closed contours; no wire tip can be left unconnected to another wire. Increased wire density is desirable near the probable locations of the antenna elements, where current densities will be maximum.

An approximate representation of the loop antenna element must then be chosen. For the purpose of pattern and resistive effects calculations, it has been shown that a single-turn loop of area  $A$  and current  $NI$ , located on the surface (no cavity) is appropriate. Here  $A$  is the anticipated area of a single turn of the multi-turn loop element,  $N$  is the anticipated number of turns such that  $N$  times the turn circumference is approximately  $\lambda/2$ , and  $I$  is the current in the center turn of the multi-turn loop element (the maximum current value).

The next step is to determine the probable number of antennas and their approximate locations. Based on structural considerations, several permissible areas for antenna locations on the airframe can be assumed. Knowing these locations, knowing that crossed-dipole excitation is desired to a first approximation and knowing the power output required of each antenna, the initial antenna locations and the number of antennas used will be easily determined. It is felt that the most probable number of

---

\* This temporary limitation will be changed as larger computers are used.

elements would be four, two located on the fuselage and two on the wings. However, two elements, one to excite currents on the wing and one for the fuselage, may be a distinct possibility. The starting locations and the limits of variation from these locations are given as input to the computer program.

Then optimization techniques can be applied to determine the locations and excitations of all the elements in order to achieve a nearly isotropic radiation pattern. Some of these techniques involving the computer program have been explained in Section III-A; these are by no means the only ones which may be applied.

It is most probable that a single wire-grid model of the aircraft will not be valid over the entire frequency band of interest; therefore it will be necessary to model the aircraft at several frequencies within the pertinent band. It is suggested that the locations of all the elements be optimized at each of the selected frequencies for a single set of excitations - for example, currents of equal magnitude on all elements. Next, choose the locations that represent the best compromise among all those obtained at the selected frequencies. Fix these as the design locations and optimize the excitations of the elements for most nearly isotropic radiation pattern at each design frequency. This can be done by altering the computer program for optimizing locations, as mentioned in Section III-A.

The results of the optimization of excitations indicate the magnitudes and relative phases of the currents on the antenna elements for best pattern at selected frequencies. It is the choice of the designer whether to have a continuously-varying excitation network or to maintain control in discrete steps. In either case, if the restrictions on elemental locations are too severe to achieve satisfactory patterns at higher frequencies, extra elements may be placed on the structure and excited at the appropriate frequencies.

#### B. Loop Design for Optimum Efficiency

The first step in designing the multiturn loop element is to determine the loop size. Since the area of each turn is the primary factor which limits element efficiency, the loop dimensions should be as large as possible. The maximum size is subject to structure limitations; specifically, the restriction on cavity size imposed by the structure. Once the dimensions of each turn have been determined, the number of turns,  $N$ , is chosen so that the total wire length is approximately  $\lambda/2$  at the lowest frequency to be transmitted.

After the loop size and number of turns have been tentatively determined, the formulas of Section II can be used to calculate the resistance properties and efficiency curves of the loop. The tuning technique is an important consideration here. The efficiency curve of the element using all its turns will be similar in shape to the curve of Fig. 33, with the first efficiency "hump" at approximately the lowest operating frequency, other "humps" occurring at 3, 5, 7, 9.....times this frequency, and with low efficiency points at frequencies in between. However, by switching out turns, these "humps" may be moved so that most efficient radiation can occur at chosen frequencies. For example, assuming a 10 to 1 operating band, it is probable that the first two regions of high efficiency corresponding to  $L \simeq \lambda/2$  and  $3\lambda/2$ , would be used, and each would be tuned over a 3 to 1 band by switching out turns on the loop antenna. Therefore, efficiency calculations for various numbers of turns switched out of the loop antenna must be made in order to obtain information on the efficiency throughout the operating frequency band.

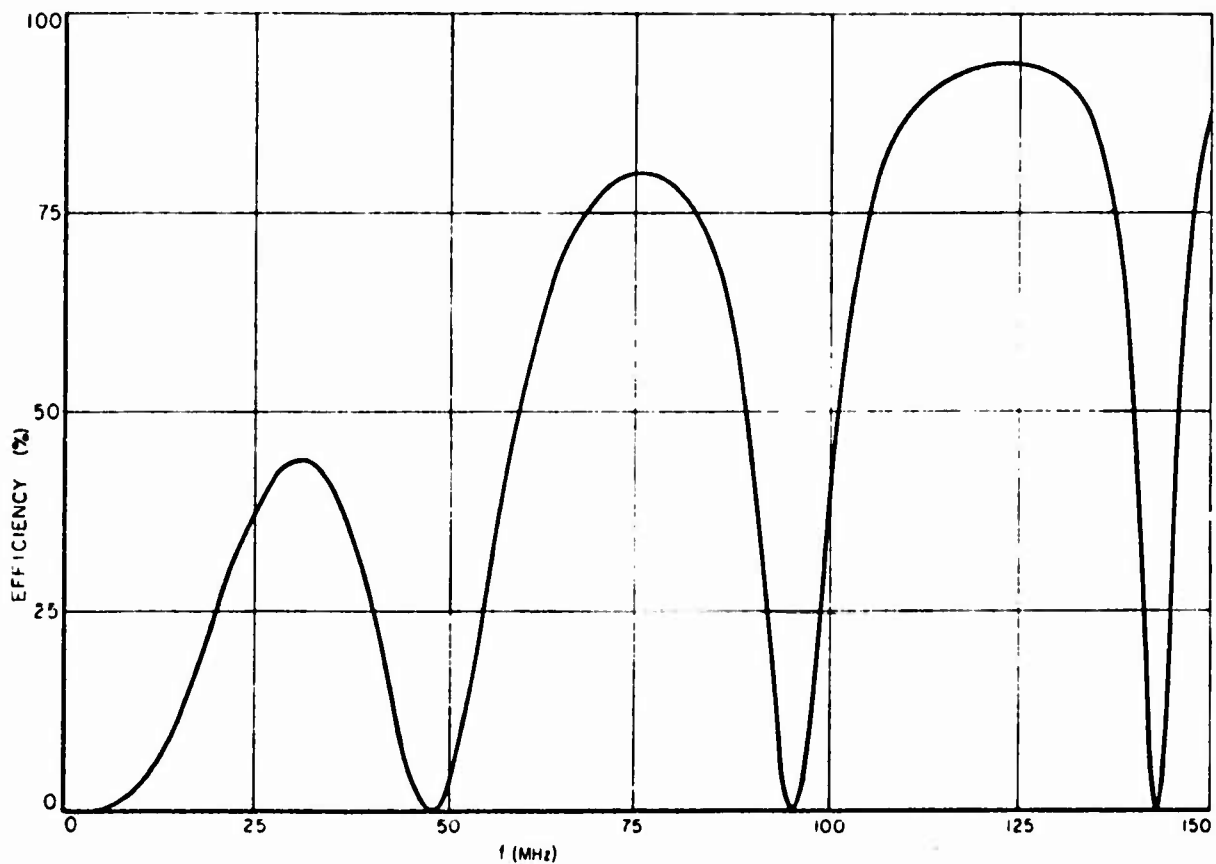


Fig. 33. Calculated efficiency of example element.

After the efficiency performance for the particular loop geometry has been analyzed, the loop conductor size and configuration, i.e., tube or wire bundle, may be chosen for an optimum combination of loop efficiency, weight, size, and complexity (see Fig. 34).

### C. System Design for Pattern and Efficiency

The next design step is to combine the optimized loop and the optimum structure location and excitation data, and analytically evaluate the pattern and efficiency of the total configuration. Providing a good test model was used for the structure design, the pattern of the system should be virtually the same as before. With a known loop configuration, the computer program for resistive effects, Section IV-B, can now be applied to obtain pertinent data on total system efficiency and the terminal resistance of each element. If the resulting system efficiency is satisfactory, the analytic stage of the design is virtually complete. If not, trade-offs involving pattern shape, loop size, weight, and complexity, and number of elements can be tried analytically to achieve a more optimum combination.

### D. Tuning and Matching Network Design

The final step is to design the tuning networks for the loop elements. Since the computer techniques for predicting the total terminal impedance, including reactance, are not available at present, this step now involves a measurement of the terminal impedances of the loop elements in proper position on the aircraft structure. With this measured data and known power amplifier output impedance, the switching network and capacitance values discussed in the element tuning and matching section (II) can be determined.

## V. CONCLUSIONS AND RECOMMENDATIONS

A new HF aircraft antenna system, which has several advantages over the conventional techniques, has been presented in this report. Its performance has been analyzed and a procedure for designing the system for use on an arbitrary aircraft has been presented. As a result of this study, several conclusions can be stated concerning the characteristics, feasibility, and relative merits of this antenna system.

As was stated in the introductory section, the two principal innovations of this antenna system are inductive coupling to the structure

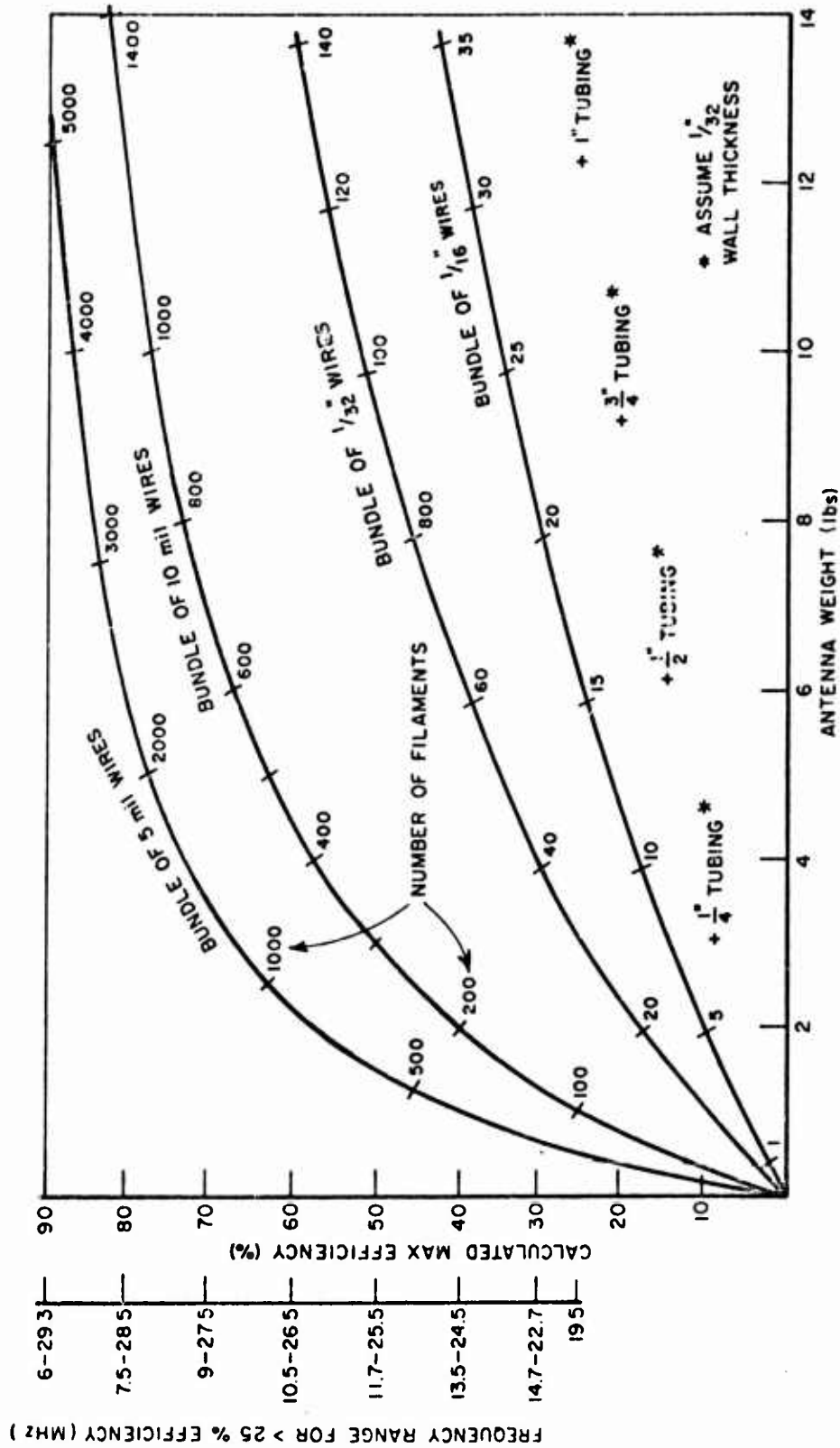


Fig. 34. Maximum predicted efficiency vs. weight for 13-turn prototype loop element using suggested construction techniques.

using several antenna elements, and the use of multiturn loop antenna elements of small area but appreciable total wire length in wavelengths. These two innovations are analyzed in Sections II and III and the Appendices. It is concluded that efficiencies on the order of 10 per cent can be obtained from practical multiturn loops with maximum dimensions of a few hundredths of a wavelength when operated near their resonant frequencies. And furthermore, the impedance characteristics of those elements, being inductive, are appropriate for efficient, capacitive matching networks. It is concluded also that the use of several individually-fed antenna elements to inductively excite radiating currents on the aircraft can produce an improved radiation pattern, and also significantly increase the effective aperture of the system, thus improving its terminal impedance properties and increasing its efficiency by as much as an order of magnitude.

The design of this system for a particular aircraft is discussed in Section IV. It is concluded that this system is applicable to virtually all aircraft, and because of the use of high-speed digital computers, the design can be completed more quickly, give a more optimum system, and require less cut-and-try effort than a conventional HF antenna system design.

Even though this system has never been actually designed and installed on a particular aircraft, some conclusions can be drawn regarding its feasibility. From the pattern computation section, it is concluded that, if a four element system were designed for a B-57 type structure, the resulting radiation pattern could be made virtually omnidirectional at frequencies below about 10 MHz, with slight degradation between 10 and 30 MHz which could possibly be improved with the addition of more antenna elements. From the combined analyses, it is concluded that the efficiency of such a system could be about 50 per cent above 15 MHz, decreasing, but still more than 10 per cent, at frequencies from 15 MHz down to 3 MHz. Also, the elements could be tuned to match conventional power amplifiers, and have sufficient bandwidth for communications-type signals. On the basis of these statements, it is concluded that this system is feasible.

It is evident that this system has many advantages over conventional HF aircraft antenna systems. Because it uses several elements, dispersed over the aircraft structure, this system is more secure than conventional antennas. Also, its patterns are superior in general to conventional antennas, and they can be more easily and precisely designed for a particular aircraft. The many individually fed elements have a multi-function capability which might become extremely beneficial. Only



electronic control circuitry is necessary to enable use of this antenna system for direction finding, homing, and other directional communications applications.

Since this project was primarily concerned with the feasibility and major aspects of this antenna system, the treatment of some specific system parameters is incomplete. As these areas are important in the actual construction of such a system, they deserve additional careful consideration.

The power handling capability of this system has not been carefully analyzed, although it is estimated that each element should handle about the same amount of power as a conventional, electric element of the same size. An experimental investigation of breakdown phenomena in this antenna should be undertaken to confirm this observation.

The effects of ferrite and dielectric loading of the antenna elements were only briefly treated in this report. Since loading might decrease the element size necessary for a given performance level, further investigation in this area would be worthwhile.

A study of practical tuning and feeding circuitry for these antenna elements should be initiated. An approach to tuning these elements was presented in Section II, but it is felt that implementation of this or other tuning schemes will be an important consideration with regard to the complexity and cost of a system of this type.

Finally, particularly in the areas of reactance and mutual impedances, it is evident that the analytical design procedures of this report are incomplete. In the interest of systematic, nonexperimental design techniques for this antenna system and others also, it is important that work in these areas continue. A thorough, computer-aided, analytical design technique, applicable to all HF aircraft antenna systems and whose capabilities are accurately known and have been demonstrated is an important breakthrough, well worth pursuing.

APPENDIX I  
EXCITATION OF RADIATING CURRENTS  
ON THE STRUCTURE

One of the basic considerations of this new HF antenna system is the utilization of radiating currents on the aircraft structure. It is to be expected that such currents will be excited by the multiturn loop element described in Section II. Since the structure is much larger than the loop element, excitation of such currents could significantly increase the total radiation resistance, and hence the efficiency, of the antenna system. This section describes an analytical and experimental effort that shows that these results may indeed, be achieved. In Section III, it is shown that these currents may be utilized in controlling the overall radiation pattern.

For the present analysis, the aircraft structure is simplified to the form of crossed cylinders, as shown in Fig. 35. Assuming the cylinder lengths are  $3\lambda/4$  or less, it is known that an approximately omni-directional radiation pattern may be achieved by exciting dipole mode currents, in phase quadrature, on the cylinders.<sup>16</sup> For this excitation, the cylinders can be considered separately to a first order approximation, with assumed sinusoidal current distributions.

Placement of the small loop elements for strong excitation of the cylinder is most easily deduced by considering the receiving antenna case and invoking the reciprocity theorem. In this instance, dipole current modes are set up on the structure by the incident field, and the small loop elements can be considered current probes. It is therefore obvious that the most efficient excitation is obtained when the elements are located at the points on the surface where the current is maximum, the loops being oriented with the plane of a turn of the loop perpendicular to the associated H-field of the current on the cylinder. For cylinder lengths less than  $\lambda/2$ , the current maximum is at the center, and the maxima move outward from the center with increasing frequency for cylinder lengths greater than  $\lambda/2$ . The dipole current modes and optimum loop locations for these cases are illustrated in Fig. 36.

Several experiments to test the validity of and performance changes resulting from this approach have been performed. A copper cylinder 68" long and 8" in diameter was built for this purpose.

For the first tests, a small rectangular 2" long by 1" high loop was mounted perpendicular to the surface of the cylinder at its center. A pattern in the horizontal plane for horizontal polarization for this

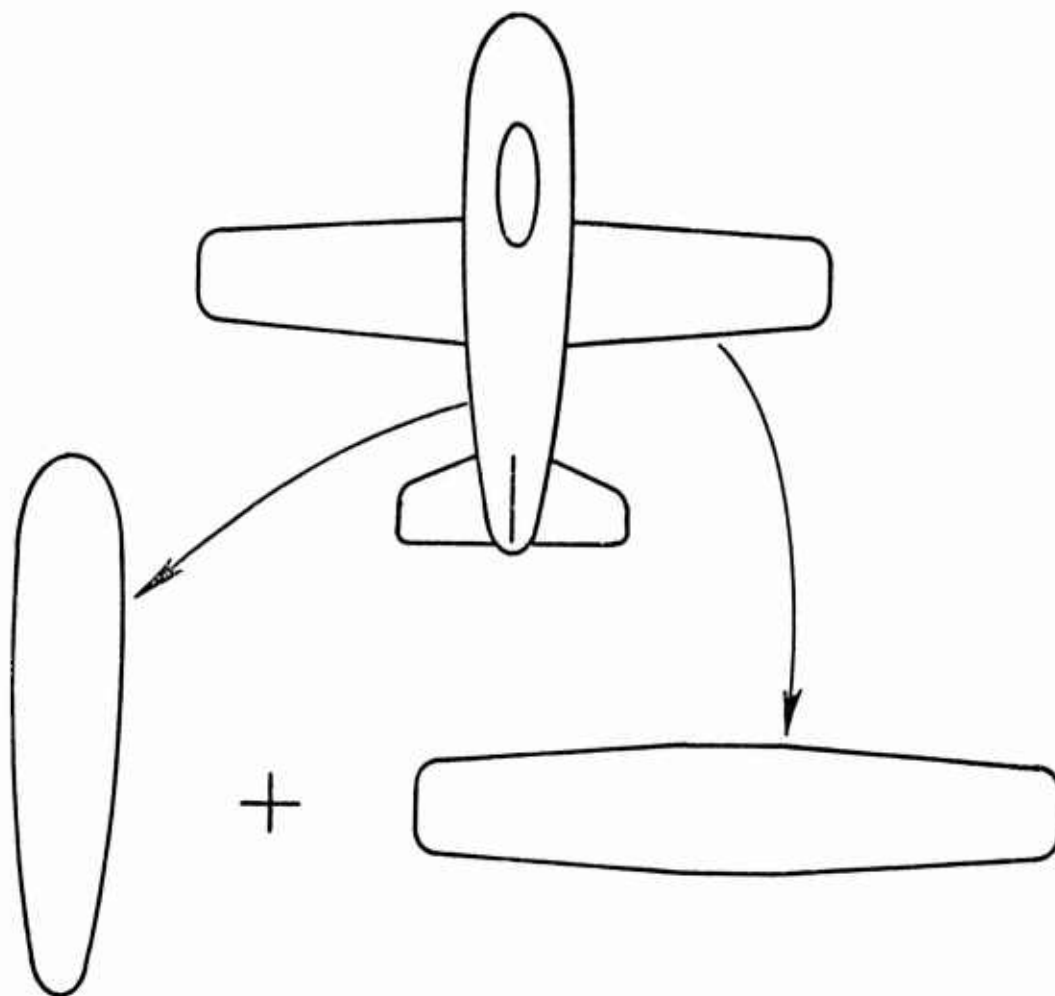


Fig. 35. Crossed-cylinder approximation of aircraft structure.

antenna with the loop oriented vertically is shown in Fig. 37. For this orientation, radiation from the loop is vertically polarized in this plane. Therefore, this pattern results entirely from radiating currents excited on the surface of the cylinder. This pattern closely approximates a half-wave dipole pattern, and, since the cylinder is one-half wavelength long at this frequency, this implies that a dipole current distribution is indeed being excited.

A pattern in the plane of the loop and with polarization parallel to the plane is shown in Fig. 38. To a first order approximation, this pattern can be considered as the sum of an isotropic pattern in the plane of a small loop and the doughnut-shaped pattern of a dipole. Based on these assumptions some conclusions on the relative power radiated in the two modes, and therefore the relative effects of the cylindrical

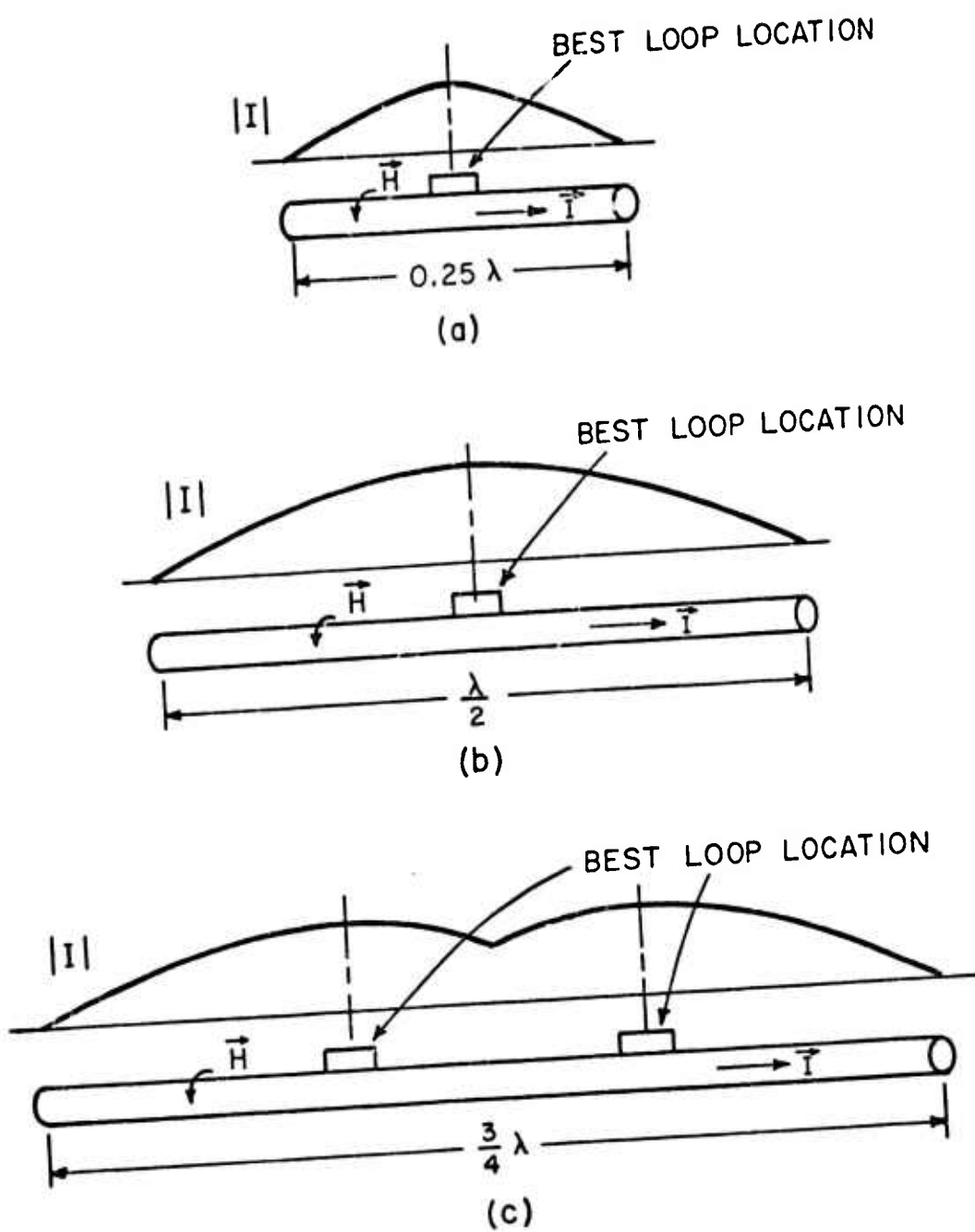


Fig. 36. Current modes and optimum loop locations for several cylinders.

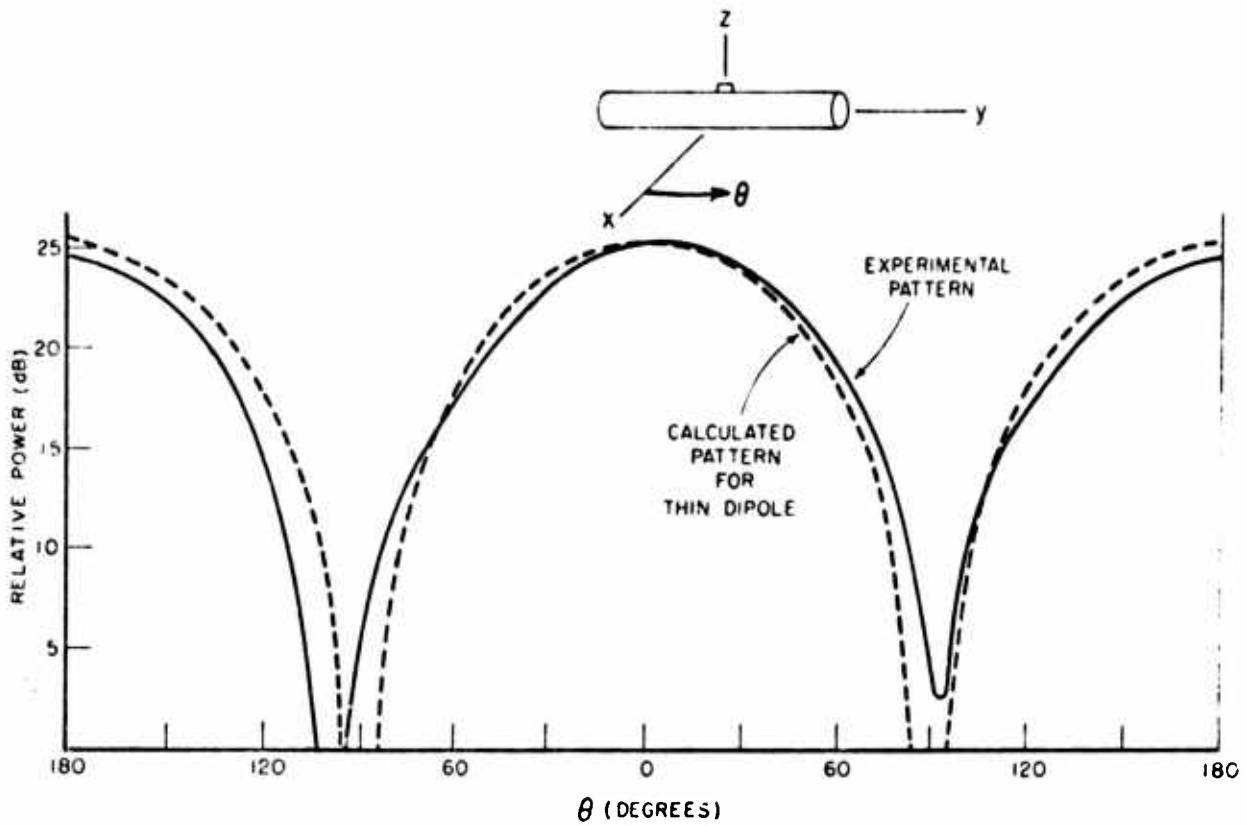


Fig. 37. Experimental pattern of loop-excited cylinder in plane perpendicular to loop.

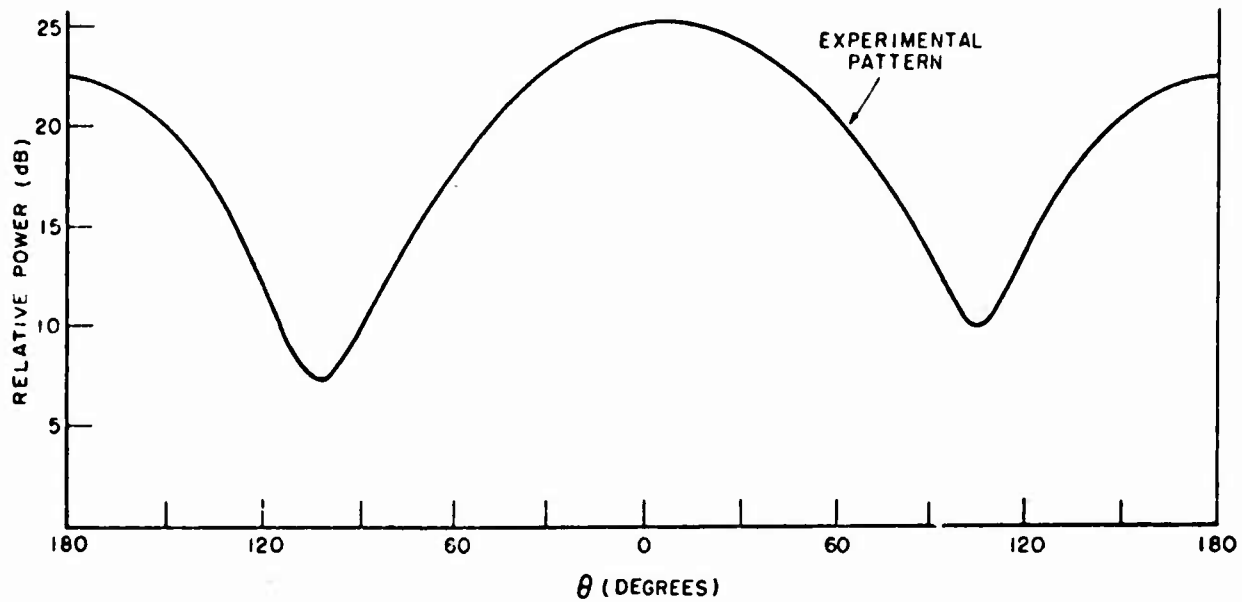


Fig. 38. Experimental pattern of loop-excited cylinder in plane of loop.

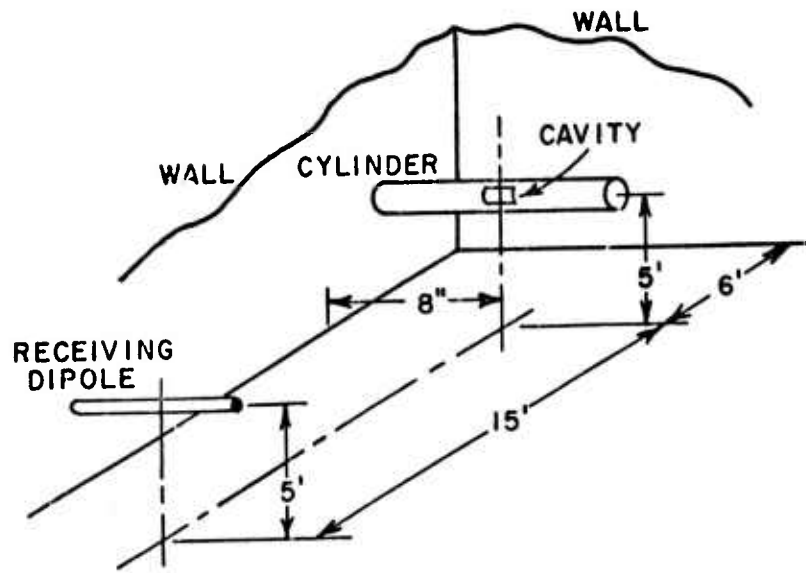
structure on the radiation resistance, can be made. Since the resultant pattern resembles a dipole pattern with filled-in nulls, it is immediately obvious that considerably more power is radiated by the dipole mode than by the loop mode. Comparing the pattern maximum (dipole pattern + loop pattern) to the pattern minimum (loop pattern), the power radiated by the dipole mode is calculated to be about 30 times that of the loop mode. The computer program of Section III gives a pattern for this case which is very close to the experimental pattern, and the ratio that is calculated is approximately 10. Based on these data, the excitation of radiating currents on the cylindrical structure has increased the power radiated for a given terminal current, i.e., increased the radiation resistance, by at least an order of magnitude.

In order to verify that the patterns in the above tests represented a change in gain for the loop-on-cylinder configuration rather than simply a change in directivity with no radiation resistance change, another test has been made.

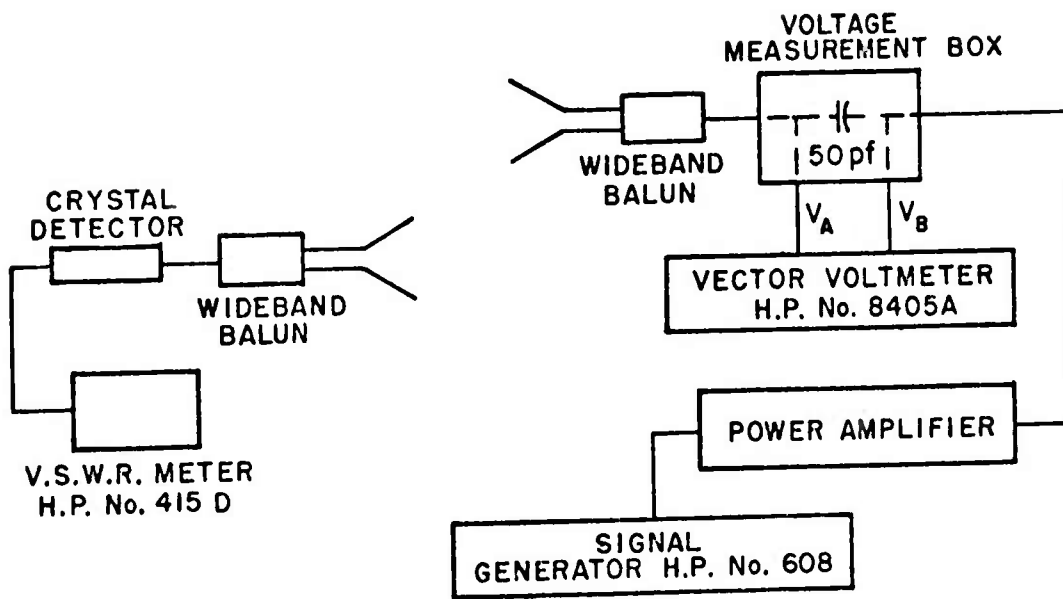
The test model in this case was the 8" by 68" cylinder, with a 2" square by 1" deep cavity built in its surface at the center of the cylinder. A 13-turn, 1/12 scale model of the 3/4" tubing prototype multiturn loop antenna was inserted into the cavity. A standard far-field gain measurement consisting of input and radiated power measurements was made on the multiturn loop antenna alone, and on the antenna-cylinder combination. The measurement system is shown in Fig. 39. There were several possible sources of error on this indoor measurement system. However, a gain improvement by a factor of 10 as a result of adding the cylinder was measured using this technique at a frequency where the cylinder was approximately  $\lambda/2$  long, thus verifying the pattern measurement results.

There are some important implications of these results. First, it has been shown that radiating currents can be excited on an airframe by using properly oriented flush-mounted loop elements, and with significant effects. As is shown in Fig. 38, the radiation of the excited structure is much stronger than that of the loop antenna element. Thus, in order to make accurate pattern predictions of an antenna system on an aircraft, it is imperative that these excited currents on the airframe be carefully accounted for.

These pattern implications give additional insight into the operation of this new HF antenna system. Instead of considering it as an array of loop antennas on a pattern-modifying airframe, it is more appropriate, to a first approximation, to treat this system as a series of multiturn loop impedance transformers between the source and the radiating structure.



(a) LAYOUT



(b) CIRCUIT DIAGRAM

Fig. 39. Indoor gain measurement system.

The locations and excitations of the loops are thus chosen so that power is coupled to this structure in a manner to obtain omnidirectional radiation with good efficiency.

The implications of the gain and efficiency effects of the structure are also important when considering the loop element. As was presented in Section II, practical efficiencies to be expected from these loops by themselves are on the order of 20 per cent or less. However, based on the results of this section, these same loops should have efficiencies of 50 per cent or possibly more when placed on the airframe in the correct manner. Thus for feasibility considerations, the effects of structure excitation make this system seem even more promising.

Because of these important results, this structure excitation concept is being used in treating this system, and provides qualitative information on element location, orientation, and expected performance. However, because an airframe is more complicated than crossed dipoles, and because of the demonstrated importance of the structure effects, it is obvious that more sophisticated, accurate, and generally applicable analyses of these effects are necessary. This is the subject of Section III.



APPENDIX II  
COMPUTER PROGRAM FOR OPTIMIZING LOCATIONS  
OF FOUR ANTENNA ELEMENTS ON A WIRE-GRID  
AIRCRAFT MODEL

This computer program in Fortran IV is a modification of the original pattern-computing program, which is explained in detail in Technical Report 2235-2. It is the purpose of this Appendix to explain the modifications to the original program and how these modifications might be further modified. First, however, the symbols for the input and output data will be identified.

The input data symbols are defined as follows:

- NWIRE = number of wires used to represent the wire-grid aircraft model;
- NEL = number of segments used to represent the antenna elements;
- NDT = number of degrees per increment of the far-field angle  $\theta$  ;
- NDP = number of degrees per increment of the far-field angle  $\phi$  ;
- DELX = unit of increment (in wavelengths) in the x-direction for the mobile antenna elements;
- DELY = unit of increment (in wavelengths) in the y-direction for the mobile antenna elements;
- DULMX = upper limit of displacement in x-direction (in wavelengths) for mobile antenna elements;
- DLLMX = lower limit of displacement in the x-direction (in wavelengths) for mobile antenna elements;
- B = wire radius (in wavelengths);
- DBDIF = allowed variation in far-field pattern (in decibels).

For the wires of the wire-grid body, B is set equal to 0.005.

The data concerning the locations and orientations of the wires of the wire-grid model are read in the subroutine LINSEG. These data are defined as follows:

X1, Y1, Z1 = Cartesian coordinates (in wavelengths) of one end of a given wire;

X2, Y2, Z2 = Cartesian coordinates (in wavelengths) of the other end of a given wire;

NINC = number of wire segments into which the given wire is to be divided.

The subroutine LINSEG calculates the length, orientation angles, and Cartesian coordinates of the center of each wire segment. These data are printed out in the following manner:

FM = the index number of segment M;

X(M), Y(M), Z(M) =  $(x_m, y_m, z_m)$ , the Cartesian coordinates (in wavelengths) of the center of segment M;

SI(M) = length (in wavelengths) of segment M;

SAL(M) =  $\sin \alpha_m$ , where  $\alpha_m$  is an orientation angle of segment M;

CCAB(M) =  $\cos \alpha_m \cos \beta_m$ , where  $\alpha_m$  and  $\beta_m$  are orientation angles of segment M;

CSAB(M) =  $\cos \alpha_m \sin \beta_m$  .

The next input data are for the current elements comprising the antenna. The symbols for these data are defined as follows:

X(J), Y(J), Z(J) =  $(x_j, y_j, z_j)$ , the Cartesian coordinates (in wavelengths) of the center of element j;

SI(J) =  $S_j$ , the length (in wavelengths) of element j;

ALP = the orientation angle  $\alpha_j$  of element j (in degrees);

BET = the orientation angle  $\beta_j$  of element j (in degrees);

CURR(J) = real component of current on segment j;

CURI(J) = imaginary component of current on segment j.

After the computer has calculated the complex current on each wire-grid segment of the aircraft model, these results are printed out under the following symbols:

FI = index number of segment i;

CURR(I) = real part of current on segment i (amperes);

CURI(I) = imaginary part of current on segment i (amperes);

CMAG = magnitude of current on segment i (amperes);

PH = phase of current on segment i (degrees).

The bulk of the statements between numbers 160 and 443 are needed to calculate the far-field pattern values for various planar cuts. At each far-field point the squares of the components of the field intensity are calculated. These are denoted by

TPR =  $|E_{\theta}(\theta, \phi)|^2$  for given field angles  $\theta$  and  $\phi$ ;

PPR =  $|E_{\phi}(\theta, \phi)|^2$ ;

FPR = TPR+PPR.

FDB is the relative power in dB of whatever field component the designer wishes to use in his optimization (here the component is PPR, which is the horizontal power component for a pattern cut in the x-y, or horizontal, plane).

Statement 305 and the one immediately following set up the maximum and minimum relative power in dB over a complete pattern cut. After the values for one complete cut have been calculated, the maximum relative power in dB (FMAX), the minimum relative power (FMIN), the difference between maximum and minimum (FDIF) and the reference, or allowable, difference (DBDIF) are printed out. The values of FDIF and DBDIF are compared to see if the pattern cut meets specifications (is within the allowed variation from isotropic). If this is so, another pattern cut is taken for the same positions of the active elements, and the comparison procedure is repeated. If at any point a pattern cut does not have the desired degree of uniformity, then testing begins to determine what set of positions are being considered.

The three "IF" statements beginning with number 310 control the course of the program. If the pattern has been found unsatisfactory (FDIF greater than DBDIF) for the first set of element positions (NEXNC=1), then the value of FDIF is stored in TEMPI, and the mobile element locations are incremented by DELX and DELY in the DO-loop beginning at statement number 330. Calculation of a pattern cut for the new element positions is then begun. The second of the three IF statements assumes that the elements have been moved at least once (NEXNC>1). The decision is whether the previous incrementing of the elements resulted in a more favorable or less favorable pattern (FDIF greater or less than TEMPI). If the newer pattern is more favorable (but still unacceptable), then the mobile elements are again incremented in the same direction as before, and the pattern calculation is performed again. If the newer pattern is less favorable than the previous one, then one of two conditions holds: either the mobile elements have been incremented only once, or the incrementing process has moved the elements beyond positions for the best pattern without obtaining an acceptable pattern. Which of the two conditions is valid is determined by the third IF statement. If the latter case holds, then the program retraces the incrementing process by one step, prints out these element locations as the best it can find, and stops. If the former case is correct, i.e., if the elements have been moved only once, then the program assumes that the direction in which the elements were originally moved was incorrect. Therefore, the direction of the incrementing process is reversed, and the mobile elements are moved to the opposite side of the original locations (statements 340 to 350). A pattern is again calculated for these new locations and the results are compared to previous locations as explained previously. If for any subsequent set of locations the quantity FDIF exceeds the value stored in TEMPI, then the preceding set of locations is assumed to be the best set for the given excitations. This set of locations of the mobile elements is printed out and the program is terminated.

If the initial locations of the elements give patterns that fall within the allowed variation between maximum and minimum strength for every pattern cut, then the values printed out as optimum locations will be in error by the amount of one increment of the locations. The clue is that the value of NEXNC will be printed out as 1.

This particular program allows the user to vary the locations of the pair of elements that are fixed during the optimizing routine described above. In its present form, the program causes the normally fixed elements to change locations by one increment, after which the locations of the mobile pair of elements are re-optimized. This option can be made more complex by modeling the whole procedure along the line of

reasoning of the routine described above. Its effect may be eliminated entirely by setting the value of the quantity NTRANS (see first page of statement listing) equal to an integer greater than zero (10, for instance).

The whole program can be converted to an optimization of current magnitudes (or phases) at given locations merely by altering the pertinent data and incrementing statements to change values of current magnitude or phase instead of locations.

```

$EXECUTE      IBJOB
$IBJOB        GO
$IBFTC MAIN   NODECK
  2 FORMAT(1H ,8F15.8)
  3 FORMAT(1H , 58HTHE OPTIMUM X- AND Y- LOCATIONS OF MOBILE ELEMENTS
  2FOLLOW  ///)
  4 FORMAT(1H ,1110,3F15.5//)
  7 FORMAT(7F10.5)
  8 FORMAT(14I5)
  9 FORMAT(//1H ,4F15.5//)
11 FORMAT(1H1)
  ZZ=376.72727
  DIMENSION D(10),X(120),Y(1*0),Z(120),SI(120),SALP(120),CURR(120),
  2CUR1(120),CAB(120),SAB(120),
  3CR(100,101),CI(100,101)
  LOGICAL LND
  PI=3.1415926
  P2=PI/2.
  TP=2.*PI
  FPP=TP*TP
  PSQ=PI*PI
  CRY=ZZ/8./PSQ
  CCST=ZZ/180./PSQ
  ZZ2=ZZ/2.
  D(1)=7.
  D(2)=32.
  D(3)=12.
  D(4)=32.
  D(5)=14.
  D(6)=32.
  D(7)=12.
  D(8)=32.
  D(9)=7.
  CNSNT=4.*PI
  TA=.01745329
  TD=57.29578
  READ(5,8) NWIRE,NEL,NDT,NDP
  READ(5,7) DELX,DELY,DULMX,DLLMX
  READ(5,7) B,DBDIF
  B2=B*B
  BK=TP*B
  BK2=BK*BK
  BK4=BK2*BK2
  NEXNC=0
  FDP=NDP
  FDT=NDT
  RDP=TA*FDP
  RDT=TA*FDT
  LMP=360/NDP+1
  LMT=180/NDT+1
  NTRANS=0
  L=0
  CALL LINSEG(NWIRE,L,X,Y,Z,SI,SALP,CAB,SAB)
  N=L
  NN=N+1
  WRITE(6,11)
  IF(N-100) 41,41,500
41 CONTINUE
  J1=1
  J2=N
  LND=.FALSE.
99 DO 300 I=1,N
  IF(LND) GOTO 45
  S=SI(I)

```

```

IF(I-1) 101,42,101
101 I1=I-1
CR(I,1)=CR(I1,I1)
CI(I,1)=CI(I1,I1)
IF(S-SI(I1)) 42,45,42
42 ST=S/2.
R=SQRT (B2+ST*ST )
SINB=ST/R
COSB=B/R
TANB=(1.+SINB+COSB)/(1.-SINB+COSB)
RK=TP*R
RK2=RK*RK
ER=-PI/3.*S*(2.-BK2/3.+BK4/60.+RK2*(BK2-8.)/120.)
E1=SINB*(1./RK2+.5+RK2*(1.-7./60.*BK2)/8.-RK2*RK2/240.)
2-(1.-BK2/4.+7./480.*BK4)*ALOG (TANB)
CR(I,1)=ZZ*ER
CI(I,1)=ZZ*E1
45 XI=X(I)
YI=Y(I)
ZI=Z(I)
CABI=CAB(I)
SABI=SAB(I)
DO 280 J=J1,J2
IF(I-J) 103,280,103
103 S=SI(J)
ST=S/2.
SS=S*S
CABJ=CAB(J)
SABJ=SAB(J)
XIJ=XI-X(J)
YIJ=YI-Y(J)
ZIJ=ZI-Z(J)
ZP=XIJ*CABJ+YIJ*SABJ-ZIJ*SALP(J)
RS=XIJ*XIJ+YIJ*YIJ+ZIJ*ZIJ
RH2=RS-ZP*ZP
RB=RH2+B2
RBK=FPP*RB
KK=8
EZR=0.
EZI=0.
ERR=0.
ERI=0.
W=-1.
T=-ST
SSS=25.*SS
IF(RS.GT.SSS) KK=4
KKK=KK+1
D(5)=(7*KK)/4
FKK=KK
DEL=S/FKK
DO 50 K=1,KKK
R2=RB+(ZP-T)*(ZP-T)
R=SQRT (R2)
RK=TP*R
COSB=COS(RK)/R/R2
SINB=SIN (RK)/R/R2
RKCS=RK*COSB-SINB
CRKS=COSB+RK*SINB
TRBR=2.-3.*RB/R2
IF(D(K)-7.) 104,104,49
104 ERR=ERR+W*CRY*RKCS
ERI=ERI-W*CRY*CRKS
W=1.
49 EZR=EZR+D(K)*(TRBR*RKCS-RBK*SINB)

```

```

EZI=EZI-D(K)*(RBK*COSB+TRBR*CRKS)
50 T=T+DEL
EZR=EZR*CCST*DEL
EZI=EZI*CCST*DEL
Q1=CABI*CABJ+SABI*SABJ+SALP(I)*SALP(J)
Q2=XIJ*CABI+YIJ*SABI-ZIJ*SALP(I)
IF(LND) GOTO 270
CR(I,J)=(EZR-ZP*ERR)*Q1+ERR*Q2
CI(I,J)=(EZI-ZP*ERI)*Q1+ERI*Q2
GO TO 280
270 CSR=(EZR-ZP*ERR)*Q1+ERR*Q2
CSI=(EZI-ZP*ERI)*Q1+ERI*Q2
CR(I,NN)=CR(I,NN)-CSR*CURR(J)+CSI*CURI(J)
CI(I,NN)=CI(I,NN)-CSR*CURI(J)-CSI*CURR(J)
280 CONTINUE
300 CONTINUE
IF(LND) GOTO 630
DO 118 L=1,N
LLL=L-1
DO 118 I=L,N
II=I+1
IF(LLL) 105,106,105
105 DO 117 K=1,LLL
CR(I,L)=CR(I,L)-CR(I,K)*CR(K,L)+CI(I,K)*CI(K,L)
CI(I,L)=CI(I,L)-CI(I,K)*CR(K,L)-CR(I,K)*CI(K,L)
CR(L,II)=CR(L,II)-CR(L,K)*CR(K,II)+CI(L,K)*CI(K,II)
117 CI(L,II)=CI(L,II)-CI(L,K)*CR(K,II)-CR(L,K)*CI(K,II)
106 CRP=CR(L,II)
CLL=CR(L,L)*CR(L,L)+CI(L,L)*CI(L,L)
CR(L,II)=(CRP*CR(L,L)+CI(L,II)*CI(L,L))/CLL
118 CI(L,II)=(CI(L,II)*CR(L,L)-CRP*CI(L,L))/CLL
JJ=N+NEL
DO 620 J=NN,JJ
READ(5,7)X(J),Y(J),Z(J),SI(J),ALP,BET
READ(5,7)CURR(J),CURI(J)
CALP=COS(TA*ALP)
SALP(J)=SIN(TA*ALP)
CBET=COS(TA*BET)
SBET=SIN(TA*BET)
CAB(J)=CALP*CBET
SAB(J)=CALP*SBET
WRITE(6,2) X(J),Y(J),Z(J),SI(J),CAB(J),SAB(J)
620 WRITE(6,2) CURR(J),CURI(J)
J1=NN
J2=JJ
LND=.TRUE.
GOTO 99
630 CONTINUE
DO 120 L=1,N
LLL=L-1
IF(LLL) 205,206,205
205 DO 119 K=1,LLL
CR(L,NN)=CR(L,NN)-CR(L,K)*CR(K,NN)+CI(L,K)*CI(K,NN)
119 CI(L,NN)=CI(L,NN)-CI(L,K)*CR(K,NN)-CR(L,K)*CI(K,NN)
206 CRP=CR(L,NN)
CLL=CR(L,L)*CR(L,L)+CI(L,L)*CI(L,L)
CR(L,NN)=(CRP*CR(L,L)+CI(L,NN)*CI(L,L))/CLL
120 CI(L,NN)=(CI(L,NN)*CR(L,L)-CRP*CI(L,L))/CLL
DO 122 L=2,N
I=NN-L
II=I+1
DO 122 K=II,N
CR(I,NN)=CR(I,NN)-CR(I,K)*CR(K,NN)+CI(I,K)*CI(K,NN)
122 CI(I,NN)=CI(I,NN)-CI(I,K)*CR(K,NN)-CR(I,K)*CI(K,NN)

```



```

DO 160 I=1,N
CURR(I)=CR(I,NN)
CURI(I)=CI(I,NN)
CR(I,NN)=0.0
CI(I,NN)=0.0
CMAG=SQRT (CURR(I)*CURR(I)+CURI(I)*CURI(I))
FI=I
PH=TD*ATAN2(CURI(I),CURR(I))
160 WRITE(6,2) FI,CURR(I),CURI(I),CMAG,PH
WRITE(6,11)
NEXNC=NEXNC+1
SUM=0.
SUMP=0.
FMAX=0.
FMIN=0.
DO 445 NP=1,LMP
DO 443 NT=1,LMT
IF (NP.GT.1) GOTO421
NPHI=NDT*(NT-1)
PHI=NPHI
CPHI=COS(TA*PHI)
SPHI=SIN(TA*PHI)
STHET=1.0
CTHET=0.0
STCP=STHET*CPHI
STSP=STHET*SPHI
CTCP=CTHET*CPHI
CTSP=CTHET*SPHI
GOTO 429
421 NPHI=NDP*(NP-2)
NTHET=NDT*(NT-1)
PHI=NPHI
CPHI=COS(TA*PHI)
SPHI=SIN(TA*PHI)
THET=NTHET
STHET=SIN(TA*THET)
CTHET=COS(TA*THET)
STCP=STHET*CPHI
STSP=STHET*SPHI
CTCP=CTHET*CPHI
CTSP=CTHET*SPHI
429 ETR=0.0
ETI=0.
EPR=0.
EPI=0.
DO 400 I=1,JJ
S=SI(I)*ZZZ
ARG=X(I)*STCP+Y(I)*STSP+Z(I)*CTHET
COSA=COS(TP*ARG)
SINA=SIN(TP*ARG)
CABI=CAB(I)
SABI=SAB(I)
P=CPHI*SABI-SPHI*CABI
Q=CTCP*CABI+CTSP*SABI+STHET*SALP(I)
FR=(SINA*CURR(I)+COSA*CURI(I))*S
FI=(SINA*CURI(I)-COSA*CURR(I))*S
ETR=ETR+FR*Q
ETI=ETI+FI*Q
EPR=EPR+FR*P
400 EPI=EPI+FI*P
TPR=ETR*ETR+ETI*ETI
PPR=EPR*EPR+EPI*EPI
FPR=TPR+PPR
FDB=10.*ALOG10(PPR)

```

```

      IF (FMAX.GT.0.0001) GOTO 305
      FMAX=FDB
      FMIN=FDB
      GOTO 443
305  IF (FDB.GT.FMAX) FMAX=FDB
      IF (FDB.LT.FMIN) FMIN=FDB
443  CONTINUE
      FDIF=FMAX-FMIN
      WRITE(6,9) FMAX,FMIN,FDIF,DBDIF
      IF (FDIF.GT.DBDIF) GOTO 310
445  CONTINUE
      GOTO 385
310  IF (NEXNC.EQ.1) GOTO 320
      IF (FDIF.LT.TEMP1) GOTO 320
      IF (NEXNC.NE.2) GOTO 399
340  DELX=(-1.)*DELX
      DELY=(-1.)*DELY
      DO 350 NIN=1,3
      L10=N+3+NIN
      X(L10)=X(L10)-DELX
      Y(L10)=Y(L10)-DELY
      X(L10+6)=X(L10+6)+DELX
350  Y(L10+6)=Y(L10+6)-DELY
      GOTO 330
320  TEMP1=FDIF
330  DO 360 NIN=1,3
      L10=N+3+NIN
      X(L10)=X(L10)-DELX
      Y(L10)=Y(L10)-DELY
      X(L10+6)=X(L10+6)+DELX
      Y(L10+6)=Y(L10+6)-DELY
360  WRITE(6,2) X(L10),Y(L10),X(L10+6),Y(L10+6)
      WRITE(6,11)
      IF (X(JJ-1).GT.DULMX.OR.X(JJ-1).LT.DLLMX) GOTO 399
      GOTO 99
399  IF (NEXNC.EQ.1) GOTO 340
385  WRITE(6,11)
      WRITE(6,3)
      WRITE(6,4) NEXNC,      TEMP1,FDIF,DBDIF
      DO370 NIP=1,3
      L11=N+NIP+3
      X(L11)=X(L11)+DELX
      Y(L11)=Y(L11)+DELY
      X(L11+6)=X(L11+6)-DELX
      Y(L11+6)=Y(L11+6)+DELY
370  WRITE(6,2) X(L11),Y(L11),X(L11+6),Y(L11+6)
      IF (NTRANS.GT.0) GOTO 500
      DO 371 NIN=1,3
      L10=N+NIN
      Y(L10)=Y(L10)-DELX
371  Y(L10+6)=Y(L10+6)+DELX
      NEXNC=0
      NTRANS=10
      GOTO 99
500  CONTINUE
      STOP
      END
$IBFTC LINDIV  NODECK
      SUBROUTINE LINSEG (NW,M,X,Y,Z,SI,SAL,CCAB,CSAB)
      12 FORMAT(1H ,8F15.8)
      13 FORMAT(6F10.5,15)
      DIMENSION X(1),Y(1),Z(1),SI(1),SAL(1),CCAB(1),CSAB(1)
      DO16 I=1,N#
      READ(5,13) X1,Y1,Z1,X2,Y2,Z2,NINC

```

```

S2=(X2-X1)*(X2-X1)+(Y2-Y1)*(Y2-Y1)
ST2=S2+(Z2-Z1)*(Z2-Z1)
S=SQRT(S2)
ST=SQRT(ST2)
FNI=NINC
DX=.5*(X2-X1)/FNI
DY=.5*(Y2-Y1)/FNI
DZ=.5*(Z2-Z1)/FNI
SL=ST/FNI
CBET=(X2-X1)/S
SBET=(Y2-Y1)/S
SLP=(Z1-Z2)/ST
CLP=S/ST
CABL=CLP*CBET
SABL=CLP*SBET
DO15 J=1,NINC
M=M+1
SI(M)=SL
SAL(M)=SLP
CCAB(M)=CABL
CSAB(M)=SABL
FJ=2*J-1
X(M)=X1+FJ*DX
Y(M)=Y1+FJ*DY
Z(M)=Z1+FJ*DZ
FM=M
15 WRITE(6,12) FM,X(M),Y(M),Z(M),SI(M),SAL(M),CCAB(M),CSAB(M)
16 CONTINUE
RETURN
END

```

\$DATA

APPENDIX III  
STRUCTURE IMPEDANCE EFFECTS COMPUTER  
CALCULATION PROGRAM

This computer program calculates the change in complex impedance due to the addition of a scattering structure near a transmitting antenna. In the form printed here, the structure is limited to a  $0.05\lambda$  diameter scattering cylinder. However, the techniques used in the program allow application to more general structures with only slight modification.

The input parameters are:

L	number of current modes on the scatterer
K	number of longitudinal current modes on the scatterer
M	number of longitudinal surface divisions on the scatterer
N	number of transverse surface divisions on the scatterer
MMMM	number of longitudinal divisions on the antenna
DR	longitudinal differential length on scatterer in $\lambda$
DS	transverse differential length on scatterer in degrees
DRS	longitudinal differential length on antenna in $\lambda$
DT	scattering surface thickness in $\lambda$
RO(I) } SO(I) }	surface coordinates of the I-th point where the field boundary coefficients will be enforced
LMULT(I) } LPHASE(I) } TMULT(I) } TPHASE(I) }	Constants which describe the longitudinal and transverse variation of the I-th sinusoidal current mode on the scattering surface

The constants relating to the scattering surface can be explained as follows. In this program, points on some generalized scattering surface are specified by two orthogonal surface coordinates,  $r$  and  $s$ , where  $r$  is called the longitudinal coordinate and  $s$  is called the transverse coordinate. For the cylinder,  $r$  corresponds to  $z$  and  $s$  corresponds to  $\theta$ , and the cylinder radius is inbedded in the program statements, #28 and 29. For a plane surface,  $r$  and  $s$  could correspond to  $x$  and  $y$ ; for a spherical surface of given radius,  $\theta$  and  $\phi$ ; etc. For integration purposes, the surface is divided into differential quasi-rectangles, each of dimensions  $DR$  by  $DS$ . The number of such divisions in each coordinate are specified by  $M$  and  $N$ .

Sinusoidal current modes are assumed on the scattering surface, as seen in statement 27 of the program. Longitudinal and transversely directed currents are allowed, with the number of modes assumed specified by  $L$  and  $K$ . Currents in both directions may have longitudinal and transverse variation also. The four constants  $LMULT$ ,  $LPHASE$ ,  $TMULT$ , and  $TPHASE$  specify this variation for each mode, and are chosen such that each mode satisfies the boundary conditions at the surface edges. For the cylindrical surface of this program, all current modes should be zero on the ends of the cylinder and be periodic to assure continuity around the circumference of the cylinder. For a planar surface, all current modes would be required to be zero on all edges.

In this program, as for the pattern computation program, the electric field boundary condition is enforced at specific points in order to solve for the current mode coefficients. The locations of these points are specified by the input parameters  $RO$  and  $SO$ . At each point, the electric field in the longitudinal and transverse direction is forced to zero; thus, the number of matching points is half the number of current modes.

Some sections of this program will now be identified. The scattering coefficients for each mode are calculated in statements 27 to 70. The source scattering coefficients are calculated in statements 70 to 99. The field boundary condition is enforced, and the current mode coefficients solved for in statements 102 to 120. Finally, the reaction integral discussed in Section III-B is computed in statements 150 to 210.

The first output list comprises the quantities  $I$ ,  $J$ ,  $REALETAN$ ,  $IMAGETAN$ , which specify the complex value of the scattering coefficient of the  $I$ -th current mode at the  $J$ -th field matching point. The second output list,

I      REAL I-TH CURRENT      IMAG I-TH CURRENT.

specifies the complex current mode coefficient for the I-th mode.  
Finally, the complex value of ZADD is printed out, where ZADD is the impedance which must be added to the original impedance of the antenna as a result of adding the scattering structure.

```

COMPLEXCURR(20),CON1,VAR1,EX,EY,EZ,
1  ETAN(20,20),VAR2,PR,QR,CCU(20),CCURRL,
2  (CURRT,ELONG,ETRAN,ZADD,CURRS(5),ELL
  DIMENSIONRO(20),SO(20),LMULT(10),LPHASE(10),TMULT(10),TPHASE(10)
  REAL LMULT,LPHASE
1  FORMAT(6F10.5)
2  FORMAT(4F10.5)
3  FORMAT(14I5)
  READ(5,3)L,K,M,N,MMMM
  READ(5,2)DR,DS,DRS,DT
  NNNN=L/2
  READ(5,1)(RO(I),SO(I),I=1,NNNN,1)
  READ(5,2)(LMULT(I),LPHASE(I),TMULT(I),TPHASE(I),I=1,NNNN,1)
  DO102 NNN=1,NNNN,1
  XO=0.0
  YO=0.0
  ZO=RO(NNN)
  XOLONG=0.
  YOLONG=0.
  ZOLONG=1.
  XOTRAN=-SIN(3.1416*SO(NNN)/180.)
  YOTRAN=COS(3.1416*SO(NNN)/180.)
  ZOTRAN=0.
  DO70 I=1,M,1
  WI=(3.+((-1.)**I))/3.
  IF(I-1) 15,14,15
14  #I=1./3.
15  IF(I-M) 17,16,17
16  #I=1./3.
17  R=- (DR/2.)+DR*FLOAT(I)-.250
  DO70 J=1,N,1
  #J=(3.+((-1.)**J))*3.1416*.025/540.0
  IF(J-1) 22,21,22
21  #J=1.*3.1416*.025/540.
22  IF(J-N) 24,23,24
23  #J=1.*3.1416*.025/540.
24  S=- (DS/2.)+DS*FLOAT(J)
  DO27 NN=1,NNNN,1
27  CURR( NN)=( SIN(3.1416*LMULT(NN)*2.*R+3.1416
  1  *LPHASE(NN)/180.)*SIN(3.1416*(TMULT(NN)*S
  2  +TPHASE)/180.))* (1.,0.)
  X=.025*COS(3.1416*S/180.)
  Y=.025*SIN(3.1416*S/180.)
  Z=R
  XLONG=0.
  YLONG=0.
  ZLONG=1.
  XTRAN=-SIN(3.1416*S/180.)
  YTRAN=COS(3.1416*S/180.)
  ZTRAN=0.
  RHO=SQRT((X-XO)**2+(Y-YO)**2+(Z-ZO)**2)
  IF(RHO) 39,61,39
39  PR=(-1.+(0.-1.)*(2.*3.1416*RHO)+(2.*3.1416*RHO)
  1  **2)/(RHO**3)
  QR=(3.+3.*(0.,1.)*(2.*3.1416*RHO)-(2.*3.1416*RHO)
  1  **2)/(RHO**5)
  DO 59 NN=1,NNNN
  IF(I.LE.1..AND.J.LE.1) ETAN(2*NNN,2*NN)=(0.,0.)
  IF(I.LE.1..AND.J.LE.1) ETAN(2*NNN-1,2*NN)=(0.,0.)
  CON1=CMPLX(0.,-376./ (3.*3.1416*3.1416))
  VAR1=(XO-X)*CURR(NN)*XLONG+(YO-Y)*CURR(NN)
  1  *YLONG+(ZO-Z)*CURR(NN)*ZLONG
  EX=CON1*CMPLX(COS(2.*3.1416*RHO),-SIN(2.*3.1416*
  1  RHO))*(PR*CURR(NN)*XLONG+(XO-X)*QR*VAR1)

```

```

2   *DR*DS*W1*WJ
EY=CON1*CMPLX(COS(2.*3.1416*RHO),-SIN(2.*3.1416*
1   RHO))*(PR*CURR(NN)*YLONG+(YO-Y)*QR*VAR1)
2   *DR*DS*W1*WJ
EZ=CON1*CMPLX(COS(2.*3.1416*RHO),-SIN(2.*3.1416*
1   RHO))*(PR*CURR(NN)*ZLONG+(ZO-Z)*QR*VAR1)
2   *DR*DS*W1*WJ
ETAN(2*NNN,2*NN)=EX*XOLONG+EY*YOLONG+EZ
1   *ZOLONG+ETAN(2*NNN,2*NN)
50 ETAN(2*NNN-1,2*NN)=EX*XOTRAN+EY*YOTRAN+EZ
1   *ZOTRAN+ETAN(2*NNN-1,2*NN)
IF(1.LE.1.AND.J.LE.1) ETAN(2*NNN,2*NN-1)=(0.,0.)
IF(1.LE.1.AND.J.LE.1) ETAN(2*NNN-1,2*NN-1)=(0.,0.)
VAR2=(XO-X)*CURR(NN)*XTRAN+(YO-Y)*CURR(NN)
1   *YTRAN+(ZO-Z)*CURR(NN)*ZTRAN
EX=CON1*CMPLX(COS(2.*3.1416*RHO),-SIN(2.*3.1416*
1   RHO))*(PR*CURR(NN)*XTRAN+(XO-X)*QR*VAR2)
2   *DR*DS*W1*WJ
EY=CON1*CMPLX(COS(2.*3.1416*RHO),-SIN(2.*3.1416*
1   RHO))*(PR*CURR(NN)*YTRAN+(YO-Y)*QR*VAR2)
2   *DR*DS*W1*WJ
EZ=CON1*CMPLX(COS(2.*3.1416*RHO),-SIN(2.*3.1416*
1   RHO))*(PR*CURR(NN)*ZTRAN+(ZO-Z)*QR*VAR2)
2   *DR*DS*W1*WJ
ETAN(2*NNN,2*NN-1)=EX*XOLONG+EY*YOLONG+EZ*
1   ZOLONG+ETAN(2*NNN,2*NN-1)
59 ETAN(2*NNN-1,2*NN-1)=EX*XOTRAN+EY*YOTRAN+EZ*
1   ZOTRAN+ETAN(2*NNN-1,2*NN-1)
GOTO 70
61 DO 66 NN=1,NNNN
IF(1.LE.1.AND.J.LE.1) ETAN(2*NNN,2*NN)=(0.,0.)
63 ETAN(2*NNN,2*NN)=ETAN(2*NNN,2*NN)+DR*DS*W1*WJ
1   *CURR(NN)*CON1*(-1.+(0.,-1.))*(2.*
2   3.1416*DT)+(2.*3.1416*DT)**2)/(DT**3)
IF(1.LE.1.AND.J.LE.1) ETAN(2*NNN-1,2*NN-1)=(0.,0.)
66 ETAN(2*NNN-1,2*NN-1)=ETAN(2*NNN-1,2*NN-1)+DR*DS*
1   W1*WJ*CURR(NN)*CON1*(-1.+(0.,-1.))*(2.*
2   3.1416*DT)+(2.*3.1416*DT)**2)/(DT**3)
70 CONTINUE
DO99 IJ=1,MMM,1
SS=J.
RS=-.25J-(DRS/2.)+DRS*FLOAT(IJ)
XS=-.5J
YS=0.
ZS=RS
XSLONG=0.
YSLONG=0.
ZSLONG=1.
WIS=(3.+((-1.)**IJ))/3.0
IF(IJ-1) 83,82,83
82 WIS=1./3.
83 IF(IJ-MMM) 85,84,85
84 WIS=1./3.
85 CURR(1)=COS(2.*3.1416*RS)*(1.,0.)
RHO=SQRT((XS-XO)**2+(YS-YO)**2+(ZS-ZO)**2)
PR=(-1.+(0.,-1.))*(2.*3.1416*RHO)+(2.*3.1416*RHO)
1   **2)/(RHO**3)
QR=(3.+3.*(0.,1.))*(2.*3.1416*RHO)-(2.*3.1416*RHO)
1   **2)/(RHO**5)
DO99 MM=1,1,1
NN=L+1
IF(IJ.LE.1) ETAN(2*NNN,NN)=(0.,0.)
IF(IJ.LE.1) ETAN(2*NNN-1,NN)=(0.,0.)
VAR1=(XO-XS)*CURR(MM)*XSLONG+(YO-YS)*CURR(MM)

```



```

1      *YSLONG+(ZO-ZS)*CURRS(MM)*ZSLONG
EX=CON1*CMPLX(COS(2.*3.1416*RHO),-SIN(2.*3.1416*
1      RHO))* (PR*CURRS(MM)*XSLONG+(XO-XS)*QR*
2      VAR1)*WIS*DRS
EY=CON1*CMPLX(COS(2.*3.1416*RHO),-SIN(2.*3.1416*
1      RHO))* (PR*CURRS(MM)*YSLONG+(YO-YS)*QR*
2      VAR1)*WIS*DRS
EZ=CON1*CMPLX(COS(2.*3.1416*RHO),-SIN(2.*3.1416*
1      RHO))* (PR*CURRS(MM)*ZSLONG+(ZO-ZS)*QR*
2      VAR1)*WIS*DRS
ETAN(2*NNN,NN)=-EX*XOLONG-EY*YULONG-EZ*
1      ZGLONG+ETAN(2*NNN,NN)
ETAN(2*NNN-1,NN)=-EX*XOTRAN-EY*YOTRAN-EZ*
1      ZOTRAN+ETAN(2*NNN-1,NN)
99 CONTINUE
100 FORMAT(76H      I      J      REALETAN      IMAGETAN      I      J      REA
1LETAN      IMAGETAN / (214,2F15.4,3H      ,214,2F15.4))
NP=2*NNN-1
NPP=2*NNN
LLL=L+1
WRITE(6,100) (NP,NN,ETAN(NP,NN),NPP,NN,ETAN(NPP,NN),NN=1,LLL,1)
102 CONTINUE
DO112 J=1,L,1
NNN=J-1
DO112 I=J,L,1
II=I+1
IF(NNN) 108,111,108
108 DO110 KK=1,NNN,1
ETAN(I,J)=ETAN(I,J)-ETAN(I,KK)*ETAN(KK,J)
110 ETAN(J,II)=ETAN(J,II)-ETAN(J,KK)*ETAN(KK,II)
111 ELL=ETAN(J,J)
112 ETAN(J,II)=ETAN(J,II)/ELL
NN=L+1
DO118 J=2,L,1
I=NN-J
II=I+1
DO118 KK=II,L,1
118 ETAN(I,NN)=ETAN(I,NN)-ETAN(I,KK)*ETAN(KK,NN)
DO120 I=1,L,1
120 CCU(I)=ETAN(I,NN)
121 FORMAT(42H      I      REAL      I TH CURRENT      IMAG      I TH CURRENT
1      / (15,5H      ,F10.4,
2      10H      ,F10.4))
122 WRITE(6,121) (I,CCU(I),I=1,L,1)
150 ZADD=(0.,0.)
DO210 I=1,M,1
WI=(3.+((-1.)*I))/3.
IF(I-1)155,154,155
154 WI=1./3.
155 IF(I-M)157,156,157
156 WI=1./3.
157 R=- (DR/2.)+DR*FLOAT(I)-.250
DO210 J=1,N,1
WJ=(3.+((-1.)*J))*3.1416*.025/540.0
IF(J-1)162,161,162
161 WJ=1.*.025*3.1416/540.0
162 IF(J-N)164,163,164
163 WJ=1.*.025*3.1416/540.0
164 S=- (DS/2.)+DS*FLOAT(J)
CCURRT=(0.,0.)
CCURRL=(0.,0.)
DO174 II=1,NNNIN
170 CCURRL=CCURRL+CCU(2*II)*CURR(II)
174 CCURRT=CCURRT+CCU(2*II-1)*CURR(II)

```

```

ELONG=(0.,0.)
ETRAN=(0.,0.)
X=.025*COS(3.1416*S/180.)
Y=.025*SIN(3.1416*S/180.)
Z=R
XLONG=0.
YLONG=0.
ZLONG=1.
XTRAN=-SIN(3.1416*S/180.)
YTRAN=COS(3.1416*S/180.)
ZTRAN=0.
DO206 IJ=1,MMMM
RS=-.250-(DRS/2.)+DRS*FLOAT(IJ)
SS=0.
XS=-.50
YS=0.
ZS=RS
XSLONG=0.
YSLONG=0.
ZSLONG=1.
WIS=(3.+(-1.**IJ))/3.
IF(IJ-1)196,195,196
195 WIS=1./3.
196 IF(IJ-MMMM)198,197,198
197 WIS=1./3.
198 DTS=1.
CURRSS=COS(3.1416*2.*RS)
RHO=SQRT((XS-X)**2+(YS-Y)**2+(ZS-Z)**2)
VAR1=(X-XS)*CURRSS*XSLONG+(Y-YS)*CURRSS*YSLONG+(Z-ZS)*CURRSS*ZS
LONG
EX=CON1*CMPLX(COS(2.*3.1416*RHO),-SIN(2.*3.1416*RHO))*(PR*CURRSS*
|XSLONG+(X-XS)*QR*VAR1)*WIS*DTS*DRS
EY=CON1*CMPLX(COS(2.*3.1416*RHO),-SIN(2.*3.1416*RHO))*(PR*CURRSS*
|YSLONG+(Y-YS)*QR*VAR1)*WIS*DTS*DRS
EZ=CON1*CMPLX(COS(2.*3.1416*RHO),-SIN(2.*3.1416*RHO))*(PR*CURRSS*
|ZSLONG+(Z-ZS)*QR*VAR1)*WIS*DTS*DRS
ELONG=ELONG+EX*XLONG+EY*YLONG+EZ*ZLONG
206 ETRAN=ETRAN+EX*XTRAN+EY*YTRAN+EZ*ZTRAN
ZADD=ZADD+(CCURRL*ELONG+CCURRT*ETRAN)*DR*DS*W1*WJ
210 CONTINUE
211 FORMAT(27H REAL ZADD IMAG ZADD / (2F15.4))
WRITE(6,211)ZADD
STOP
END

```

APPENDIX IV  
RADIATION RESISTANCE FROM FAR-FIELD  
PATTERN INTEGRATION

This Appendix explains a simple alteration of the digital computer program for calculating the far-field patterns of an antenna mounted on a wire-grid aircraft model. The alteration allows the computation of the radiation resistance of the system by, in effect, an integration of the Poynting vector over the surface of the sphere at infinity. A statement listing accompanies this explanation.

The exact form for the radiation resistance is

$$(28) \quad R_R = \frac{1}{Z_0 I^2} \int \int E^2 ds = \frac{W}{I^2} ,$$

where  $Z_0$  is the impedance of free space,  $I$  is the rms terminal current in amperes,  $E$  is the rms electric field intensity,  $W$  is the radiated power, and

$$(29) \quad ds = d\theta d\phi \sin\theta ,$$

the differential area of the surface of the sphere in square radians. The integration is performed using the trapezoidal rule applied to a spherical surface in a strip-wise fashion. The square of the electric field intensity (FPR) is calculated at a given point  $(\theta, \phi)$ , and this quantity is multiplied by a finite surface area  $\sin\theta \Delta\theta \Delta\phi$  whose center is assumed to be the point  $(\theta, \phi)$ . For each value of  $\phi$ , incremented by  $\Delta\phi$ , the quantity  $E^2$  is calculated for each value of  $\theta$ , incremented by  $\Delta\theta$ , between 0 and  $\pi$  radians, not including the end points. The quantity SUMT represents the contribution to the integral from the products of all the quantities  $E^2$  and the respective surface areas at the center of which each  $E^2$  is calculated, less the contributions from the polar surfaces ( $\theta = 0$  and  $\theta = \pi$ ). The contributions from these two nearly circular areas are calculated separately, owing to the way in which the program divides up the spherical surface. The combined contributions from these two areas is represented by the quantity SUMP. Finally, SUMM represents the value of the integral of Eq. (28). The total power radiated by the composite system is given by the quantity PWR, and the radiation resistance is represented by RRAD. CMAX denotes the maximum (not rms) terminal current.

All that has been offered in the statement listing is the altered final portion of the main program which was originally a pattern-calculating vehicle. To see where the alterations begin, note the statement listing of the complete program (altered in a different manner) in Appendix II of this report. The alterations listing begins with statement number 160. Except for a minor change in input data (that of leaving out the pertinent data for performing optimization) the preceding portion of the main program remains unchanged. The subroutine for calculating pertinent quantities concerning the wire-grid segments of the aircraft also remains unchanged. One option that is available but is not included in the statement listing is the ability to print out desired far-field pattern information. This can be easily added by inserting a WRITE statement immediately preceding statement number 305. The quantities one might want to examine are PHI (spherical field angle  $\phi$ ), THET (spherical field angle  $\theta$ ), PPR( $|E_{\phi}(\theta, \phi)|^2$ ), TPR( $|E_{\theta}(\theta, \phi)|^2$ ), and FPR( $|E_{\phi}|^2 + |E_{\theta}|^2$ ).

```

.
.
.
160 WRITE(6,2) FI,CURR(I),CURI(I),CMAG,PH
WRITE(6,11)
SUM=0.
SUMP=0.
FDP=NDP
FDT=NDT
RDP=TA*FDP
RDT=TA*FDT
LMP=360/NDP
LMT=180/NDT-1
DO 305 NP=1,LMP
NPHI=NDP*(NP-1)
PHI=NPHI
CPHI=COS(TA*PHI)
SPHI=SIN(TA*PHI)
DO 305 NT=1,LMT
NTHET=NDT*NT
THET=NTHET
STHET=SIN(TA*THET)
CTHET=COS(TA*THET)
STCP=STHET*CPHI
STSP=STHET*SPHI
CTCP=CTHET*CPHI
CTSP=CTHET*SPHI
ETR=0.
ETI=0.
EPR=0.
EPI=0.
DO 400 I=1,JJ
S=SI(I)*ZZ2
ARG=X(I)*STCP+Y(I)*STSP+Z(I)*CTHET
COSA=COS(TP*ARG)
SINA=SIN(TP*ARG)
CABI=CAB(I)
SABI=SAB(I)
P=CPHI*SABI-SPHI*CABI
Q=CTCP*CABI+CTSP*SABI+STHET*SALP(I)
FR=(SINA*CURR(I)+COSA*CURI(I))*S
FI=(SINA*CURI(I)-COSA*CURR(I))*S
ETR=ETR+FR*Q
ETI=ETI+FI*Q
EPR=EPR+FR*P
400 EPI=EPI+FI*P
TPR=ETR*ETR+ETI*ETI
PPR=EPR*EPR+EPI*EPI
FPR=TPR+PPR
305 SUM=SUM+FPR*STHET
SUMT=SUM*RDP*RDT
PHI=0.
THET=0.
STHET=SIN(TA*THET)
CTHET=COS(TA*THET)
SPHI=SIN(TA*PHI)
CPHI=COS(TA*PHI)
412 CONTINUE
STCP=STHET*CPHI
STSP=STHET*SPHI
CTCP=CTHET*CPHI
CTSP=CTHET*SPHI
ETR=0.
ETI=0.

```

```

EPR=0.
EPI=0.
DO 410 I=1,JJ
S=SI(I)*ZZ2
ARG=X(I)*STCP+Y(I)*STSP+Z(I)*CTHET
COSA=COS(TP*ARG)
SINA=SIN(TP*ARG)
CABI=CAB(I)
SABI=SAB(I)
P=CPHI*SABI-SPHI*CABI
Q=CTCP*CABI+CTSP*SABI+STHET*SALP(I)
FR=(SINA*CURI(I)+COSA*CURI(I))*S
FI=(SINA*CURI(I)-COSA*CURI(I))*S
ETR=ETR+FR*Q
ETI=ETI+FI*Q
EPR=EPR+FR*P
410 EPI=EPI+FI*P
TPR=ETR*ETR+ETI*ETI
PPR=EPR*EPR+EPI*EPI
FPR=TPR+PPR
310 SUMP=SUMP+FPR*PI*(RDT**2.)/4.
IF(THET.GT.90.) GOTO 320
THET=180.
STHET=SIN(TA*THET)
CTHET=COS(TA*THET)
GOTO 412
320 SUMM=SUMT+SUMP
PWR=SUMM/(ZZ*2.)
RRAD=2.*PWR/(CMAX**2.)
WRITE(6,9) SUMM,SUMT,CMAX,RRAD
450 WRITE(6,11)
500 CONTINUE
STOP
END

```

APPENDIX V  
MAGNETIC DIPOLE REPRESENTATION OF A  
SMALL ELECTRIC CURRENT LOOP

The present form of the pattern-calculating digital computer program and all its modifications employ the same statements to calculate the tangential electric field at the center of each wire-grid segment due to the active elements as are used to calculate the scattering coefficients among the wire-grid segments themselves. This is possible if the active elements themselves can be represented by a collection of short electric current segments. In the case of the multiturn loop antenna, the core storage necessary to hold data for the large number of current segments required for adequate representation would become excessive. One approach which will ease this storage problem may be employed if the circumference of each turn in the loop is small compared to a wavelength. For this case a constant current may be assumed on each turn of the multiturn loop. Kraus<sup>2</sup> has shown that the small electric loop with constant current has the same field pattern as a short magnetic dipole located at the center of the loop and oriented along the axis of the loop, provided both the electric loop and the magnetic dipole have dipole moments related as follows:

$$(30) \quad I_m l = -j 240 \pi^2 I_e A ,$$

where  $I_m$  and  $I_e$  stand for the magnetic and electric currents, respectively,  $l$  is the length of the magnetic dipole in wavelengths, and  $A$  is the area of the loop in wavelengths squared. Of course,  $I_m l$  and  $I_e A$  are the dipole moments of the magnetic dipole and the small electric loop, respectively. In addition, the medium is assumed to be free space.

Assume that the magnetic dipole is located at coordinates  $(x_m, y_m, z_m)$  in some fixed coordinate system. Let the dipole be oriented along the  $z$ -axis of a rotated coordinate system with orientation angles  $\alpha_m$  and  $\beta_m$ . Further, let a particular wire segment of the wire-grid aircraft, the  $i$ -th wire segment, be similarly located and oriented with respect to the same fixed coordinate system; that is, let the wire segment be located at  $(x_i, y_i, z_i)$  and have orientation angles  $\alpha_i$  and  $\beta_i$ . These angles are now defined for all subscripts: the angle  $\alpha$  is measured positively downward from the  $x$ - $y$  plane of the fixed coordinate system toward the negative  $z$ -axis; the angle  $\beta$  is measured positively from the  $x$ -axis of the fixed coordinate system toward the  $y$ -axis.

First, the coordinates of the center of the i-th wire segment are expressed in the rotated coordinates of the magnetic dipole. These are given as

$$(31) \quad x_i' = - (x_i - x_m) \sin \alpha_m \cos \beta_m - (y_i - y_m) \sin \alpha_m \sin \beta_m \\ - (z_i - z_m) \cos \alpha_m$$

$$(32) \quad y_i' = - (x_i - x_m) \sin \beta_m + (y_i - y_m) \cos \beta_m$$

and

$$(33) \quad z_i' = (x_i - x_m) \cos \alpha_m \cos \beta_m + (y_i - y_m) \cos \alpha_m \sin \beta_m \\ - (z_i - z_m) \sin \alpha_m$$

The radial distance from the center of the magnetic dipole to the center of the i-th wire segment is

$$(34) \quad r_i = \sqrt{(x_i - x_m)^2 + (y_i - y_m)^2 + (z_i - z_m)^2} .$$

The other spherical coordinates of the center of the i-th wire segment in the rotated system of the magnetic dipole are the angles  $\theta_i$  and  $\phi_i$ , defined in the accepted manner for spherical coordinates. These may be computed as follows:

$$(35) \quad \phi_i = \arctan \left( \frac{y_i'}{x_i'} \right)$$

and

$$(36) \quad \theta_i = \arctan \left( \frac{y_i'}{z_i' \sin \phi_i} \right) .$$

The instantaneous electric field at the point  $(r_i, \theta_i, \phi_i)$  generated by the magnetic dipole in its rotated system is given by <sup>2</sup>



$$(37) \quad E_{\phi_m}(r_i, \theta_i, \phi_i) = \frac{I_m l \sin \theta_i}{4\pi} \left( \frac{jk}{r_i} + \frac{1}{r_i^2} \right) e^{-jk r_i} .$$

The Cartesian components in the rotated system are denoted by

$$(38) \quad E_{x_m} = -\sin \phi_i E_{\phi_m},$$

and

$$(39) \quad E_{y_m} = \cos \phi_i E_{\phi_m} .$$

One last relationship must be established. Given that an element is in a rotated system with orientation angles  $\alpha$  and  $\beta$ , and given that the Cartesian unit vectors are denoted by  $\hat{x}$ ,  $\hat{y}$ , and  $\hat{z}$ , respectively, then the Cartesian unit vectors in the rotated system are related to those in the fixed system as follows:

$$(40) \quad \hat{x}' = -\hat{x} \sin \alpha \cos \beta - \hat{y} \sin \alpha \sin \beta - \hat{z} \cos \alpha$$

$$(41) \quad \hat{y}' = -\hat{x} \cos \beta + \hat{y} \sin \beta$$

$$(42) \quad \hat{z}' = \hat{x} \cos \alpha \cos \beta + \hat{y} \cos \alpha \sin \beta - \hat{z} \sin \alpha .$$

Now recall that the  $i$ -th wire segment is oriented along the  $z$ -axis in its own rotated coordinate system. Then the electric field generated by the magnetic dipole tangential to the  $i$ -th wire segment is given by the dot product

$$(43) \quad \vec{E}_i^{\text{tang}} = E_{\phi_m}(r_i, \theta_i, \phi_i) \cdot \hat{z}' ,$$

or in rotated Cartesian coordinates,

$$(44) \quad \vec{E}_i^{\text{tang}} = E_{\phi_m}(-\sin \phi_i \hat{x}_m' + \cos \phi_i \hat{y}_m') \cdot \hat{z}' .$$

In programming the above method, the input data for the magnetic dipole are read into the computer program just as the data for the electric current segments were previously, except that the equivalent dipole moment should be substituted for the data concerning current on the dipole. The unconditional transfer statement

GO TO 99

immediately preceding statement number 630 is eliminated, and the statements for programming the method suggested above for calculating  $E_i^{\text{tang}}$  for all  $i$  are inserted there. The quantities  $E_i^{\text{tang}}$  for all  $i$  are in general complex numbers whose real and imaginary parts become the elements

$$(45) \quad \text{Real}(-E_i^{\text{tang}}) = \text{CR}(I, NN)$$

and

$$(46) \quad \text{Imaginary}(-E_i^{\text{tang}}) = \text{CI}(I, NN) \quad .$$

One other change must be noted. The present approach uses the same far-field formulas to calculate the  $\theta$ - and  $\phi$ -components of the field from the whole system, including the radiating elements. This would be changed to use the present formulae for calculating only the field components scattered from the wire-grid structure. The far-field contribution at the observation point  $(R, \theta, \phi)$  due to the magnetic dipole may be determined in the following manner. First, consider the radial distance to the center of the magnetic dipole negligible compared to the distance to the point  $(R, \theta, \phi)$ . Next, by referring to Eqs. (31) - (33), define the quantities

$$(47) \quad x_f^i = -\sin\theta \cos\phi \sin\alpha_m \cos\beta_m - \sin\theta \sin\phi \sin\alpha_m \sin\beta_m \\ - \cos\theta \cos\alpha_m$$

$$(48) \quad y_f^i = -\sin\theta \cos\phi \sin\beta_m + \sin\theta \sin\phi \cos\beta_m$$

$$(49) \quad z_f^i = \sin\theta \cos\phi \cos\alpha_m \cos\beta_m + \sin\theta \sin\phi \cos\alpha_m \sin\beta_m \\ - \cos\theta \sin\alpha_m \quad .$$

The angular spherical coordinates of the observation point  $(R, \theta, \phi)$  in the rotated system of the magnetic dipole are, then,

$$(50) \quad \phi_f = \arctan \left( \frac{y_f^i}{x_f^i} \right)$$

and

$$(51) \quad \theta_f = \arctan \left( \frac{y_f^i}{z_f^i \sin \phi_f} \right) .$$

Then, after dropping any further reference to the far-field radial distance  $R$ , the  $\phi$ - and  $\theta$ -components of the electric field of the magnetic dipole referred to the fixed coordinate system are respectively

$$(52) \quad E_{\phi_m}(\theta, \phi) = F_{\phi} \cdot E_{fm}$$

and

$$(53) \quad E_{\theta_m}(\theta, \phi) = F_{\theta} \cdot E_{fm} ,$$

where<sup>2, 12</sup>

$$(54) \quad E_{fm} = \frac{jk I_m l \sin \theta_f}{4\pi} e^{jk(x_m \sin \theta \cos \phi + y_m \sin \theta \sin \phi + z_m \cos \theta)} ,$$

$$(55) \quad F_{\phi} = \cos \phi_f (\sin \beta_m \sin \phi + \cos \beta_m \cos \phi) \\ + \sin \phi_f (\sin \alpha_m \sin \beta_m \cos \phi - \sin \alpha_m \cos \beta_m \sin \phi),$$

and

$$(56) \quad F_{\theta} = \cos \phi_f (\cos \beta_m \cos \theta \sin \phi - \sin \beta_m \cos \theta \cos \phi) \\ + \sin \phi_f (\sin \alpha_m \cos \beta_m \cos \theta \cos \phi + \sin \alpha_m \sin \beta_m \cos \theta \sin \phi \\ - \cos \alpha_m \sin \theta) .$$

(Note that the factor  $(1/R) e^{-jkR}$  in Eq. (54) is suppressed so that the phase of the far-field term is referred to the origin of the fixed coordinate system.)

By programming the above quantities, the far-field contribution from a magnetic dipole may be directly combined with the far-field quantities radiated by the currents induced on the wire-grid aircraft structure.

The above paragraphs have described a method for representing a small square electric loop by a single magnetic dipole. By a direct extension of this method, a multiturn loop of, say, 16 turns can be represented by 16 small magnetic dipoles instead of 64 short electric wire segments. This modification to present techniques should make computations involving perhaps four multiturn loops much more practical.

## REFERENCES

1. Foster, D., "Loop Antennas with Uniform Current," Proc. IRE. Vol. 32, (October 1944), pp. 603-607.
2. Kraus, J.D., Antennas, pp. 155-172.
3. Munk, B.A. and Flaig, T.L., "Radiation Resistance and Efficiency of Multiturn Loop Antennas," Report 2235-4. (Report in Process).
4. Walter, C.H., Traveling Wave Antennas, McGraw-Hill Book Co., Inc., (1965), p. 61.
5. Ramo, S., and Whinnery, J.R., Fields and Waves in Modern Radio, Second Edition, John Wiley and Sons, Inc., (1953), pp. 234-248.
6. Walter, op. cit., pp. 253.
7. Annual Summary Report, Report 2235-1, 27 July 1967, Electro-Science Laboratory, The Ohio State University Research Foundation, pp. 6-9.
8. Flaig, T.L., "Impedance and Efficiency of Multiturn Loop Antennas," Report 2235-3, 3 April 1968, ElectroScience Laboratory, The Ohio State University Research Foundation, pp. 21-23.
9. Jasik, H., Antenna Engineering Handbook, Section 34, pp. 34-10 to 34-16.
10. Wheeler, H.A., "The Radian Sphere Around a Small Antenna," Proc. IRE, Vol. 47, pp. 1325-1331.
11. Terman, F.E., et al., Electronic and Radio Engineers Handbook, McGraw-Hill Book Co., Inc., (1955), p. 354.
12. Richards, G.A., "A Boundary-Value Technique for Computing the Patterns of an Antenna Near a Conducting Body of Arbitrary Shape," Report 2235-2, September 1967, ElectroScience Laboratory, The Ohio State University Research Foundation.
13. Richmond, J.H., "A Reaction Theorem and Its Application to Antenna Impedance Calculations," IRE Transactions on Antennas and Propagation, Vol. AP-9, No. 6, (November 1961), pp. 515-520.

14. King, R.W.P., E.A. Aronson, and C.W. Harrison, Jr., "Determination of the Admittance and Effective Length of Cylindrical Antennas," Radio Science, Vol. 1, (New Series), No. 7 (July 1966), pp. 835-850.
15. Kraus, J.D., op. cit., pp. 262-272.
16. Kraus, J.D., op. cit., pp. 424-428.